Suzuki and Kumada Surface Initiated Polycondensations: Novel Engineering Route to Conjugated Polymer Systems

DISSERTATION

Zur Erlangung des akademischen Grades

Doktor rerum naturalium
(Dr. rer. nat.)

vorgelegt

der Fakultät Mathematik und Naturwissenschaften
der Technischen Universität Dresden

von

Kseniya Boyko

geboren am 18 Februar 1985 in Wladiwostok, Russland

Eingereicht am . . .

Die Dissertation wurde in der Zeit von Juli/2007 bis
Januar/2011 im Leibniz-Institut für Polymerforschung Dresden e.V. angefertigt.

To my wonderful mother

Contents

Introduction

Motivation & actuality. In the field of electronic organic materials, conjugated polymers (CPs) have attracted much attention in recent years. These materials may combine the processability and outstanding mechanical characteristics of polymers with the electrical, optical and magnetic properties of functional organic molecules. The light weight, mechanical flexibility, thermal and chemical stability and simple processing, as well as the optoelectronic properties of these materials may significantly improve device efficiency and manufacturing processes. A remarkable advantage of these polymers is that their optoelectronic properties can be modified by designing chemical functions based on the constituent molecules and doping conditions. It has been well-established that performances of thin-film devices based on π-conjugated polymers, such as light-emitting diodes, field-effect transistors and photovoltaic (PV) cells, are strongly dependent on the organisation of the polymer molecules and their interactions with other constituents in multicomponent devices. Further progress in organic electronics will require the development of new CPs which have not only improved optoelectronic characteristics, but also guidable self-assembly properties. In this regard, well-defined conjugated polymers with controllable architecture, such as block copolymers or polymer brushes, are potentially interesting, but not yet a readily available class of materials. On the other hand, the use of CPs in integrated circuits, solar cells, light-emitting diodes or sensors often requires their covalent fixation and patterning on various surfaces. CPs can be grafted to functionalized surfaces by (electro)chemical cross-linking; however, it is difficult to control a structural order within the cross-linked films. The attachment of CP chains to substrates by their end-points to form polymer brushes would be an interesting alternative, and could possibly be crucial for many devices requiring charge injection and charge transport processes. Surface-initiated polymerization is the most efficient way to generate polymer brushes with high grafting densities and tunable thickness. Various chain-growth polyaddition reactions, including radical and anionic polymerization of olefins, ring-opening polymerisation of olefins and polypeptides, etc., have already been adapted for the preparation of brushes. Surface-initiated polymerizations assume the generation of polymerizing species by surface-immobilized initiators and growth of polymer chains via one-by-one addition of monomers at the propagating point. Since the synthesis of most conjugated polymers involves a $step - growth$ polycondensation mechanism, the preparation of CP brushes remained problematic for a long time. Therefore, the main aim of this thesis was to develop a surface-initiated polymerization process based on $chain - growth$ polycondensations that would provide straightforward access to conjugated polymer brushes.

Outline of the thesis. The first chapter provides an introduction to the conjugated polymers and reviews the main synthetic approaches. In particular, it describes step- and chain-growth polymerization mechanisms, their drawbacks and benefits. It also covers the field of polymer brushes, their main characteristics and different manufacturing feasibilities. The second chapter focusses on different experimental techniques used in this work. Chapters three, four and five describe experiments performed during the course of this work and discussion of the achieved results. The third and fifth chapters report the grafting of poly(9,9-dioctylfuorene) and poly[(9,9-bis(2-ethylhexyl)fluorene] from different substrates such as Si-wafers, quartz slides and poly(4-bromostyrene) (PS(Br)) latex nanoparticles. The fourth chapter investigates in detail the catalyst activation process which precedes the grafting stage. The sixth chapter considers organic light-emitting diodes, their constituents, basic working principles and main characteristics. The final, seventh chapter presents general conclusions and gives an outlook on future work in the field.

Results and novelty. In this work, I developed a surface-initiated and site-specific palladium-catalyzed Suzuki polycondensation method to graft and pattern semiconducting fluorescent poly[9,9-bis(2-ethylhexyl)fluorene] (PF2/6). To the best of my knowledge, this is the second example for the preparation of conjugated polymer brushes via a grafting-from procedure (the first one was based on Kumada catalyst-transfer polycondensation and was reported in 2007) [1], and this is also the first grafting-from method that utilizes Suzuki catalyst-transfer polycondensation. Using the developed procedure, grafting of polyfluorenes can be performed from surface-immobilized PS(Br) films, as well as from monolayers of small molecules or patterned initiators. The described process leads to mechanically robust CPs films which are stable against delamination and can be easily produced in a very economical way. That means that the monomer is consumed on polymerization of brushes. The developed process seems to be very promising for the fabrication of plastic devices by covering functional substrates with different shapes. We believe that the method will become a powerful surface engineering tool, useful for the fabrication of optoelectronic devices and sensors. In the next step, it would be desirable to develop grafting from electrically conductive substrates for application of the electroluminescent properties of the grafted polyfluorenes, as well as to determine the scope and limitations of surface-initiated polycondensation.

Publications

- T. Beryozkina, K. Boyko, V. Senkovskyy, M. Horecha, N. Khanduyeva, U. Oertel, M. Stamm, A. Kiriy. Surface-Initiated Suzuki Polycondensation of Polyfluorene. Angew. Chem. Int. Ed. 2009, 48, 2695-2698.

Conferences

- 4th International Symposium on Nanostructured and Functional Polymer-Based Materials and Nanocomposites, Rome, Italy, 2008 (poster presentation)
- European Polymer Congress, Graz, Austria, 2009 (poster presentation)
- 8th International Conference on Advanced Polymers via Macromolecular Engineering, Dresden, Germany, 2009 (poster presentation)
- 5th Annual Plastic Electronics Europe, Dresden, Germany, 2009 (poster presentation)
- SPIE Photonics Europe, Brussels, Belgium, 2010 (poster presentation)

1 Conjugated Polymers and Polymer Brushes

1.1 Conjugated Polymers

1.1.1 Main Synthetic Routes and their Applicability for Preparation of Polymer Brushes

Conjugated polymers (CPs) are organic macromolecules which consist of alternating single and double bonds. Typical CPs are polyacetylene, polyphenylvinylene, polythiophene and polyfluorene (Figure 1). They have received considerable attention with the development of the information technology industry. In the 1980s they had become a great interest of research following the discovery, that insulating polyacetylene turns it into an excellent "organic metal" which shows perfect metal-like conductivity if oxidized or reduced ("doped") [2]. The main drawback of this method is related to the insolubility and to the impossibility of treating the polymer after synthesis. Attempts to solubilize it were performed with two main approaches: the precursor route and direct polymerization. Historically, the first efforts to get conjugated polymers were based on the "precursor route". Afterwards they were replaced with much more efficient "direct routes".

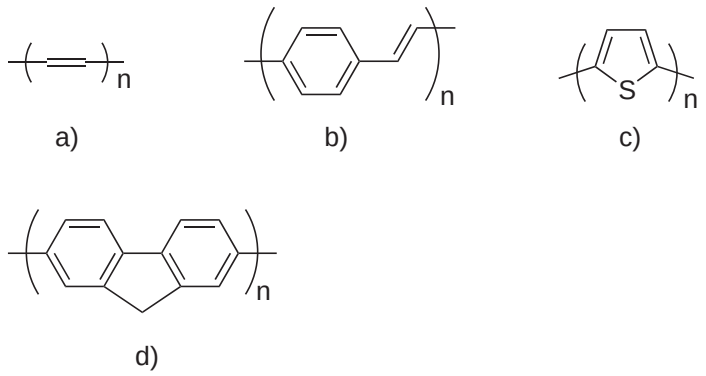

Figure 1: The chemical structures of a) polyacetylene, b) polyphenylvinylene, c) polythiophene, d) polyfluorene.

1.1.2 Precursor Routes

The idea was to prepare a soluble precursor, which upon elimination of some molecular substituents via a thermal treatment, may produce the conjugated form of the polymer. Early attempts to synthesize poly(phenyl vinylene) (PPV)-type polymers had started from variations of Ullmann [3] or Wurtz-Fittig [4] reactions. Other methods used Kovaci's [5, 6] and Wessling methods (Figure 2) [7, 8, 9]. Gilch [10] route utilizes halide leaving groups.

The general restrictions of these methods are limited efficiency, various side reactions during post-polymerization processing and toxic by-products. A key issue in the synthesis of any CPs is the minimization of defects, which have a large, usually negative, influence on the optical and electronic properties. These defects can act as a charge traps or specific sites for nonradiative decay, which significantly reduce the performance of devices.

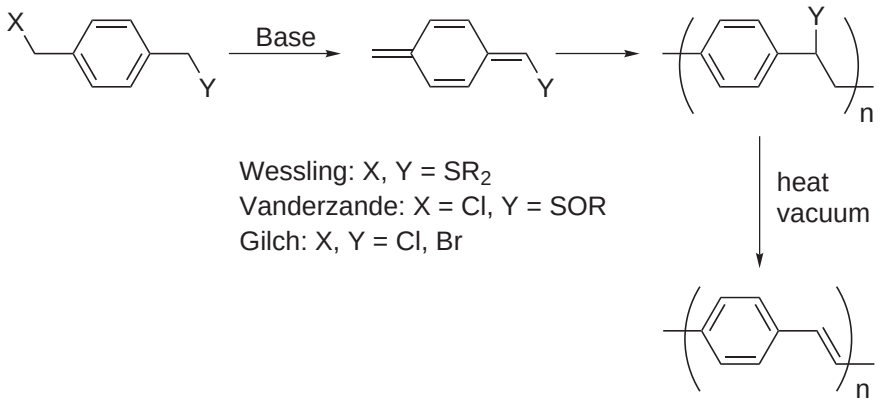

Figure 2: Precursor polymer route to PPV via a quinodimethane.

Moreover, during the synthesis of precursors or their polymerization, carbonyl groups can be formed by the oxidation of benzylic positions [11].

More powerful direct routes to conjugated polymers are step-growth and chain-growth condensation polymerizations.

1.1.3 Step-Growth Polycondensation

Step-growth polymerization proceeds through a mechanism in which all the end groups of monomers and oligomers in the reaction mixture react equally with each other (Figure 3). In a so-called AA/BB approach "AA-type" and "BB-type" monomer molecules can be used. Thus, two different monomers are required, each carrying two of the same functional groups (A or B type) [12]. One huge restriction of this approach is that AA and BB monomers need to be combined in exact molar ratio of 1:1 in order to obtain a high molar mass product. Carothers equation describes the dramatic loss in molar mass caused by mismatched stoichiometry. AB monomers (where each monomer has two different functional groups) are intrinsically nonsymmetric and $a\ priori$ have an equal amount of both functional groups. Moreover, in polymers obtained by this method, monomer units are incorporated in head-to-tail fashion. This provides a good opportunity to avoid structural defects that is important in such applications as organic light-emitting diodes (OLEDs), solar sells and so

on. A drawback of the AB-polymerization method is a limited availability of monomers, so the AA/BB approach is predominantly used.

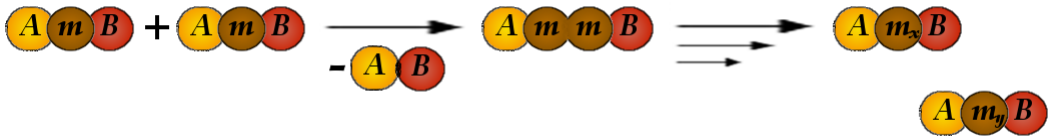

Figure 3: Step-growth polymerization model, AB-approach.

1.1.4 Direct Routes

Oxidative polycondensation. Polymerizations based on oxidative coupling reactions were widely used during the early stages of conjugated polymer research. Aryl and heterocyclic compounds such as thiophene, aniline and fluorene, having electron-rich sites around their ring system are treated with oxidative reagents (ammonium persulfate, $FeCl_3$, etc.) to get CPs (Figure 4) [13, 14, 15]. Typical degrees of polymerization are 10 to 100 together with usually broad molecular weight distributions.

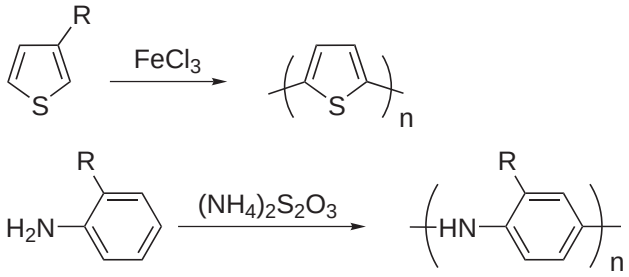

Figure 4: An example of oxidative polycondensation route to CPs

Fridel-Crafts polymerization is similar to direct oxidative polymerization. Lewis acids, such as $AlCl_3$, $AlBr_3$ and $FeCl_3$ can promote condensation polymerizations [16]. Depending on the reaction conditions and the nature of the polymerization agent both, cross-linked and branched polymers can be synthesized. Only oligomeric materials can be obtained by this method [17].

Electrochemical polycondensation is a direct route to $in\ situ$ formation of polymer from a monomer solution induced electrochemically [18]. Owing to a current passing through the cell, monomers like pyrrole, thiophene and fluorene can be easily oxidized into reactive radicals followed by polymerization. The film thickness can be easily controlled by the integrating current.

The McMurry reaction is the coupling of aromatic dialdehydes with low-valent titanium reagents (Figure 5) [19, 20]. This method allows for the synthesis of polymers with a $cis/trans$ ratio of about 0.4 [21].

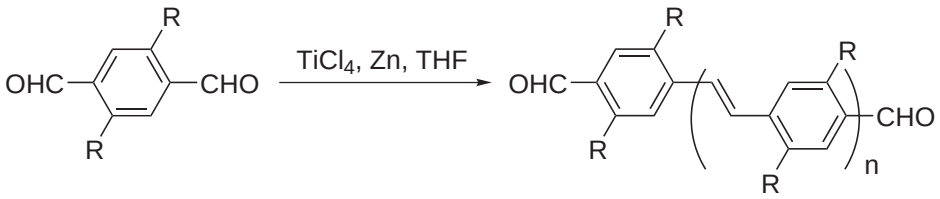

Figure 5: An example of McMurry polycondensation reaction

Wittig and Wittig-Horner reactions. The Wittig reaction is the coupling of an aldehyde with aryl triphenyl phosphonium salts to yield alkenes (Figure 6) [22]. One drawback of this method is the simultaneous production of cis- and $trans$-isomers [23]. The selectivity can be improved by using phosphonates instead of phosphonium salts (Wittig-Horner reaction), which produces almost all $trans$-alkenes [24].

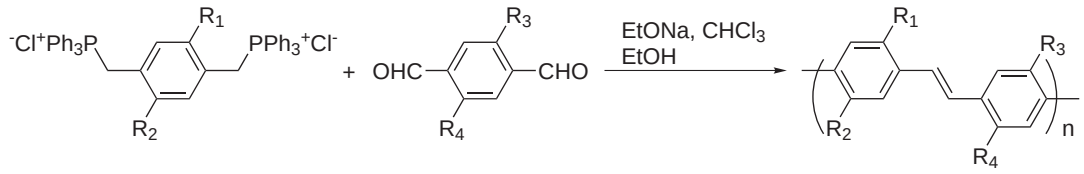

Figure 6: Wittig reaction.

The Knoevenagel reaction is a base-catalyzed condensation of a dialdehyde and an arene possessing two relatively acidic sites (benzylic protons) [25]. This method is widely used for the synthesis of CN-PPV and its derivatives [26].

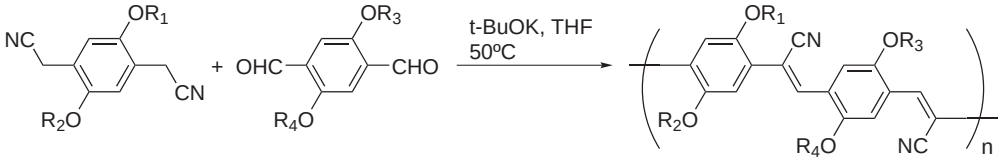

Figure 7: Synthesis of CN-PPV via Knovenagel condensation route.

Polycondensation of organomagnesium monomers. Grignard reagents can be easily prepared by the direct reaction of an organic halide with magnesium metal [27]. Poly(phenyl phenylene)s (PPPs) with long alkyl side chains can be prepared through nickel-assisted coupling of organomagnesium reagents. However, the typical degree of polymerization for polymers prepared by this method is about 8-20 units.

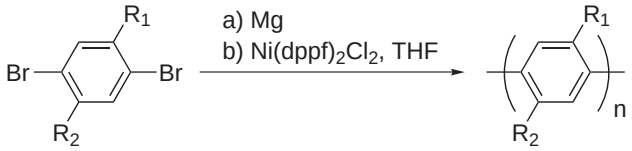

Figure 8: Synthesis of PPP through coupling of Grignard reagents.

The McCullough method for polythiophenes (PTs) utilizes bromination at the 2^{nd} position of 3-alkylthiophene precursors and selective lithiation at the 5th position with lithium diisopropylamine followed by quenching with $MgBr_2{\cdot}OEt_2$. The polymerization is catalyzed by $Ni(dppf)_2Cl_2$. The overall reaction is controlled by the metal site to give stereoregular structures [28].

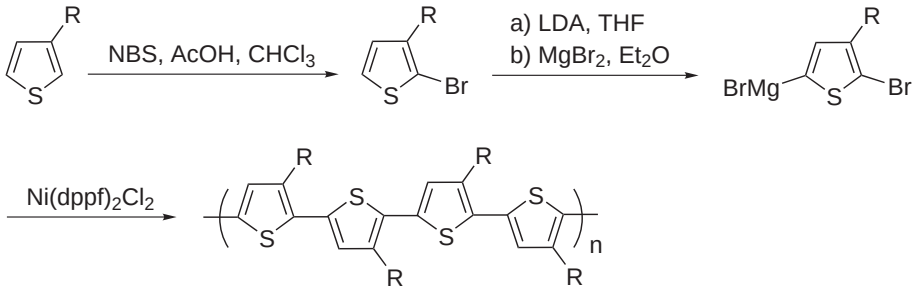

Figure 9: McCullough method for the synthesis of regioregular P3ATs.

The Rieke method allows one to get CPs under mild conditions. For orienting linkage selectivity, this method relies on organozinc reagents [29, 30] which react with aryl halides at -78^{o}C to afford the corresponding Grignard reagents. The higher reactivity of zinc toward iodide, relative to bromide, leads to selective incorporation at the site opposite the alkyl substitution.

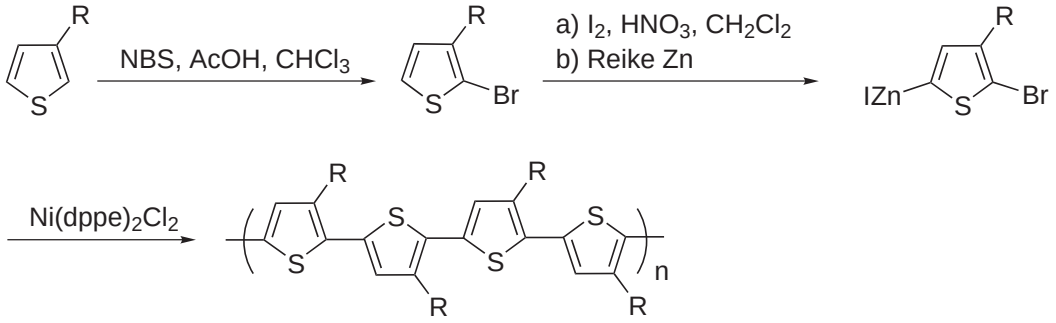

Figure 10: Rieke method for the regioregular P3ATs.

The Heck reaction is a palladium-catalyzed formation of carbon-carbon double bond between organic halides and olefins, in mostly $trans$ configuration, with very few side reactions [31]. The reaction is compatible with a suitable range of chemical functionalities. The regioselectivity can be controlled by the reaction conditions, by the substituents on the arylene component, by living groups and by the choice of olefinic monomer [32].

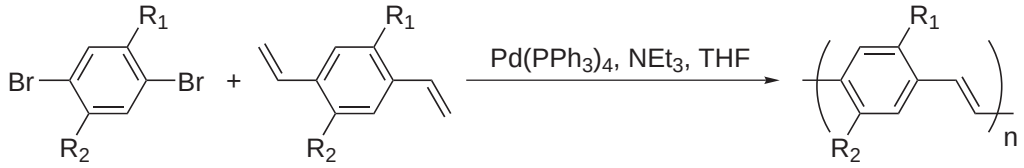

Figure 11: Heck reaction for the synthesis of PPVs.

The Suzuki reaction refers to the cross-coupling of aromatic organic electrophiles such as aryl or vinylic halides (or triflates) with organoboron reagents (aryl boronic acids and their esters) in the presence of a base [33]. The most commonly used palladium catalysts are $Pd(PPh_3)_4$, $Pd(PPh_3)_2Cl_2$ and $Pd(OAc)_2$ with triphenylphosphine. Typical reaction is illustrated in Figure 12. The Suzuki reaction is tolerant to a broad range of functional groups and is unaffected by the presence of water. Boronic derivatives are easier to handle than their corresponding acids and non-toxic by-products are formed. It has been noted that 2,5-dialkylbenzene-1,4-bis(trimethyleneborate)s polymerize smoothly to give higher molecular weight polymers than those obtained with the parent boronic acids [34, 35].

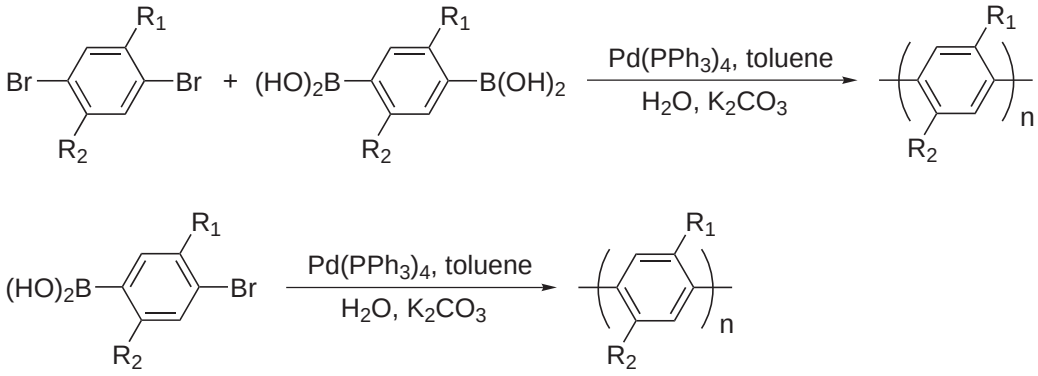

Figure 12: Suzuki coupling reaction.

The Stille coupling reaction is the palladium-catalyzed coupling between an organostannane and halides or pseudohalides to form C-C bond with very few limitations on the R-groups [36]. The advantages are that organostannanes are not oxygen or moisture sensitive; however they are toxic and possess low polarity, which makes them poorly soluble in water.

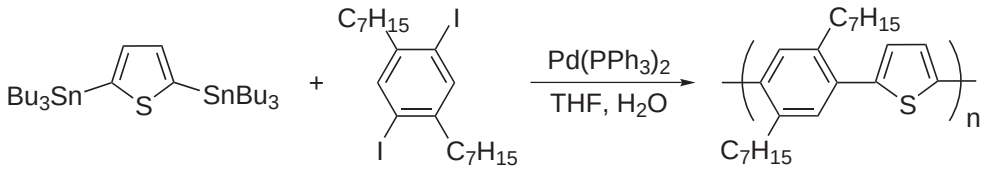

Figure 13: Synthesis of PATs via Stille coupling route.

The Sonogashira-Hagihara reaction is the coupling of terminal alkynes with aromatic bromides or iodides performed in the presence of palladium catalyst, a copper (I) co-catalyst and an amine base [37]. The corresponding iodides react considerably faster and lead to the higher yield at lower reaction temperatures. Polymers obtained by this method have a molecular weight from thousands to hundreds of thousands.

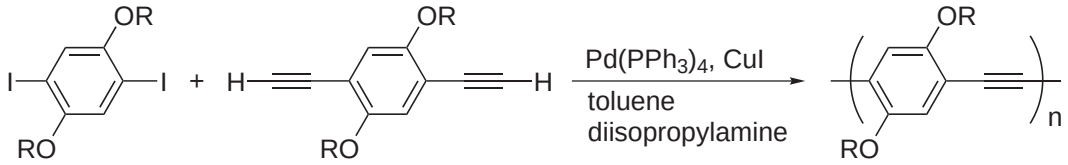

Figure 14: Sonogashira-Hagihara coupling.

Yamamoto-type cross-coupling refers to the C-C coupling via the condensation of dihaloaromatic compounds [38]. By this approach, high molecular weight polymers (up to M_n = 200 000 g/mol [39]) can be obtained through the Ni(COD) (COD = cyclooctadiene) catalyst and dihalosubstituted monomers. A major advantage of this method is the straightforward preparation of the dihalohenated reactants. As compared to the $FeCl_3$-catalyzed oxidative polymerization, Yamamoto coupling yields minimized branching. A disadvantage is the difficulty in removing catalyst residues from the product.

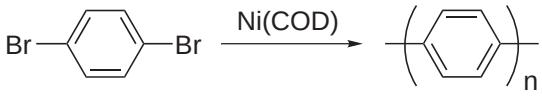

Figure 15: An example of the Yamamoto polycondensation.

All the aforementioned synthetic routes are powerful methods to obtain CPs with the limited amount of defects. However, polymers synthesized through these approaches possess broad molecular weight distributions. That is because these methods employ step-growth polymerization mechanisms, where all end groups of monomers and oligomers in the reaction mixture react equally with each other. In addition, the preparation of complex architectures of conjugated polymers such as brushes or block copolymers is hardly possible with these step-growth polycondensation methods.

1.1.5 Chain-Growth Condensation Polymerization for Conjugated Polymers

Although many controlled chain-growth polymerizations (RAFT, ROMP, ATRP, etc.) have been developed to polymerize "vinyl-type" monomers, examples of chain-growth polymerization routes to conjugated polymers are rare. Typical $catalyst - transfer\ polycondensation$ mechanism involves a catalytic cycle consisted of three consecutive steps: oxidative addition, transmetalation, and reductive elimination (Figure 16).

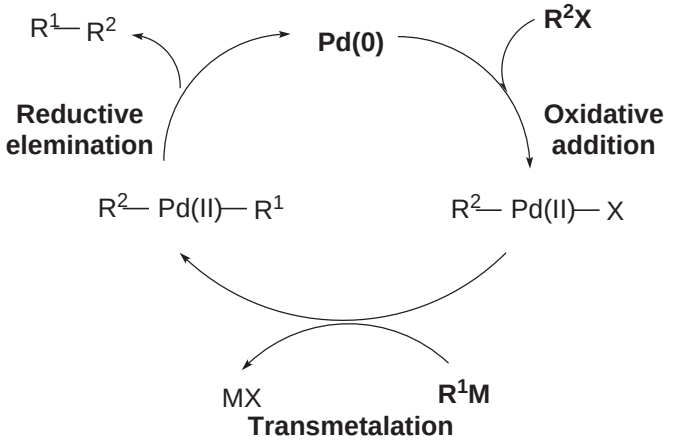

Figure 16: Generalized mechanism for palladium-catalyzed Suzuki-Miyaura cross-coupling reaction.

The key step in this mechanism is $intra$molecular catalyst transfer to and activation of only the elongated polymer end group. With this mechanism, one can achieve conjugated polymers with narrow molecular weight distributions, which lead to improved conductive properties. Hu et al. have found that employing Pd(0)/t-Bu_3P for the cross-coupling of dihalobenzenes with one equivalent of arylboronic acid leads to preferential intramolecular catalyst transfer [40]. Later, Scherf and co-workers demonstrated that a strictly intramolecular motion of the regenerated Pd(0) catalyst was observed for extended 2,7-substituted fluorene monomers. These promising results showed that a controlled, intermolecular Pd-insertion in Suzuki-type cross-coupling reactions is also possible across the "large" distance of the monomer unit.

Yokozawa et al. [41] found that the chain-growth mechanism is quite general for metal-catalyzed polymerization of AB-type monomers. They found, in particular, that polycondensation of monomers like 7-bromo-9,9-bis(2-ethylhexyl)-9H-fluoren-2-ylboric acid ester catalyzed by Pd complexes with bulky and electron-reach phosphine ligands (Suzuki-Miyaura polycondensation) can also be performed in a chain-growth manner. They used a stable aryl palladium(II) halide complex as an externally-added initiator. The aryl group of the initiator served as the end group of the growing polymer chain. The molecular weight of the obtained polymer increased linearly in proportion to the conversion of monomers with low polydispersity. The degree of polymerization was strongly dependent on the feed ratio of the monomer to the initiator. All these facts confirm the chain-growth polymerization mechanism for Suzuki-Miyaura cross-coupling polymerization. This reaction will be considered in more detail in Chapter 3.

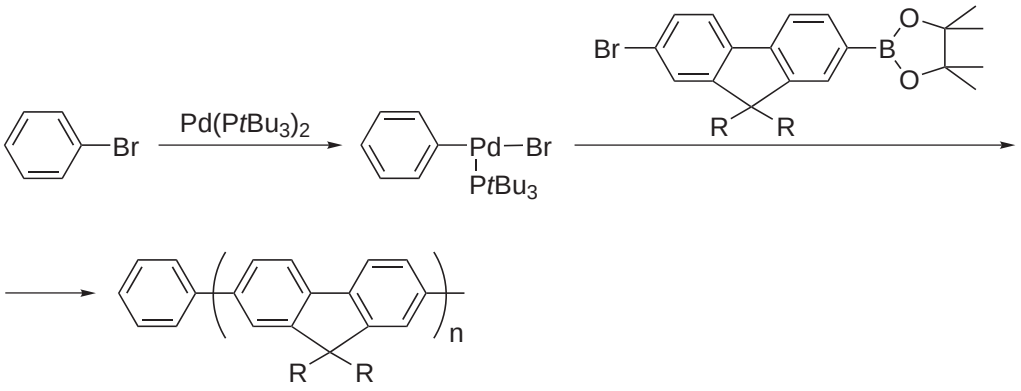

Figure 17: Synthesis of PF2/6 via Suzuki-Miyaura chain-growth polymerization.

Recently, Yokozawa and McCullough developed a method to polymerize alkylthiophenes via the catalyst-transfer polycondensation route. The proposed catalyst-transfer condensation polymerization mechanism is depicted in Figure 18.

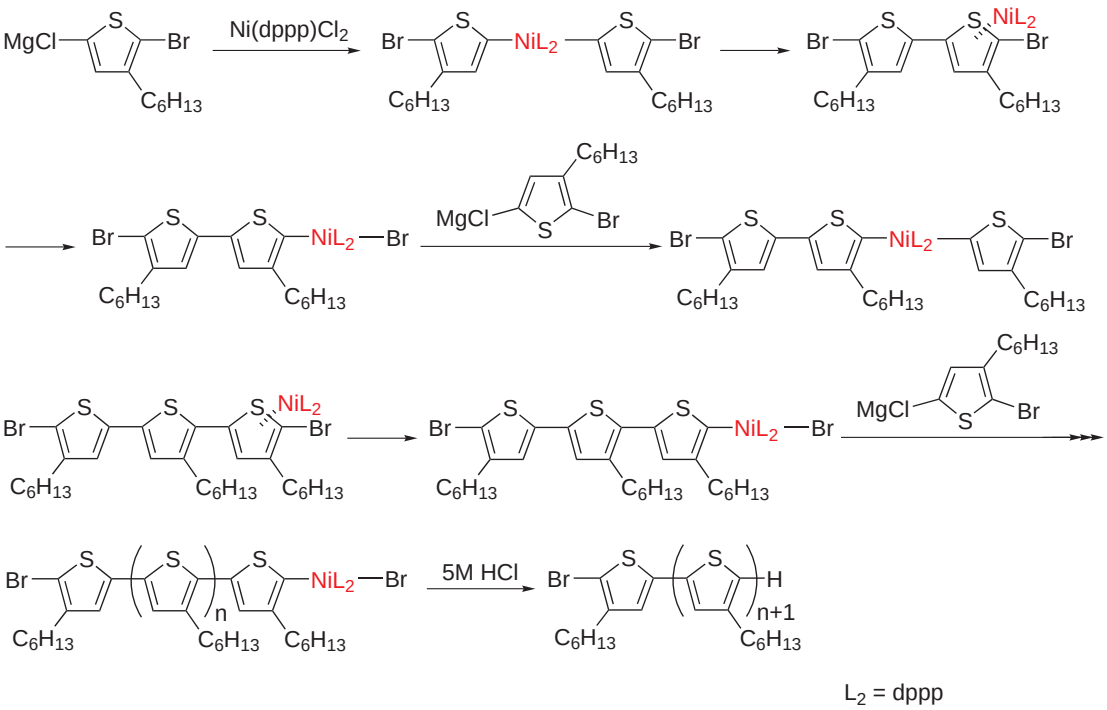

Figure 18: Catalyst-transfer condensation polymerization mechanism.

Thus, Ni(dppp)Cl_2 reacts with two equivalents of Grignard thiophene monomer, and the coupling reaction occurs with concomitant generation of a zero-valent Ni complex. The Ni(0) complex does not diffuse into the reaction mixture, but is instead inserted into the intramolecular C-Br bond. Another Grignard thiophene monomer reacts with this Ni, followed by the coupling reaction and transfer of the Ni catalyst to the next C-Br bond. Growth continues in such a way that the Ni catalyst moves to the polymer end group [42].

The effect of the catalyst structure was investigated by Lucht et al. [43]. It was shown that the Ni complexes stabilized by bidentante phosphine ligands possess a higher efficiency than those supported by monodentante ligands. On the other hand, Ni complexes are more efficient than Pd complexes.

The influence of the phosphine ligand of the Ni catalyst on the catalyst-transfer condensation polymerization was also investigated by Yokozawa and co-workers [44, 43]. Ni(dppe)Cl_2 and Ni$(PPh_3)_4$ gave a polymer with a slightly

lower M_n and a slightly broader molecular weight distribution, whereas $Ni(PPh_3)Cl_2$, $Ni(dppb)Cl_2$ and $Ni(dppf)Cl_2$ gave polymers with low M_ns and a broad molecular weight distribution. $Ni(dppp)Cl_2$ resulted in a M_n value close to the theoretical value based on the feed ratio of monomers to the catalyst and the narrowest M_w/M_n ratio.

Also, it was shown that the quenching method plays a crucial role on the polydispersity of obtained polymers. Yokozawa et al. found that the polymerization of 2-bromo-3-hexyl-5-iodothiophene with $Ni(dppp)Cl_2$ followed by quenching with 5M hydrochloric acid instead of water results in regioregular hexylthiophene-poly(3-hexylthiophene) (HT-P3HTs) with very low polydispersity, and that the M_n is also controlled by the feed ratio of 2-bromo-3-hexyl-5-iodothiophene to $Ni(dppp)Cl_2$ under this quenching method [45].

Geng and co-workers have recently reported on the polymerization of Grignard-type fluorene monomer with $Ni(dppp)Cl_2$ [46]. The monomer was generated from the corresponding bromoiodofluorene with i-PrMgCl/LiCl (1:1). The polymerization proceeded very quickly at 0^oC and was nearly completed in 10 min. High molecular weight polyfluorene (M_n = 18 800 – 86 000) was obtained at the very beginning, and the M_n almost remained identical at different conversions of the monomer. The M_w/M_n of the resulting polymers was in the range 1.49-1.77.

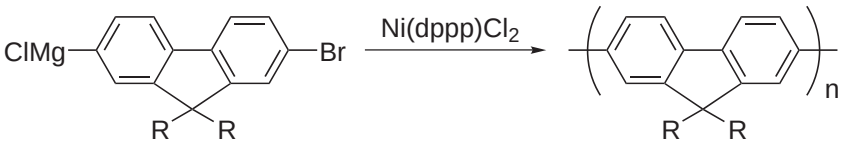

Figure 19: Synthesis of poly(octyl fluorene) (PFO) by the GRIM method.

In order to control the physical properties of thin-film devices based on π-conjugated polymers, it is necessary to enable the organisation of the polymer molecules and their interactions with other constituents in multicomponent devices. Moreover, guidable self-assembly properties may result in improved device performance. Thus, covering functionalized substrates (planar surfaces, functionalized particles and so on) with covalently grafted conjugated polymers could be a powerful tool to obtain desirable functionalized surfaces.

1.2 Polymer Brushes: Definition and Classification

1.2.1 Types of Polymer Brushes

The term "polymer brush" refers to an assembly of polymer molecules which are attached at one or several anchor points to a surface or an interface at sufficient grafting density [47, 48, 49]. Tethering can be sufficiently dense that the polymer molecules are crowded and forced to stretch away from the surface or interface due to excluded volume effect [50, 51]. This situation, in which polymer chains are stretched along the direction normal to the grafting surface, is found to be present under equilibrium conditions. It is quite different from the behaviour of flexible polymer chains in solution where chains are present in a random-walk configuration [52].

Thanks to polymer brushes, it is possible to achieve different special polymer systems such as polymer micelles, block copolymers at fluid-fluid interfaces, grafted polymers on a solid surface, adsorbed diblock copolymers and graft copolymers at fluid-fluid interfaces (Figure 20).

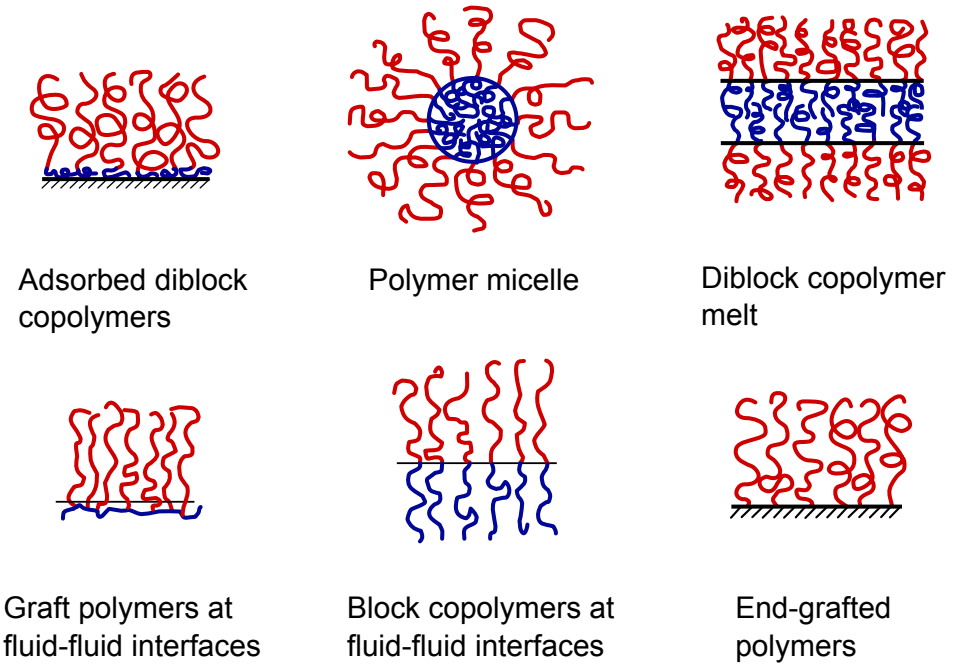

Figure 20: Examples of polymer systems comprising polymer brushes.

The conformation of grafted polymer chains mostly depends on the grafting density and interactions with the surface. At low grafting density, tethered chains do not overlap, due to the distance between grafting sites, which is larger than the size of the chains. If interactions between molecular chains

and the surface are attractive, then a "pancake-like" conformation can be observed. In the case of non-attractive interactions, polymer chains display so-called "mushroom" conformation (Figure 21). At high grafting density, because of the balance between the elasticity of the chains and segment-segment repulsion, the grafted molecules are stretched away from the surface to form brushes. If the chains are charged, electrostatic interactions generally affect the conformations. Hence, the ionic strength and pH of the surrounding medium sometimes have great influence on the formation of brushes [53].

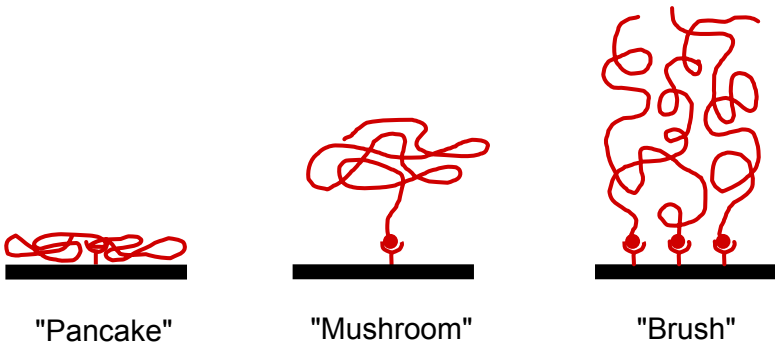

Figure 21: Conformations of polymer molecules attached to a surface: pancake, mushroom and brush.

In any case, polymer brushes show a deformed configuration, different from untethered random-walk polymer chains in solution. In the presence of a good solvent, they tend to maximise contact with solvent molecules and try to avoid interactions with each other. In melting conditions (without a solvent), polymer molecules stretch away from the surface to avoid overfilling incompressible space [52, 54].

In terms of polymer chemical compositions, polymer brushes can be divided into homopolymer brushes, mixed homopolymer brushes, random and block copolymer brushes [55]. Homopolymer brushes can be further divided into neutral and charged polymer brushes. In terms of rigidity of the polymer chain they may be flexible, semiflexible and or liquid crystalline polymer brushes [56]. These different structures are depicted in Figure 22.

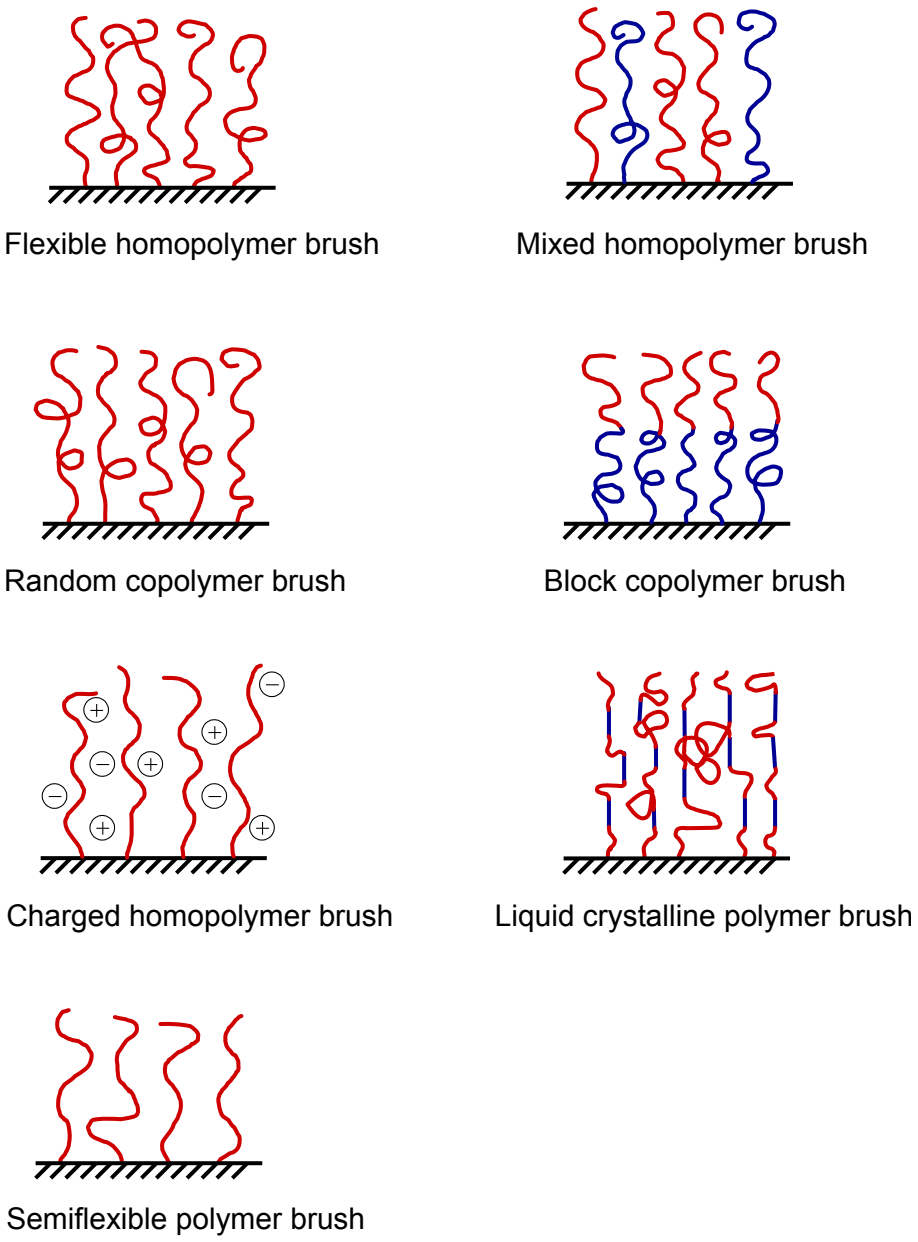

Figure 22: Classification of linear polymer brushes.

The conformation of surface-immobilized polymers can be evaluated via brush heigh h as a function of graft density σ (A (cm^2 per molecule) or C (mol per cm^2)), average distance of the anchor points d_g and the molecular weight of the surface-tethered chains. In polymer brushes, the interval between the grafting points of tethered chains is much smaller than the radius of gyration r_g of the same unperterbed chain which is not in contact with the surface.

To describe the equilibrium thickness of the grafted layer, Alexander

proposed a model which considers a flat, nonadsorbing surface to which monodisperse polymer chains are tethered. The polymer chains consist of N statistical segments of diameter a and the average distance between the tethering points is d_g, which is much smaller than the radius of gyration of a free, undeformed chain. The key concept is that the free energy per chain F includes two terms: interaction energy between two statistical segments F_{int} and elastic free energy F_{el} caused by the entropy loss of the chains.

$$F = F_{int} + F_{el} \tag{1}$$

The two assumptions are necessary. The first one is that the depth profile of statistical segments is step-like. The concentration of statistical segments is a constant within brushes. The second note is that all free ends of grafted chains are located in a single plane at a distance L from the tethering surface.

Regarding brushes in a good solvent, calculation and minimization of interaction energy of binary monomer-monomer interactions and the elastic energy of a Gaussian chain leads to the following equation:

$$h \sim N \cdot \sigma^{1/3} \tag{2}$$

In the case of a poor solvent - that is, close to θ conditions - the influence of grafting density is slightly different:

$$h \sim N \cdot \sigma^{1/2} \tag{3}$$

It is worth noting, that the dependence of the brush heigh on the polymer molecular weight is more important than that of the size of a polymer coil in solution. The radius of gyration of untethered macromolecules in solution close to θ conditions corresponds to $r_g \sim N^{1/2}$.

The degree of deformation of polymer chains depends on the environmental conditions to which tethered polymer chains are exposed. It is interesting to see that the linearity of L with N is preserved in theta and poor solvents, but polymer chains are still distorted at the theta point. In the case of melt brushes (without solvent), the grafted polymer chains are also deformed comparably with the free polymer chains in the same conditions. Thus, despite theta conditions, a good solvent or the absence of a solvent (melt conditions), the polymer chains in grafted polymer brushes demonstrate deformed configurations.

Alexander's approach is a simple free energy balance argument. It does not make an effort to describe the conformation of polymer chains or the density profile of chains at a distance from the grafting surface. This model can be used only to evaluate the hydrodynamic thickness, permeability of a brush

and the force per area required to compress a brush. Nevertheless, it allows us to predict and understand such essential properties of polymer brushes as lubrication and wetting behaviour. More advanced models are required to characterise the segment density profile correctly or to describe the variety of charged polymer molecules [57].

With the aim of describing the segment density profile of brushes, more advanced self-consistent field theories were developed [58, 59, 60]. The following basic assumptions were accepted: for strong stretching and high molecular weights of the brushes, fluctuations around the most favourable configuration of the polymer chain are minimized. As a consequence, the calculated segment density profile is parabolic as long as the grafting density is reasonable and molecular weight of polymer chains is high. The only restriction for this theory is a high grafting density. Zhang et al. studied the mechanism of the formation of polymer brushes with quartz crystal microbalance and found a three-regime kinetic of grafting. The first step is the formation of disordered grafted polymer chains in a mushroom regime, which then rearrange themselves to avoid local overlapping and form an ordered mushroom. The changed conformation allows subsequent grafting of additional polymer chains to the surface with the final formation of a brush regime.

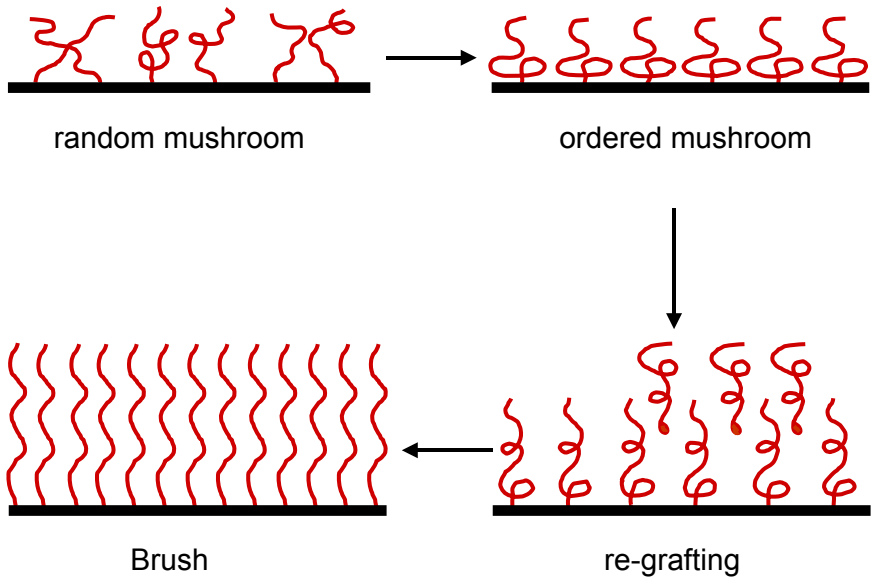

Figure 23: Formation of polymer brushes through the three-regime-kinetic of grafting.

1.2.2 Synthesis of Polymer Brushes

Generally, there are two principal requirements to force tethered polymers into a brush-like conformation. The first one is that the polymer chains are firmly and irreversibly fixed to the surface of the substrate. Another requirement is that the synthetic route allows for obtaining a system with rather high grafting density to cause the repulsion between polymer segments and, as a result, significant chain stretching. Thus, synthetic strategies can be classified into three approaches with respect to the driving force for brush formation: phase-separation, physiosorption and chemisorption.

The $Phase - separation$ approach consists of spreading of an amphiphilic block copolymer at an air-water interface. Hence, water-soluble blocks tend to dissolve in the aqueous phase whereas the anchored water-insoluble part attempts to prevent it. During the compression of this Langmuir layer, the distance between the anchor points decreases and the hydrophilic parts are stretched away from the surface into the water phase. It is worth noting, that the hydrophilic balance has to be taken into account to avoid the formation of micelles. The obtained films can be crosslinked photochemically and transferred to a solid substrate.

Tethering of polymer chains onto a solid surface can be a reversible or irreversible process. $Physisorption$ is a reversible process, when block copolymers or end-functionalized polymers are physisorbed to a solid surface (Figure 24) [48]. In the case of selective solvents [61], an ideal solvent leads to precipitation of one block (or end-group) which forms an "anchor" layer on the surface, whereas interactions between another part of the polymer and the solvent are much stronger. Hence, polymer brushes are formed in solution. The same concept is applicable for selective surfaces [62, 63]: one block is preferentially adsorbed on the surface and another one forms a polymer brush. Preparation of polymer brushes by this method is not difficult. However, due to the weak interactions (van der Waals forces or hydrogen bonding) between the substrate and the block copolymers, polymer brushes are highly unstable towards thermal and solvent treatments [64]. Some of these drawbacks could be overcome by covalently tethering polymer chains to substrates.

An alternative and more powerful approach is chemisorption of polymer molecules. This irreversible process leads to chains which are covalently bound to the surface [65, 66, 67, 68]. The method can be divided into "grafting from" and "grafting to" approaches.

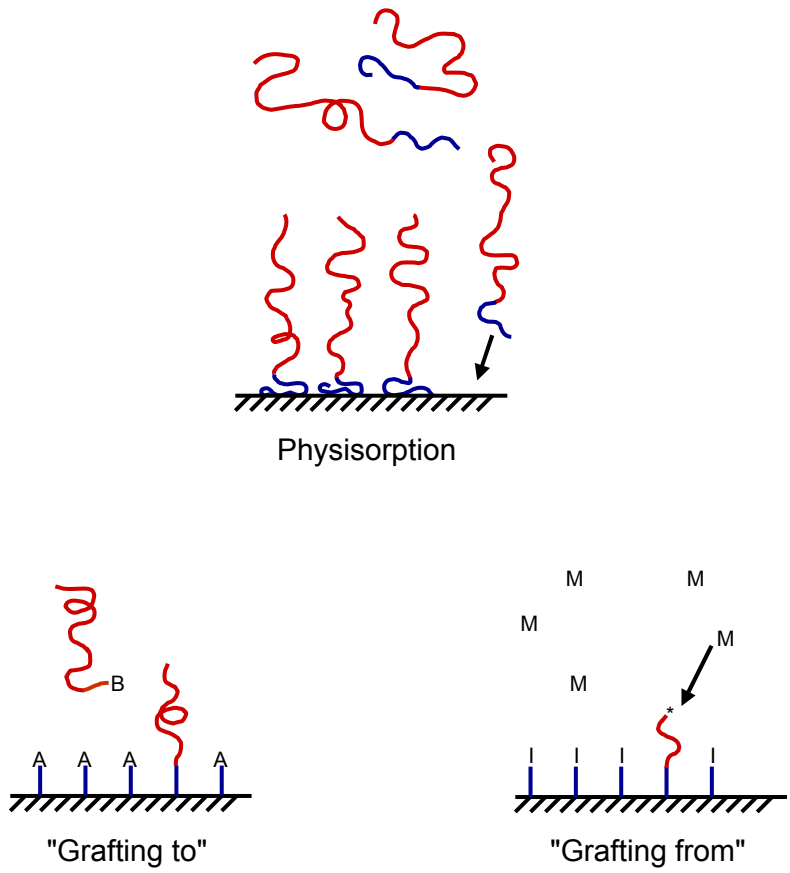

Figure 24: Preparation of polymer brushes by "physisorbtion", "grafting to" and "grafting from" approaches.

Via the "grafting to" route, one can prepare tethered polymer brushes by reacting end-functionalized polymers with a suitable surface under appropriate conditions. This is a simple and direct route, which hovewer has several limitations. The benefit is that end-functionalized polymer molecules can be synthesised by living anionic, cationic or radical polymerizations and, thus, possess narrow polydispersity and controllable molecular weight. On the other hand, only a small amount of polymer can be immobilized onto the surface by this method. During this process, macromolecular chains must diffuse through the existing polymer film to reach the reactive sites on the surface. Overcoming this barrier becomes more and more difficult at higher grafting densities. Therefore, the thickness of films is usually in the range of 3-5 nm and the grafting density is also rather low. To avoid these drawbacks, the "grafting from" approach was developed.

The "grafting from" method is a powerful tool to prepare tethered polymers on a solid substrate surface. Obtained brushes usually possess high grafting

density and a thickness up to 2000 nm in the dry state. At the first stage, the initiator must be immobilized onto the surface and after that via surface initiated polymerization tethered polymers are generated. Chain-growth living polymerizations, such as controlled radical polymerization (NMP, ATRP, etc.), anionic polymerization or ROMP were used. They allow for the preparation of surface-attached polymer chains with desirable molecular weight and narrow polydispersity. Thus, the "grafting-from" method is obviously a very powerful way to prepare polymer brushes with different functionalities.

1.2.3 Chain-Growth vs. Step-Growth Polymerization Routes to Conjugated Polymer Brushes

In spite of its obvious promise, little research has been performed in the field of CP brushes [69, 70] because of great difficulties in their preparation [71, 72].

The "grafting-to" approach, based on the coupling of end-functional polymers with a complimentarily terminated surface, usually provides rather low grafting densities [73]. This method has been widely employed in the modification of particles by nonconjugated polymers and has also been exemplified in the grafting of conjugated polymers, for example, by the attachment of thiol end-functionalized polyacetylene to gold nanoparticles [74] or amino-functionalized P3HT to quantum dots [75]. Typically, the synthesis of conjugated polymers involves polycondensation reactions employing a step-growth polymerization mechanism [76, 77]. In this case, polymer chains propagate randomly by the coupling of monomers and/or earlier formed oligomeric fragments via the abstraction of small molecules. Thus, even if an appropriate anchoring group (able to couple with the monomer) was immobilized on the surface, the process in the best case leads to a mixture of grafted chains and a large amount of unattached polymer. In practice, this approach fails to produce CP brushes with reasonable grafting densities, since polymerization products form faster in solutions, precipitate onto the surface, and hinder growth from the surface. There are few examples in the literature describing the "reactive-grafting onto" or "grafting-through" approach whereby growing CP polymer chains are grafted onto properly functionalized reactive surfaces [78]. Following this strategy, Schanze et al. performed grafting of polyacetylene that resulted in polymer brushes that were limited to athickness of 12 nm [79].

Surface-initiated polymerization, or the "grafting-from" approach [80], a method of growing polymer chains selectively from functionalized particles via one-by-one addition of monomers to surface-immobilized initiators, is one of the most powerful synthetic approaches for the creation of polymer brushes of variable composition and a tunable grafting density. However, this approach is problematic for the grafting of conjugated polymers because of the

step-growth character of most of synthetic routes to CPs [81].

In general, for the realisation of surface-initiated polymerization, suitable initiators should be attached to the surface, and the polymerization reaction has to involve the chain-growth mechanism. Since the synthetic procedure developed by Yokozawa et al. [41] fulfils the crucial last requirement, we explore the possibility of employing Suzuki catalyst transfer polycondensation in the preparation of polyfluorene brushes.

2 Experimental Techniques

2.1 Ultraviolet-Visible Spectroscopy: Basic Principle, Beer-Lambert Law, Spectrometr Construction

Ultraviolet-visible spectroscopy involves the spectroscopy of photons in UV-visible region, where the molecules undergo electronic transitions. Visible wavelengths cover a range from approximately 400 to 800 nm. The longest visible wavelength is red and the shortest is violet, corresponding to 36-72 kcal/mole respectively. This is enough to excite a molecular electron to a higher energy orbital.

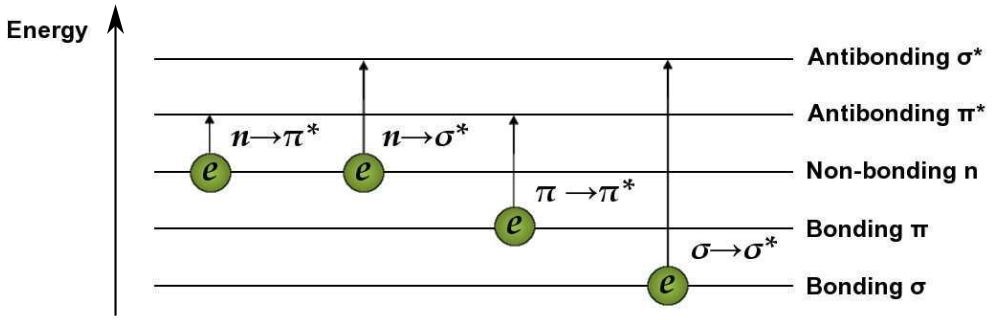

Figure 25: Schematic diagram of possible molecular electronic levels.

At room temperature, the majority of molecules are in the "ground state", the lowest vibrational state of the lowest electronic energy level. Absorption of UV or visible light leads to the excitement of an electron from E_1 to E_2 level. The UV-vis absorption bands are characteristically broad because the promotion of electron can occur from the E_1 to any of the vibrational or rotational levels of E_2. Thus, according to the aforementioned and also selection rule, the most probable transitions are $n \to \pi^*$ and $\pi \to \pi^*$.

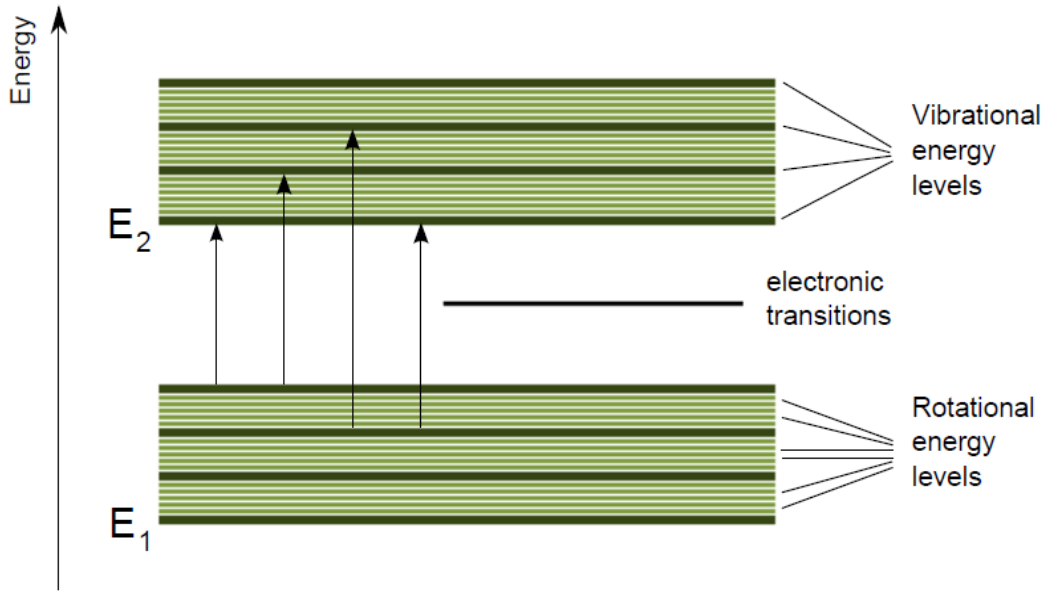

Figure 26: Schematic diagram showing possible molecular electronic transitions, and vibrational and rotational levels.

Conjugated polymers usually demonstrate bathochromic shifts in the absorption maxima. That is because the increased conjugation brings the HOMO and LUMO orbitals closer together. The energy required to effect the electron promotion is therefore less, and the wavelength is increased correspondently. The same situation is observed for planar conjugated polymer systems. Improved planarity leads to the bathochromic shifts in the absorption maxima.

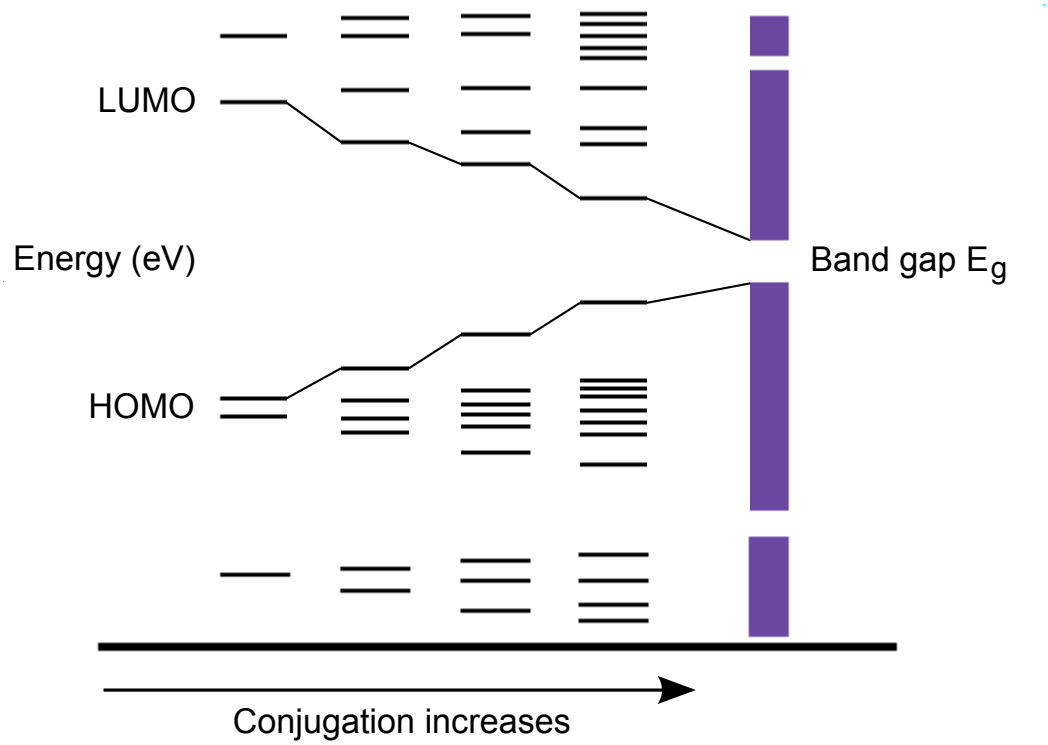

Figure 27: Decreasing of HOMO-LUMO band gap while conjugation increases.

In the double-beam UV-vis spectrophotometer (Figure 28) the light is split into two parallel beams, each passes through the cell. One cell contains the sample (solution, or film on a solid substrate) while the other one include reference (pure solvent, or in case of solid analyte, transparent substrate).

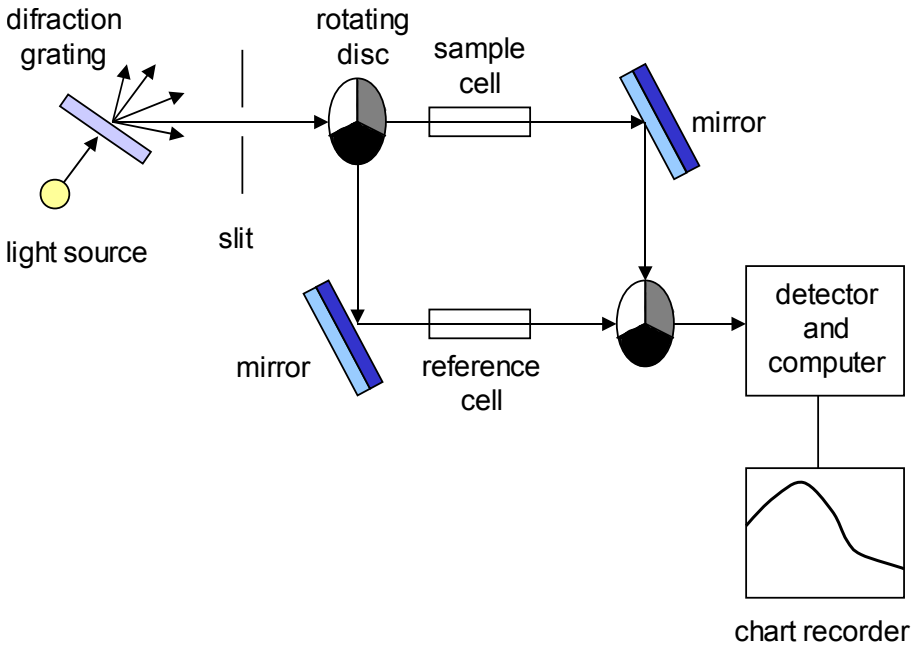

Figure 28: Schematic representation of a double beam spectrometr.

The detector measures the intensity of the light transmitted through the reference, I_0, and through the sample. The absorbance is calculated from the relationship:

$$A = lg\frac{I}{I_0} \tag{4}$$

According to the Beer-Lambert law, the absorbance A of the solution is proportional to the path length (l, length of cell, in cm) and the concentration of adsorbing molecule (c, moles per litre), according to the equation

$$A = \epsilon cl \tag{5}$$

where ϵ the molar extinction coefficient. The absorbance of a solution will vary as the concentration or the size of container varies. Molar absorptivity is independent from it being divided by the concentration and the length of the solution that the light passes through.

Thus, this is an efficient technique for determination of concentration as well as various parameters of conjugated systems, such as planarity, degree of polymerization.

In this work UV-vis measurements were carried out using a Perkin Elmer UV/vis Spectrometr Lambda 800.

2.2 Fluorescence Spectroscopy

Fluorescence spectroscopy is a technique complimentary to the UV-vis absorption spectroscopy, which analyzes fluorescence from a sample [82]. Using the beam of light, usually ultraviolet light, the electrons in molecules are excited and directly after that emit photons with a lower energy. Depending on the nature of excited state, fluorescence or phosphorescence takes place. If in excited state the electron is paired to the second electron in the ground state (so-called singlet state), return to the ground state is spin allowed and occurs rapidly by emission of photon. The emission rates of fluorescence are typically 10^8 s^{-1}, so that typical fluorescence lifetime is about 10 ns. The alternative process is phosphorescence. This is the emission of light from triplet excited states, in which the electron in the excited orbital has the same spin orientation as the ground-state electron. The processes that occur between the absorption and emission are usually illustrated by the Jablonski diagram (Figure 29) [83].

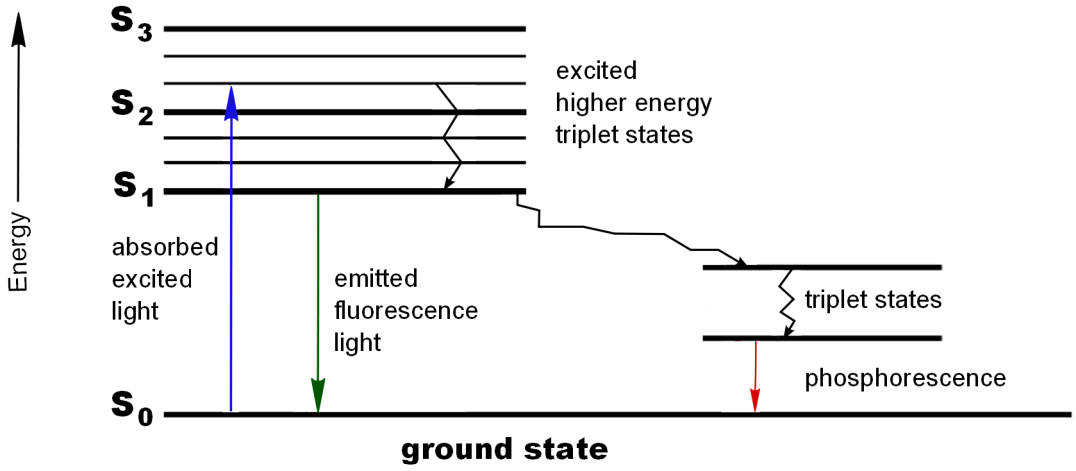

Figure 29: One form of a Jablonski diagram.

The transitions between states are depicted as vertical lines to illustrate the instantaneous nature of light absorption. Transition occurs in about 10^{-15} s, a time too short for significant displacement of nuclei. This is a Frank-Condon principle. After absorption of light fluorofor is usually excited to some higher vibrational levels and then rapidly relaxed to the lower one. This process is called internal conversion and generally occurs within 10^{-12} s or less. Since fluorescence lifetime is typically about 10^{-8} s, internal conversion is complete before emission starts.

When instead of conversion from excited to ground state electron undergo a spin conversion to the triplet state, then intersystem crossing happen. Transition to the singlet ground state is forbidden, and as a result the rate

constants for triplet emission are several orders of magnitude smaller than those for fluorescence.

The phenomenon of fluorescence displays a number of general characteristics. The energy of emission is typically less than that of absorption. After excitation system can relax not only emitting a photon, but also loose some energy via non-radiative decay (heating, quenching and so on). The energy difference between absorbed and emitted photons is the Stokes shift [84].

The fluorescence lifetime and quantum yield are also perhaps the most important characteristics of a fluorophore. The quantum yield is a ratio of numbers of emitted photons to the absorbed photons and can be schematically presented by a simplified Jablonski diagram (Figure 29). The fraction of fluorofores that decay through emission, and hence quantum yield Q, is given by (6), where the emissive rate of the fluorofore is depicted by Γ and κ_{nr} refers to the non-radiative decay (quenching). Quenching can be induced by electron transfer from one molecule to the other, intersystem crossing to the triplet state and variety of other trivial mechanisms. Thus, it is clear, that the largest quantum yield leads to the brightest emission, but it's meaning is always less than unity because of Stokes losses.

$$Q = \frac{\Gamma}{\Gamma + \kappa_{nr}} \tag{6}$$

The fluorescence lifetime is defined by the average time the molecule stays in the excited state before emitting a photon. Generally it proceeds around 10 ns. In case of fluorofore illustrated in Figure 29 the lifetime is

$$\tau = \frac{1}{\Gamma + \kappa_{nr}} \tag{7}$$

Figure 30 shows a schematic diagram of a spectrophotometer. Light source generates luminescence, which passes through a filter or monochromator, and strikes the sample. A portion of light is absorbed by the sample, and some of the molecules fluorescent. Part of this emitted light passes through a second monochromator and reaches a detector, which is usually placed at $90°$to the incident light beam to minimize the risk of transmitted or reflected incident light reaching the detector.

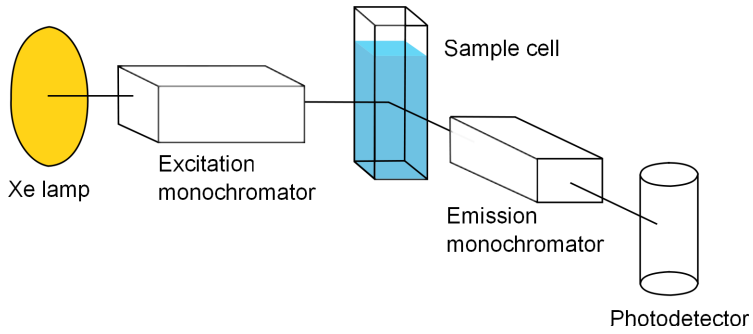

Figure 30: Schematic representation of spectrophotometer.

2.3 Ellipsometry

Ellipsometry is a non-destructive and contactless method for the characterization of thin layers at solid substrates. This method is used to get information about layers that are thinner than the wavelength of the probing light itself [85]. It measures changes of polarization of the light reflected (or transmitted) on films surface. Therefore the obtained value depends on thickness and complex refractive index. It is worth to mention that for a simple interpretation the sample must be composed of a small number of discrete, well-defined layers that are optically homogeneous and isotropic.

Electromagnetic radiation is emitted by a light source and goes through polarizer and compensator. After reflection on the sample the light passes second compensator, analyzer and falls into the detector.

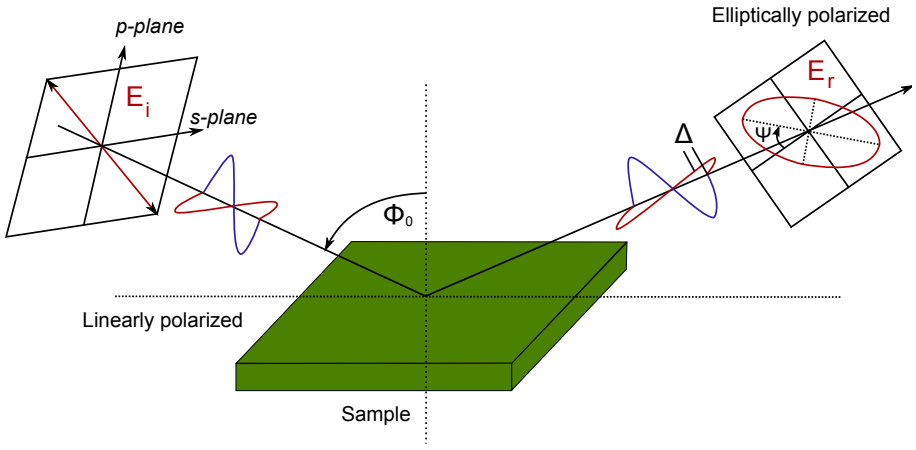

Figure 31: Schematic representation of ellypsometry.

Ellipsometry is a specular optical technique. That means, the angle of incidence equals the angle of reflection. The incident and the reflected beam

span the plane of incidence. Light, which is polarized parallel to this plane, is named "p-polarised". A perpendicular polarization direction (and parallel to the sample surface) is called "s-polarised". The amplitudes of s and p components after reflection and normalization are expressed by R_s and R_p, respectively. Ellipsometry measures the ratio of R_s and R_p.

$$\rho = \frac{R_p}{R_s} = tan(\psi)e^{i\Delta} \tag{8}$$

where $tan(\psi)$ is the amplitude ratio upon reflection and Δ is the phase shift [85]. Because ellipsometry measures the ratio of two values, it is very accurate and highly reproducible.

Ellipsometry is an indirect method. In general the measured ψ and Δ cannot be converted directly into the optical constants of the sample. A model analysis must be performed. Direct inversion of ψ and Δ is only possible in very simple cases of isotropic, homogeneous and infinitely thick films. In all other cases a layer model must be established, which considers the optical constants and thickness of all individual layers of the sample. Using an iterative procedure unknown optical constants and/or thickness parameters are varied, and ψ and Δ values are calculated. The calculated ψ and Δ values, which match the experimental data best, provide the optical constants and thickness parameters of the sample.

Optical constants. The interaction of light with the substrate can be described through the optical constants. The complex refractive index can be represented by:

$$\widetilde{n} = n + ik \tag{9}$$

where n is the real part of refraction and describes the phase velocity of light in material. The following equation describes the relationships between n, c (speed of light in vacuum) and υ (speed of light in the material).

$$n = \frac{c}{\upsilon} \tag{10}$$

The imaginary part κ (or extinction coefficient) describes how fast the amplitude of the wave decreases. The extinction coefficient is related to the absorption coefficient α by:

$$\alpha = \frac{4\pi\kappa}{\lambda} \tag{11}$$

where λ is the wavelength of light [86].

The thickness of polymer layers was measured at λ = 633 nm and 90° of incidence light with SENTECH SE-402 microfocus null-ellipsometr (lateral resolution is defined by the beam spot of about 20 μm in diameter). A multilayer model for films covering or grafted on the silicon substrate has been used for the calculation the thickness of the polymer layers. The refractive indices used in the calculations were n=1.459 for native silicon oxide layer SiO_2, n=1.525 for PGMA, n=1.63 for PS(Br), n=1.683 for PVK(Br), n=1.42 for silane and n=1.7 for PF2/6 [87].

2.4 Atomic Force Microscopy

Atomic Force Microscopy (AFM) belongs to a broad family of methods named Scanning Probe Microscopy (SPM) for imaging and characterization of surfaces on a microscopic scale. The development of the AFM was preceded by the development of the Scanning Tunneling Microscope (STM) in 1982 at IBM Zurich Research Laboratory by G. Binnig and H. Rohrer [88]. Later Binnig and co-workers [89] invented AFM, enabling one to image surfaces on the nanometer scale [90, 91]. During the scanning process cantilever with a sharp tip interacts with the specimen to form three-dimensional surface topography image of nanometer lateral and subangstrom vertical resolution. A principal schematic of AFM is shown in Figure 32.

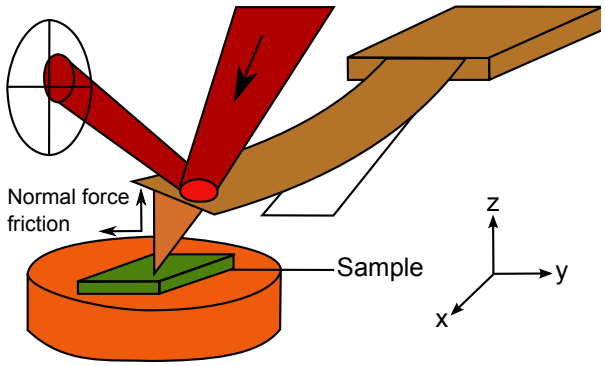

Figure 32: Schematic representation of AFM working principle.

The forces between them (van der Waals, electrostatic, magnetic) are not measured directly, but calculated by measuring the deflection of cantilever. Hook's law gives $F = -kz$, where F is the force, k is the spring constant (stiffness of the lever) and z is the displacement from the equilibrium conditions. Knowing k and z, it is easily to calculate the force. The relation between force and distance is shown in Figure 33.

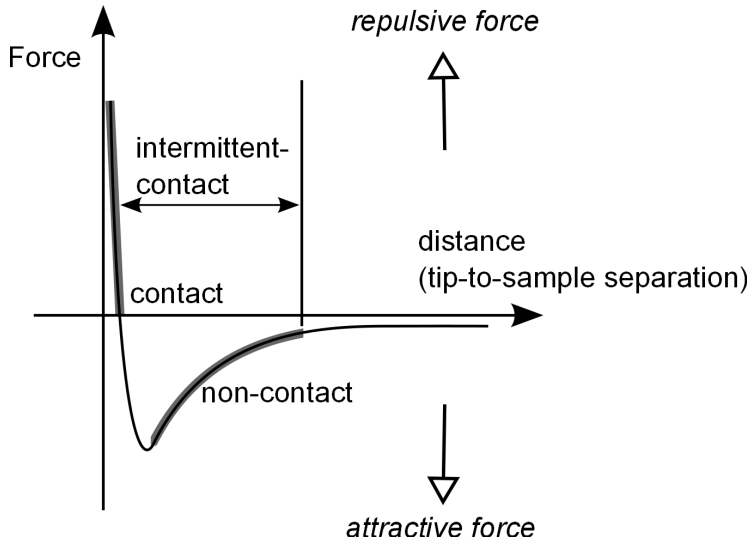

Figure 33: Plot of van der Waals force vs. distance.

In the contact region, the distance between canteliver and sample is less than a few angstroms, and the force is repulsive. In the non-contact region the force between the canteliver and the sample is attractive and the distance is in order of tens to hundreds angstroms. The choice of operating scanning mode depends on the region of this curve. Non-contact mode is used to be used in the attractive region, whereas contact mode in the repulsive. Tapping mode fluctuates between two of them.

The smoothness of the polymer layer can be measured using root mean square (RMS) roughness parameter. RMS value can be calculated from the following equation:

$$RMS = \sqrt{\frac{\sum_{i=1}^{N}(Z_i - Z_{ave})^2}{N}} \tag{12}$$

where $Z_{ave} = \frac{\sum_{i=1}^{N} Z_i}{N}$, Z_i is height at certain point of measured area, Z_{ave} is average Z value within the area, N is number of measured points within area. The rougher surface gives the larger value of RMS parameter.

In this work the Multimode AFM (Digital Instruments, Santa Barbara) was operated with amplitude feedback and in a "light" tapping mode configuration. The amplitude setpoint was set to the maximum possible value. Silicon tips with a spring constant of 0.3 N m^{-1} and a resonance frequency of 250-300 KHz were used.

2.5 Other Experimental Techniques

^{1}H and ^{31}P spectroscopies. ^{1}H and ^{31}P NMR spectra were recorded on a Bruker DRX-500 spectrometr operating at 500.13 MHz for ^{1}H using $CDCl_3$ and THF-d_8 as a solvents. The spectra were referenced on the solvent peak $\delta(^{1}H)$=7.26 ppm.

Gel Permission Chromatography (GPC). GPC measurments were carried out on a Knauer, Hewlett-Packard normal-temperature size exclusion chromatograph, equipped with refractive index detector and two column PL MIXED-C (Polymer Laboratories Ltd, UK), eluent - chloroform. Calibration was baced on polystyrene standarts obtained from Polymer Standarts Service.

X-Ray Photoelectron Spectroscopy (XPS). XPS studies were performed using of an AXIS ULTRA photoelectron spectrometer (Kratos Analytical, Manchester, England). The spectrometr was equipped with a monochromatic Al Kα (hν = 1486.6 eV) X-ray source of 300 W at 15 kV. The kinetic energy of the photoelectrons was determined with a determined with a hemispherical analyzer set to a pass energy of 160 eV for wide-scan spectra and 20 eV for high resolution spectra. During all measurements electrostatic charging of the sample was compensated by low-energy electron source.

3 Grafting of PF2/6 by Chain-Growth Suzuki Polycondensation

3.1 Introduction

Currently, palladium-catalyzed Suzuki coupling polycondensation of aryl halides with organoboron reagents is a remarkably efficient route to conjugated polymers [92]. In its classical performance, Suzuki polycondensation is catalyzed by $Pd(PPh_3)_4$ or similar complexes and involves a step-growth mechanism. As in the parent Suzuki cross-coupling, the mechanism of Suzuki polycondensation involves three basic consecutive steps: transmetallation, reductive elimination and oxidative addition (Figure 16).

Recently, Yokozawa et. al reported on the chain-growth Suzuki polycondensation of AB-type aromatic monomers [41] mediated by an unusual three-coordinate tBu$_3$PPd(Ph)Br, **1**, complex [93], prepared in an independent step by oxidative addition of a Pd(0)-catalyst to PhBr (Figure 34).

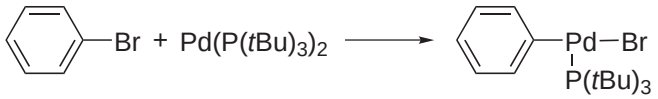

1

Figure 34: Oxidative addition of Pd(0) to PhBr.

The expected polymerization mechanism is shown in Figure 35. Within the initiation step, the initiator **1** is added to the first molecule of the monomer **2** via transmetallation. As usually for Suzuki coupling, the next step is reductive elimination which is responsible for liberation of the Pd(0) complex and the formation of a C-C bond between the phenyl group of the initiator and the monomer residue. It is essential that the Pd(0) complex supported by a single bulky and electron-rich phosphorus ligand which does not diffuse from the polymerizing chain but undergoes oxidative addition to the nearest C-Br bond located in the newly added monomer unit. Thus, intramolecular oxidative addition has been found to be a more favourable pathway than the intermolecular one. The addition of new monomer molecules to the polymerizing chain end occurs in a one-by-one manner, typical chain-growth polymerizations. Due to the peculiarity of this mechanism, most of the polyfluorene chains formed upon the polycondensation have phenyl starting groups which were transferred from the initiator and present.

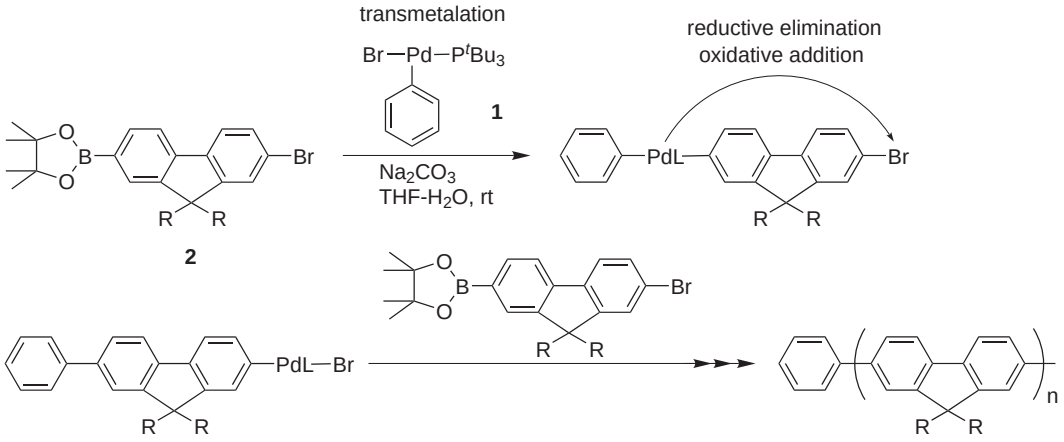

Figure 35: Mechanism of the chain-growth polycondensation according to Yokozawa et al.

It is believed that the observed chain-growth mechanism is due to a highly reactive coordination-unsaturated tBu$_3$PPd(0) catalytic intermediate [40, 94]. Because this polymerization involves the chain-growth mechanism and can be initiated by an externally-added initiator, it would be, in principle, suitable for preparation of conjugated polymer brushes on different substrates (Figure 36 and 37).

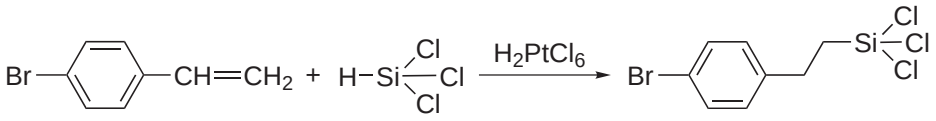

Figure 36: Preparation of reactive silane.

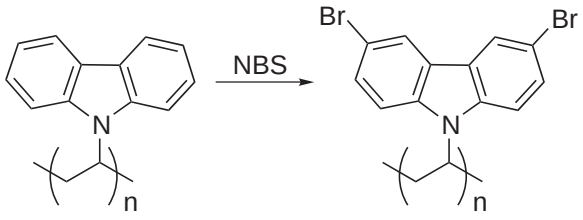

Figure 37: Preparation of poly-4-bromo-(N-vinylcarbazole).

3.2 The Development of Chain-Growth Suzuki Polycondensation

As follows from the literature, preparation of polymer brushes via the grafting-from approach possess very severe requirements on the quality of the chain-growth polymerization process. Indeed, the formation of thick enough and densely-grafted brush layers is only possible if irreversible chain-termination processes are avoided completely or at least minimized. One can approximately estimate the required molecular weight of the polymer formed via a termination-free chain-growth process to obtain a certain thickness of the brush assuming completely stretched chains. For example, to prepare a 16 nm-thick brush using monomer **2** (contour length of the monomer unit is about 0.8 nm) one needs to achieve a polymerization degree (DP) that exceeds a value of 20. Previous studies have shown that grafting densities achievable even for very high quality living polymerizations are always several times less (at least three times) than the maximum theoretical value. So, taking into account this factor, the chain-growth Suzuki polycondensation used in this study must provide polyfluorene with M_w higher than 30 000 g/mol. To examine applicability of the chain-growth Suzuki-Miyaura polycondensation for brush preparation, several experiments were performed in solution. In these experiments, an influence of initiator-to-monomer **2** (7-bromo-9,9-bis(2-ethylhexyl)-9H-fluoren-2-ylboric acid ester) ratio as well as the catalysis nature on the polymerization cource have been studied.

Entry	Cat[1](init[2]):monomer	Time	Conversion (mol %)	M_w(g/mol)	M_w/M_n
1	1% init	10 min	5%	-	-
2	1% init	2 hours	5%	-	-
3	1% init	12 hours	50%	75 000	3.75
4	5% init	30 min	70%	47 500	4.78
5	5% init	12 hours	100%	61 100	3.01
6	22% init	30 min	100%	1100	2.88
7	22% init	12 hours	100%	1700	2.50
8	5% cat	30 min	15%	5200	5.57
9	5% cat	8 hours	65%	7800	4.29
10	5% cat	12 hours	100%	16 500	3.61

Table 1: Pd(0)- and Pd(II)-catalyzed Suzuki-Miyaura polycondensation.

The initiator:monomer ratio has been varied to verify the character of the polymerization (chain-growth versus step-growth). If the polymerization follows the chain-growth mechanism, polymers with higher molecular weights should be attainable for lower initiator:monomer ratios. Furthermore, in chain-growth polymerizations, high molecular weight polymers should coexist with unreacted monomer at incomplete conversions.

The resulting polymerization mixtures were analyzed by NMR and GPC. Molecular weight and polydispersity were determined using polysterene standarts. It was found that ∼70% of monomer **2** was converted into poly(9,9-bis(2-ethylhexyl)-9H-fluorene) (PF2/6) having M_n = 9 900 g/mol and M_w = 47 500 g/mol already after 30 minutes of polymerization when 5 mol % of the initiator was used (Entry 4 of Table 1).

NMR and GPC were used to analyze the polymerization mixtures. As a representative example, Figure 38 shows the ^{1}H NMR spectrum of PF2/6 initiated by 5 mol % of tBu$_3$PPd(Ph)Br (Entry 5). The broad peaks at ∼7.65 and 7.83 ppm correspond to the protons in the benzene rings of the PF2/6 moiety. The small peaks at 7.45-7.55 ppm can be assigned to the phenyl group at the initiator end. A comparison of the integral intensity of this peak with the integral intensity of the main polymeric peak at 7.65-7.83 ppm allows for estimation of the average degree of polymerization. From this spectrum, it is clearly seen that the estimated degree of polymerization (DP) is much less than DP expected for the [monomer]/[initiator] ratio used in the experiment assuming defect-free chain-growth mechanism. This reflects a large contribution of termination and reinitiation reactions. Therefore, this

[1]cat - Pd^0(PtBu$_3$)$_2$
[2]init - tBu$_3$PPd(Ph)Br

polymerization cannot be denoted as a "living" or controlled polymerization but it certainly involves the chain-growth mechanism with a high PDI of 3.01.

PF2/6 with a much lower molecular weight was obtained when 22 mol % of the initiator was used. This result is consistent with the chain-growth mechanism, proposed for this reaction by Yokozawa, although it demonstrates that the polymerization is not controlled, since for controlled polymerizations the DP of the resulting polymer should be strictly equal to the ratio between the converted monomer and the initiator, and low polydispersities (e.g., below 1.5) should be attainable. Low monomer conversions and poorly reproducible polymerization results at low initiator content (i.e., at 1 mol %) may be explained by a catalyst deactivation process. We propose that oxygen may be unintentionally present in the reaction mixture in trace amounts and could result in oxidation of the ligand. This process is, obviously, less critical for higher concentrations of the initiator when only some part of the available initiator is deactivated. It was also interesting to compare polymerization results obtained with different forms of catalyst (e.g., tBu$_3$PPd(Ph)Br and Pd(PtBu$_3$)$_2$, entries 4 and 8 respectively). The main difference between the catalyst structure is that Pd(PtBu$_3$)$_2$ is a precursor of tBu$_3$PPd(Ph)Br since the later is forming via oxidative addition of Pd(PtBu$_3$)$_2$ to the aryl halide (Ph-Br). As seen from the Table 1 (compare entries 4 and 8), polymerization proceeds much faster and provides higher monomer conversions with tBu$_3$PPd(Ph)Br catalyst than with Pd(PtBu$_3$)$_2$. It becomes clear upon careful consideration of the polymerization mechanism that both these polymerizations during the chain-propagation involve identical Pd(0) catalyst species (i.e., PdPtBu$_3$), however the chain-initiation step is different for these catalysts. Thus, tBu$_3$PPd(Ph)Br at the initiation step undergoes transmetalation with the monomer, which (monomer) reacts with the initiator by the boronic acid end. Obviously, this initiation process is analogous to the transmetalation process that takes place at every chain-propagation step, so in this case the chain-initiation should proceed with approximately the same rate as the chain propagation. In other words, there are no problems with the initiation step for tBu$_3$PPd(Ph)Br initiated polycondensations.

The situation is different when Pd(PtBu$_3$)$_2$ initiator is used. Pd(PtBu$_3$)$_2$ requires oxidative addition as the first step that is responsible for the coupling of the catalyst and the first monomer molecule. There are two problems here that complicate the initiation process. First, because of a high bulkiness of the PtBu$_3$ ligand, Pd(PtBu$_3$)$_2$ should eliminate one ligand to produce more reactive Pd(PtBu$_3$) prior to oxidative addition. Since the equilibrium - Pd(PtBu$_3$)$_2$ = Pd(PtBu$_3$) + PtBu$_3$ - is largely shifted to the left side, Pd(PtBu$_3$) is present in very low quantities that slows down the oxidative addition step. It is worth mentioning here that preparation of the initiator tBu$_3$PPd(Ph)Br by oxidative addition of Pd(PtBu$_3$)$_2$ to PhBr requires quite hard conditions (70°C and prolonged stirring for 2.5 hours in neat PhBr). It is clear that

this reaction would proceed even slower at polymerization conditions (room temperature and lower concentration of the aryl halide). On the other hand, oxidative addition of Pd(PtBu$_3$)$_2$ to the C-Br bound of the monomer seems to be even more problematic process than the oxidative addition to PhBr because of electron-donating character of boronic acid group in the monomer. As a result, Pd(PtBu$_3$)$_2$ is not efficient initiator for Suzuki polycondensation. This result has very important practical implications since it shows in which form palladium catalyst must be introduced into polymerization mixture to efficiently initiate polymerization. It is noteworthy that this issue is much less important for "classical" catalysts, e.g., Pd supported by PPh$_3$, which can be introduced into polymerization in a very different forms (e.g., PdCl$_2$(PPh$_3$)$_2$ or Pd$_2$(dba)$_3$ + PPh$_3$, etc.) with an approximately equal polymerization results.

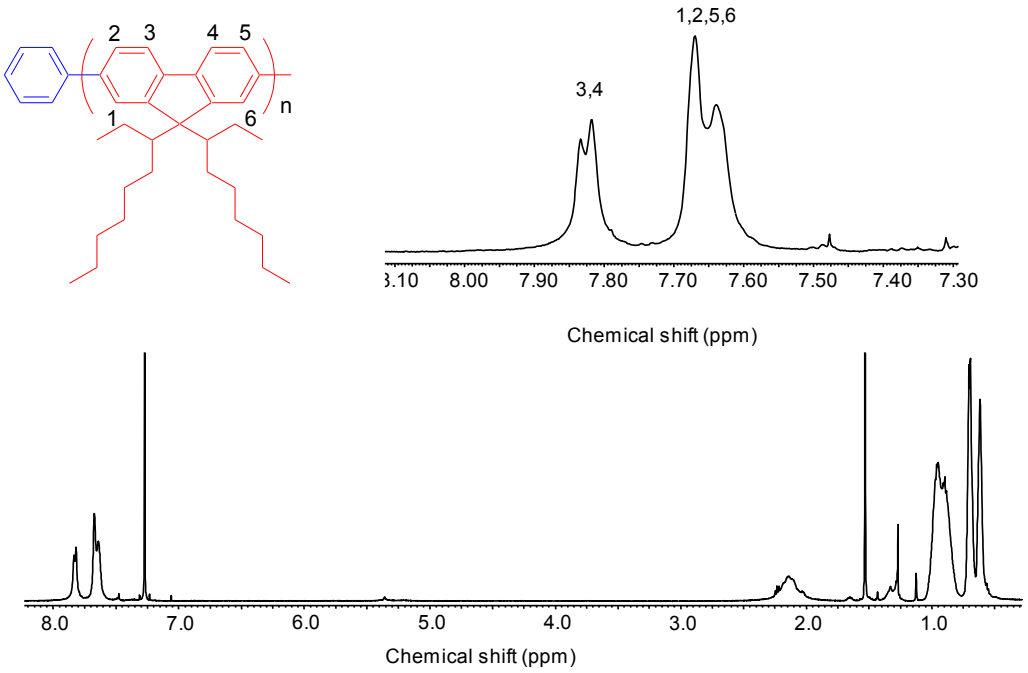

Figure 38: NMR spectrum of PF2/6 grown from adduct of bromobenzene and Pd(PtBu$_3$)$_2$ in chloroform-d.

What is important for the main task of this work is that the conducted experiments showed the general feasibility of rapid polymerization of **2** into PF2/6 with a relatively high MW. The latter might be limited by the solubility of the polymer in the water-saturated reaction mixture, as shown by Yokozawa et al. and follows from our experiments. This factor of limited solubility might be less critical for surface-initiated polymerization (SIP), when the growing surface-bound chains are more stretched and are therefore less prone to fold back upon the aggregation to hide the growing end-points. This would lead to

the formation of longer PF2/6 chains in the case of SIP than the polymerization in solution. However, if the grafting process will provide MW similar to those observed in the model bulk solution experiments, the thickness of the resulting brushes should be quite low. Another conclusion from these experiments is that polymerization is extremely sensitive to the presence of oxygen and it is especially critical for a low concentration of the Pd initiator. Since the absolute amount of the Pd initiator that could be immobilized on surface is even smaller than in the model bulk solution experiments, additional measures should be taken to avoid the penetration of oxygen into polymerization vessels during SIP.

With the idea in mind to investigate the influence of bases through the improvement of homogeneity of the system, several bases were tested and the results are summarised in Table 2. All reactions were performed at room temperature and were allowed to react overnight. To adjust the homogeneity of the biphasic water-THF solution, the appropriate amounts of methanol were utilized.

Entry	Base	Conversion (mol %)	M_w(g/mol)	M_w/M_n
1	KF [95]	-	-	-
2	K_3PO_4	-	-	-
3	NH_4OH	-	-	-
4	$(CH_3)_3N^{\oplus}CH_2PhOH^{\ominus}$	19.5%	4800	1.92
5	$(C_3H_7)_3N^{\oplus}CH_3OH^{\ominus}$	18.1%	6000	2.2
6	$(CH_3)_4N^{\oplus}OH^{\ominus}\cdot 5H_2O$	18.0%	3800	1.65
7	$(CH_3)_4N^{\oplus}F^{\ominus}\cdot 4H_2O$	19.7%	9800	2.36

Table 2: Effect of bases on Suzuki-Miyaura polycondensation (all reactions were performed in the presence of 5 mol. % of the initiator. Polystyrene (PS) was used as a standart for determination of M_w and M_w/M_n).

It is clearly seen, that reactions with KF, K_3PO_4 and NH_4OH bases were not efficient. Most of the tested alkyl ammonium bases showed better results, but nevertheless the yields of the resulting polymers were low. Therefore, in our further work only Na_2CO_3 was used as the base for surface-initiated polymerizations.

3.3 Grafting of PF2/6 From the Planar Surfaces

In general, for the realisation of surface-initiated polymerization, a suitable initiator should be attached to the surface. In this work, because of their structural similarity to bromobenzene which was used by Yokozawa et al., we utilized slightly cross-linked poly(4-bromostyrene) (PS(Br)) films as a

precursor for the preparation of the macroinitiator. For the same reason, we have also focused our attention on the [2-(4-bromo-phenyl)-ethyl]-chloro-dimethyl-silane and poly-4-bromo(N-vinylcarbazole) supporting layers.

In the next step, we tried to perform SIP of 7-bromo-9,9-bis(2-ethylhexyl)-9H-fluoren-2-ylboric acid ester from activated surfaces. First, freshly cleaned silica wafers were covered with a 2 nm thick poly(glycidyl methacrylate) (PGMA) layer, which was used as an adhesive layer. Then, the samples were annealed at 150°C for 2 hours to cross-link PGMA. Afterwards, PS(Br) was spincoated from a toluene solution and slightly cross-linked by brief UV-light irradiation. Typically, 10 nm thick photo cross-linked PS(Br) anchoring films were used. The substrates were placed vertically into a reactor and under an argon atmosphere a solution of Pd(PtBu$_3$)$_2$ was added. The tubes were heated at 70°C for 2.5 hours. The samples were then extensively washed with dry THF under an argon atmosphere to remove unreacted Pd(PtBu$_3$)$_2$. Afterwards, the monomer was added in a degassed mixture of THF and aqueous sodium carbonate solution (Figure 39). The grafting experiments were conducted at room temperature with stirring. The technical parameters were found to be very important for successful grafting.

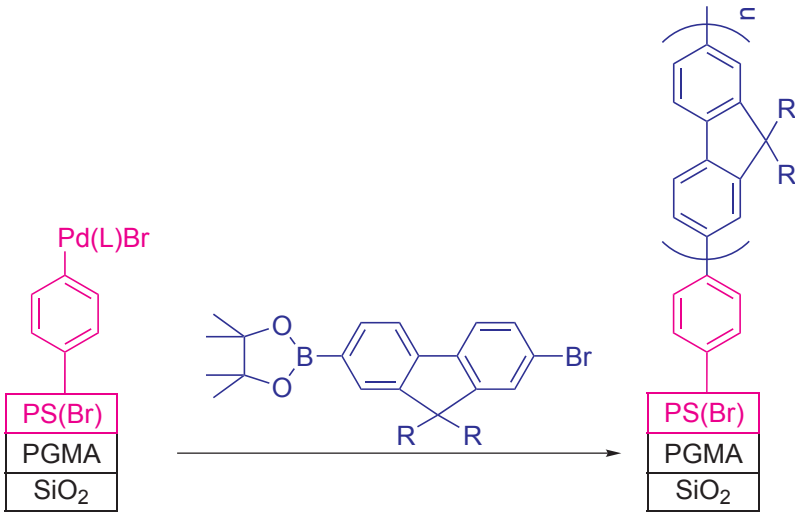

Figure 39: SIP of PF2/6 from PS(Br)-anchoring layer.

After very extensive stirring, almost no grafted PF2/6 was observed. This was possibly due to the covering of the surface with water droplets, which prevent the polymerization process. The greatest thicknesses of grafted PF2/6 were achievable with gentle stirring that provided sufficient diffusion of Na_2CO_3 dissolved in water. Only a marginal amount of water solution was used; however, it was found to play a crucial role in the polymerization process. No grafting of PF2/6 occured in those parts of the substrates which

appeared to be in a direct contact with the water (bottom) phase of the biphasic reaction mixture, possibly because of etching of the silicon and low solubility of the monomer in water. Under optimal conditions, the grafting procedure resulted in uniform PF2/6 films with a thickness up to 50 nm, and in some cases up to 100 nm (Figure 40). The thickness measurements were conducted by Null-ellipsometry and confirmed by the AFM cross-section test. Analysis of the AFM topography images of grafted PF2/6-films (Figure 41, a) revealed a root-mean-square roughness (RMS) of about 10 nm, whereas the starting PGMA/PS(Br) layers were significantly smoother (RMS = 1.3 nm) (Figure 41, b). The grafting resulted in strongly adherent PF2/6 films, which were stable against extensive rinsing with various organic solvents in an ultrasonic bath or Soxhlet apparatus. Since the consumption of the monomer upon grafting is negligible, the reaction mixture can be used for many polymerizations. Importantly, an increase of the anchoring PS(Br) layer had only a small positive effect on the grafting process (this issue is discussed in more detail below on page 50), suggesting that polycondensation proceeds predominantly from the topmost part of the PS(Br) film, in contrast to the previously reported Kumada SIP [1, 96, 97].

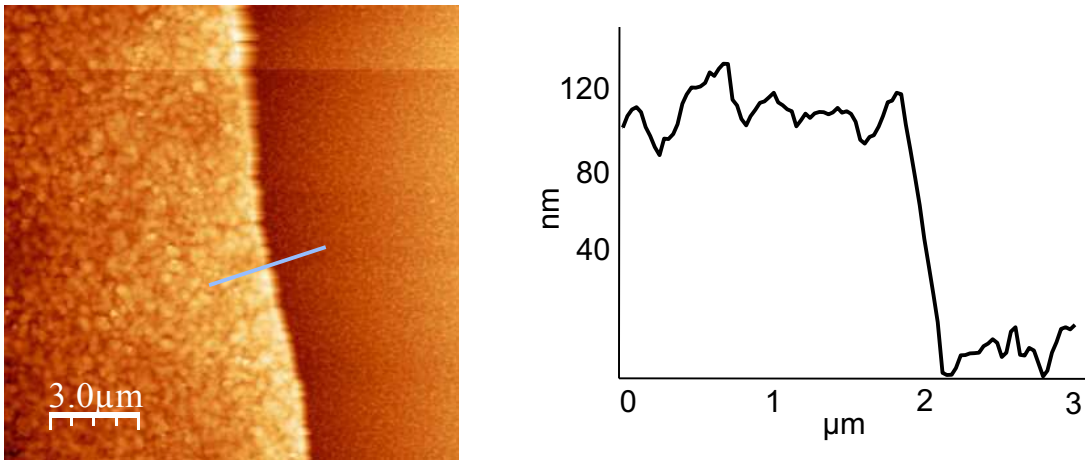

Figure 40: AFM cross-section of the scratched area of a 100 nm thick PS(Br)-graft-PF2/6 brush film.

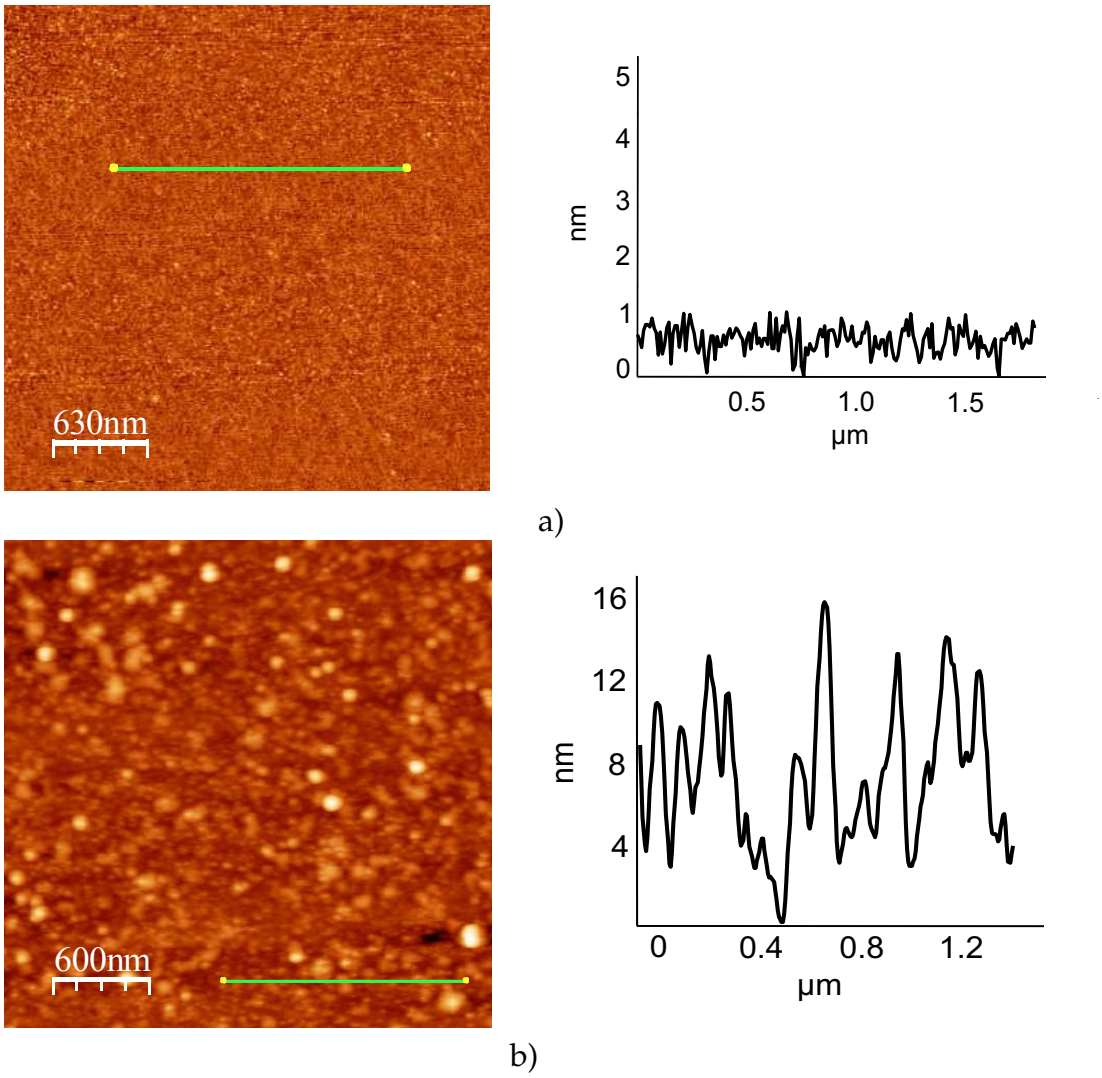

Figure 41: a) AFM topography image (left) and cross-section (right) of a cross-linked PS(Br)-anchoring layer on top of a coated PGMA layer on Si-wafer, b) AFM topography image (left) and cross-section (right) of grafted PF2/6 from a cross-linked 10 nm PS(Br) layer.

Figure 42, a) shows the UV-vis spectra of the PS(Br)-anchoring layer and grafted PF2/6 brush. The polyfluorene brush sample exhibits a relatively broad and featureless peak with λ_{max} about 370 nm. The photoluminescence (PL) spectrum of PF2/6 show well-resolved vibronic features with maxima at 415 and 435 nm (Figure 42, b), which is similar to the spectrum of unbound, high MW PF2/6 (Figure 42, c). The spectrum is represented predominantly by a fluorescent amorphous α-phase (415 nm), whereas the contribution from the more ordered, so-called "β-phase" (435 nm) is negligible here. The β-phase of PF-type polymers was first observed by Grell and Bradley et al. for polyfluorenes having a propensity for crystallization [98, 99]. The phase formation is induced by side chain interactions between adjacent polymer backbones. This causes interchain "zipping", which has the direct consequence of planarizing the PF backbone, yielding the characteristic β-phase optical properties. The amorphous character of the PF2/6 brush is not surprising, taking into account the branched nature of the alkyl substituents in PF2/6.

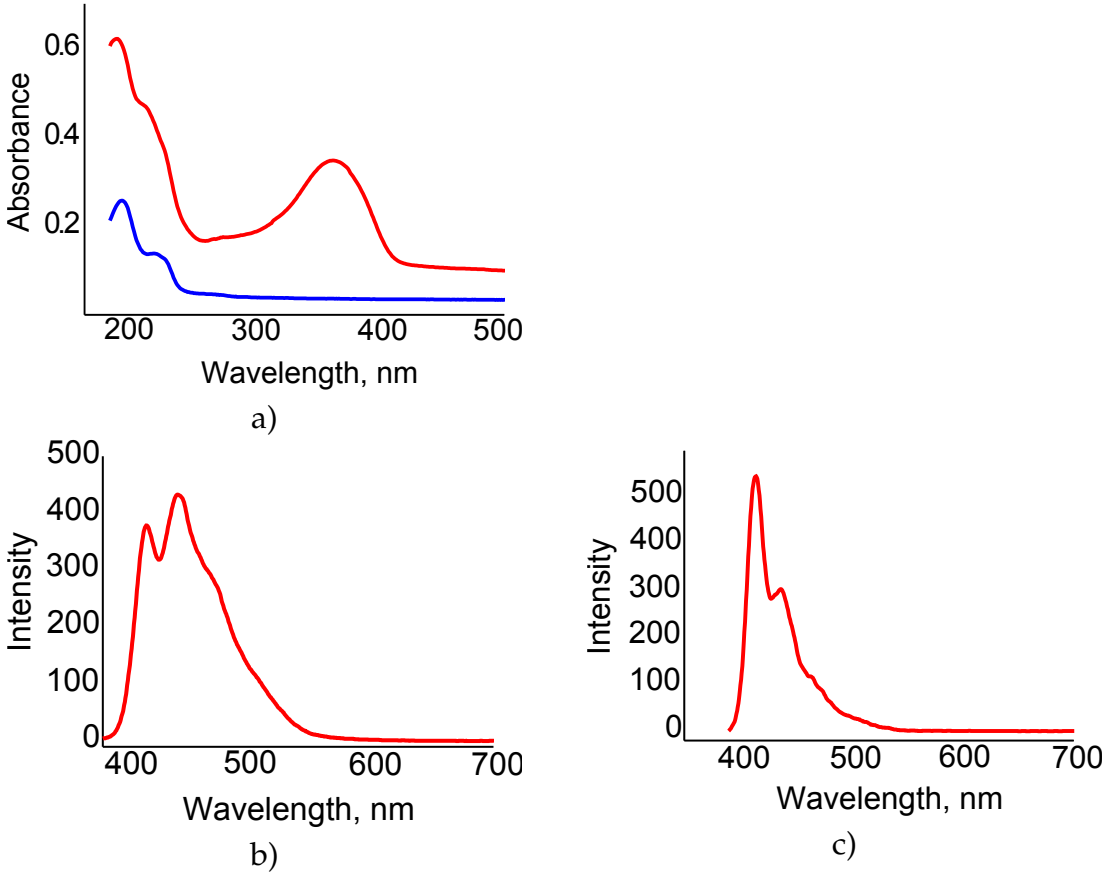

Figure 42: a) UV-vis spectra of the PS(Br)-anchoring layer (blue) and grafted PF2/6 (red), b) photoluminescence spectrum of unbound, high MW PF2/6, c) photoluminescence spectrum of PF2/6 grafted from the surface.

As evident from a fluorescent micrograph, the PF brushes display a strong emission in a dry state (Figure 43) that can be exploited in optoelectronical devices.

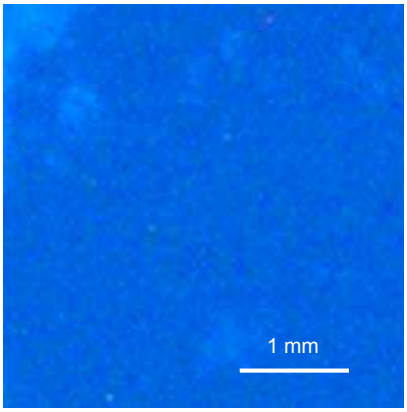

Figure 43: Fluorescent micrograph of PF 2/6 grafted from 2 nm thick PS(Br) layer deposited on a quartz slide illuminated by UV-light lamp at 360 nm.

Alternatively, the substrate was coated with a 10 nm thick smooth (RMS = 1.32 nm) photo crosslinked poly-(4-bromo-vinylcarbazole), PVK(Br) film. PVK(Br) was used because the parent PVK is a semiconductor, possesses good hole-injection properties and is frequently used in OLEDs. The morphology of anchoring PVK(Br) layers deposited from different solvents was studied with AFM. It was found that PVK(Br) deposited from a dioxane solution (Figure 44) gave smoother films than ones formed from tetrahydrofuran (Figure 45) or other solvents.

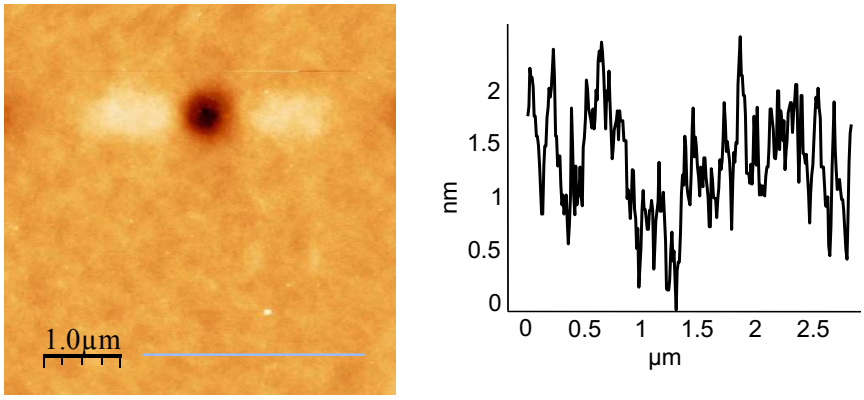

Figure 44: AFM topography image and cross-section of the 10 nm thick (as determined using ellipsometry) PVK(Br) film on a Si-wafer substrate covered with 2 nm thick PGMA. PVK(Br) was deposited from a dioxane solution.

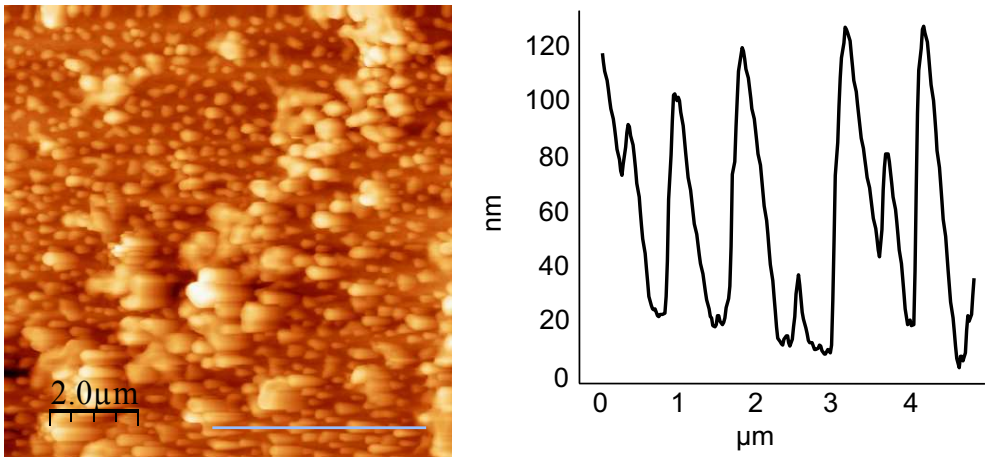

Figure 45: AFM topography image and cross-section of the 10 nm thick (as determined using ellipsometry) PVK(Br) film on a Si-wafer substrate covered with 2 nm thick PGMA. PVK(Br) was deposited from a THF solution.

Si-wafers or quartz glass with PVK(Br) layers of different thicknesses (from 10 to 80 nm) deposited from dioxane solutions were cross-linked by UV irradiation and then grafting of PF2/6 was attempted. To this end, the substrates with PVK(Br) layers were activated by Pd(P*t*Bu$_3$)$_2$ as described above for PS(Br) supported samples, and afterwards the monomer solution was added to attempt the grafting of PF2/6. UV-vis spectroscopy (Figure 46) revealed almost no absorption from PF2/6.

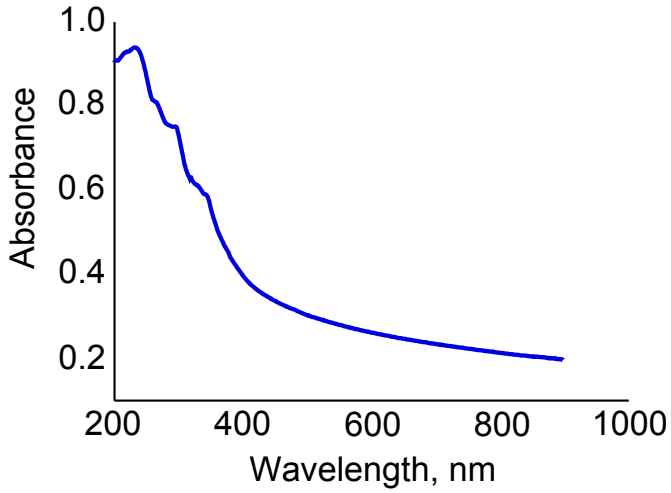

Figure 46: UV-vis spectrum of PF2/6 grafted from reactive PVK(Br).

Fluorescence spectrum (Figure 47, b) detected the emission peak assignable to PF2/6 with rather low intensity. Ellipsometry showed that the film thicknesses as well as surface morphology remained practically unchanged after these attempts (Figure 48). These facts imply that almost no grafting of PF2/6 occurs if PVK(Br) is used as the supporting layer.

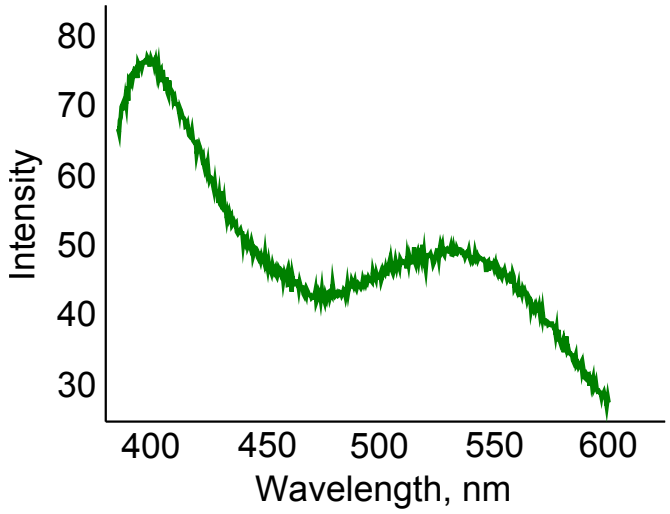

a)

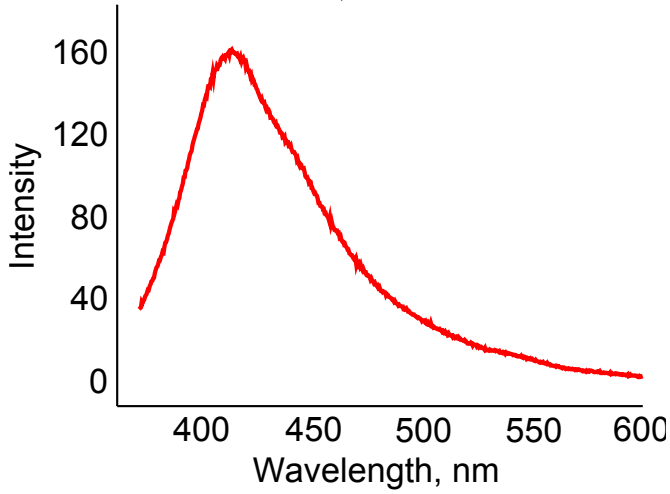

b)

Figure 47: Fluorescence spectra of a) the PVK(Br)-anchoring layer and b) PF2/6 grafted from PVK(Br).

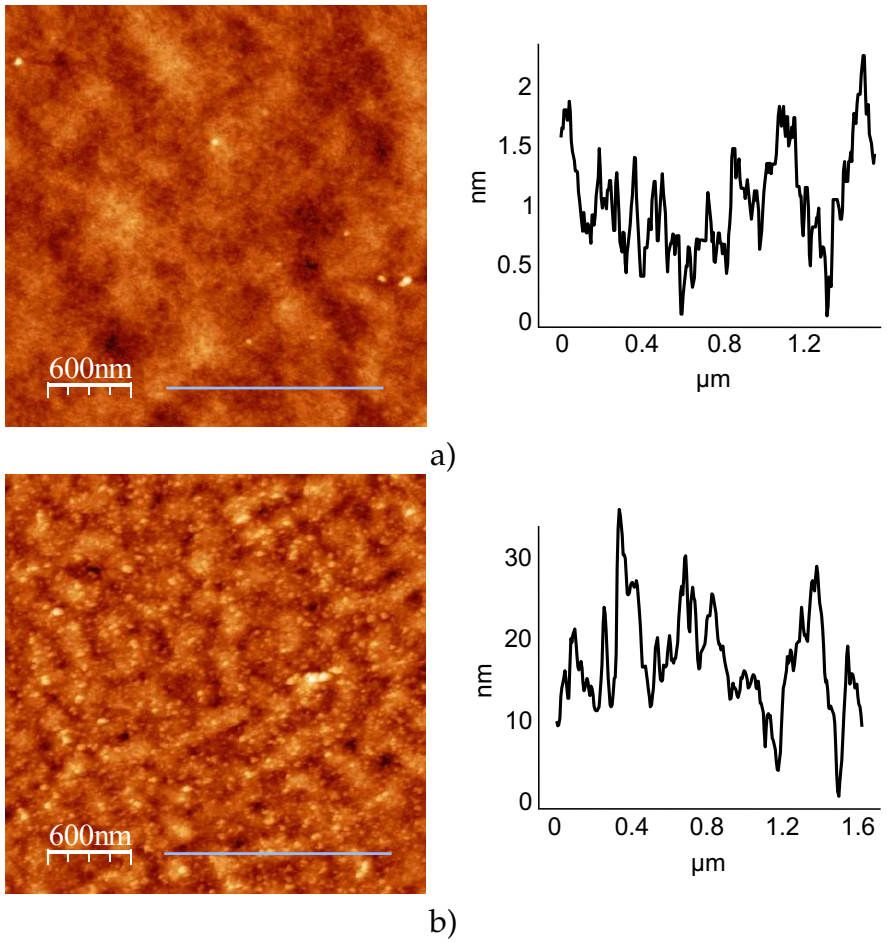

Figure 48: AFM topography image (left) and cross-section (right) of the a) PVK(Br)-anchoring layer; b) PF2/6 grafted from PVK(Br).

To investigate the influence of anchoring layer thickness on the grafting process, PF2/6 was grafted from a monolayer of reactive silane [2-(4-bromo-phenyl)-ethyl]-chloro-dimethyl-silane as well as from a 2 nm thick PS(Br) film.

[2-(4-bromo-phenyl)-ethyl]-chloro-dimethyl-silane was deposited from the gas phase onto silica wafers or quartz slides. Substrates after deposition were extensively rinsed with chloroform to wash out physiosorbed molecules. This resulted in 1 nm thick self-assembled monolayers (SAMs), as revealed by ellipsometry. The AFM topography image illustrates the smooth surface with an RMS of 0.26 nm (Figure 49, a). Deposition from the liquid phase, i.e., from a solution of silane in dry toluene, was attempted, but this approach resulted into films much thicker than monolayer films of about 5 nm, so therefore gas phase deposition was predominantly used. The same procedures of catalyst immobilization and polymerization were used in the grafting from PS(Br) anchoring layers as previously were used for the grafting from SAMs.

Thicknesses of grafted PF2/6 films up to 10 nm were achieved. Analysis of the AFM images showed that the obtained brushes had a granular morphology with a grain size of about 20-70 nm in height (Figure 49, b). The origin of the observed surface granularity is not fully understood, but it could be due to inhomogeneous immobilisation of the initiator or segregation (clustering) of PF2/6 chains during their growth. Indeed, PF2/6 is a highly hydrophobic polymer where hydrophobicity increased with increased polymerization degree. Thus, water-saturated THF might become a nonsolvent for high MW PF2/6 causing phase separation at the surface.

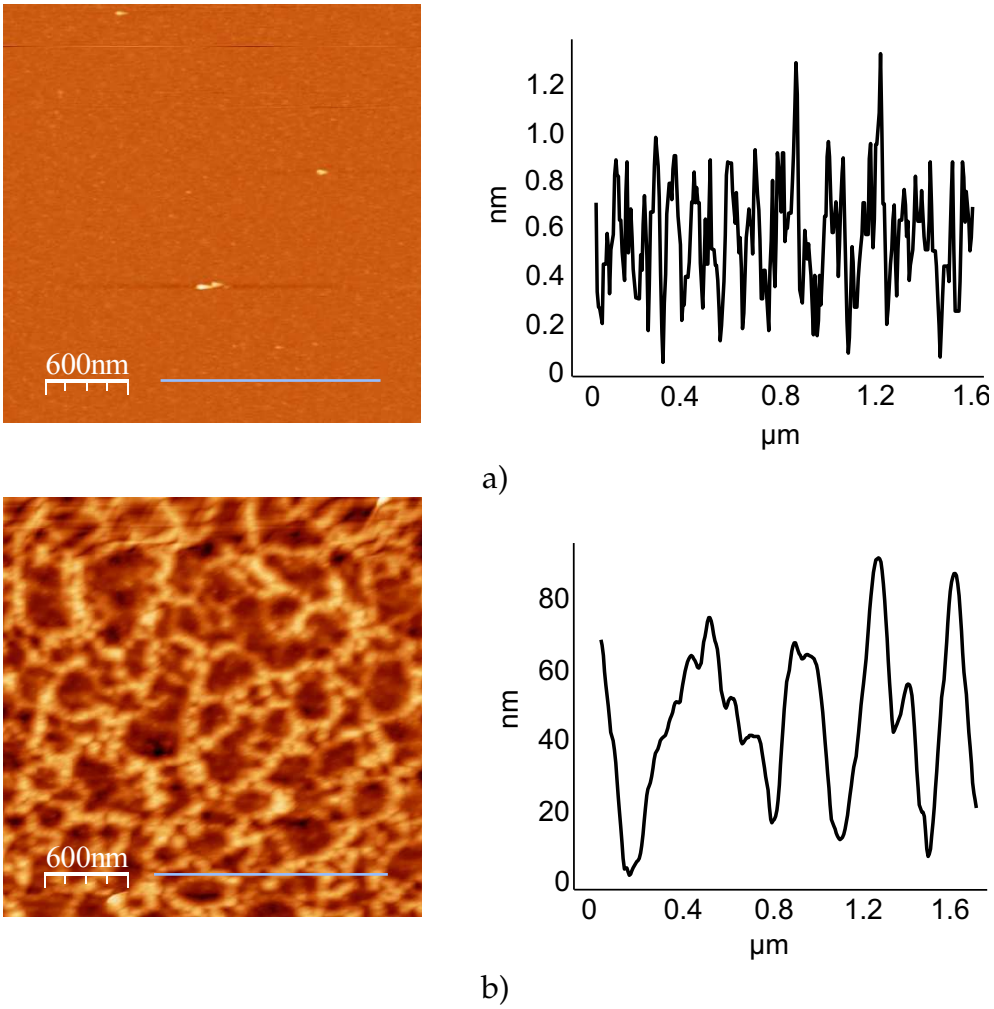

Figure 49: AFM topography image (left) and cross-section (right) of the a) 1 nm silane anchoring layer; b) PF2/6 grafted from reactive silane.

The UV-vis spectra of reactive silane before and after polymerization did not reveal any significant changes, whereas the photoluminescence spectrum demonstrated peaks typical PF2/6 at 415 and 435 nm of moderate intensity (Figure 50). The observed results can be explained by a high sensitivity of photoluminescence to fluorescent compounds. It is well known that UV-vis spectroscopy is much less sensitive method compared to fluorescence spectroscopy.

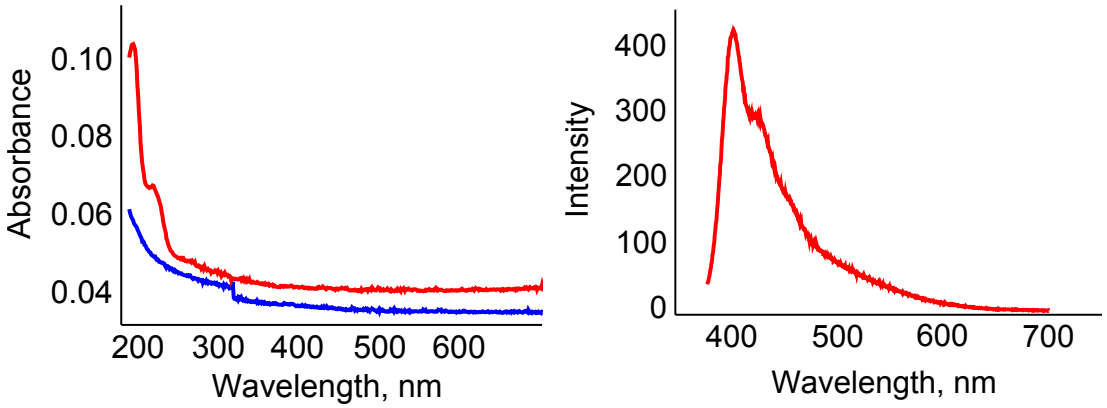

Figure 50: a) UV-vis spectra of silane-anchoring layer (blue) and grafted PF2/6 (red); b) Fluorescence spectrum of PF2/6 grafted from silane.

The same procedure was carried out using 1-2 nm thick PS(Br) films giving 10-20 nm thick PF2/6 brushes. The grafting process was found to be much more sensitive to the presence of oxygen for thin (1-2 nm) PS(Br) and silane-based anchoring films than for rather thick PS(Br) (10-100 nm) supports. In particular, the following dependence of the grafting result on the anchoring layer thickness was found. Whenever the thickness of the latter layer exceeded 10 nm, the maximal graftable thickness of the PF2/6 brush was independent of the thickness of the supporting layer. For example, 100 nm thick PF2/6 brushes could be reproducibly grown from 10 nm-thick as well as from 100 nm-thick PS(Br) films. In contrast, the maximal graftable thickness becomes dependent on the thickness of the anchoring layer for thinner than 10 nm anchoring layers. Such results may imply that the Pd species are no longer involved in the polycondensation process and only the inner layers of the initiating films are responsible for polymerization. If so, the initiator degradation process would be especially critical for thin anchoring films for which the whole quantity of the immobilized Pd catalyst may be completely degraded. On the other hand, for thicker than 10 nm anchoring films, degradation of the initiator is no more a limiting factor and the maximal

thickness of grafted PF2/6 is controlled by other processes, such as by chain-termination reactions.

3.4 Kinetic Studies

To analyze the kinetics of the grafting process, eight Si-wafers and eight quartz slides were each coated with 2 nm thick PS(Br) anchoring layers and polymerization was conducted for different times, from 0.5 to 60 hours, under otherwise identical conditions. We found that the resulting PF2/6 films reached a thickness of ∼30 nm already within 30 minutes of the polymerization, and approached maximal thicknesses within the first hour of polymerization (Figure 51).

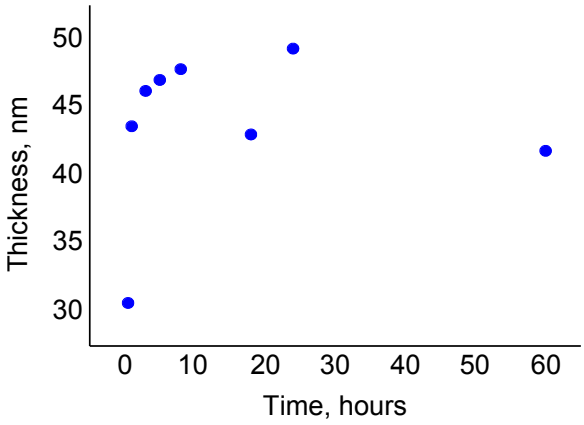

Figure 51: Kinetics of the PF2/6 grafting process.

Such results are consistent with bulk solution polymerization experiments with PF2/6 for which rather high molecular weight PF2/6 of 45 000 g/mol formed within 30 minutes of the polymerization.

3.5 Grafting of PF2/6 from Silica Nanoparticles

To confirm that the prepared grafted films are indeed brush-like structures and not a cross-linked PF2/6-network, degrafting of surface-immobilised PF2/6 and their analysis would be advisable. It is, however, clear that for the collection of a quantity of the polymer material necessary for standard investigations like GPC or NMR, graft-polymerization should be formed on quite a large substrate (in the order of one square meter), which is not technically feasible. To circumvent this problem, we attempted SIP of PF2/6 from modified submicrometre organosilica particles that would mimic planar substrates. Because of a high surface-to-volume ratio for microparticles, it was

feasible to collect the necessary amount of degrafted material from a single experiment. Other benefits of using these microparticles are as follows: nearly monodisperse silica spheres of controlled size and surface chemistry are easily available by a Stöber method [100]; the relatively large size and high density of the particles facilitate separation of surface-grafted materials from ungrafted ones by a simple centrifugation procedure; silica particles can be selectively etched under mild conditions without the destruction of attached polymers, and therefore, the grafted polymers can be released from the support for further analysis. This is in a contrast to the case when planar surfaces are used as supports.

Silica-core organosilica-shell particles, ∼300 nm in diameter, were prepared by a modified Stöber method [101] via sequential sol-gel hydrolysis of tetramethyl orthosilicates (TMOS) and [2-(4-bromo-phenyl)-ethyl]-triethoxy-silane under controlled conditions (Figure 52). Organosilane was obtained by standard hydrosililation of 4-bromostyrene by triethoxisilane in the presence of a chloroplatinic acid catalyst, and was used in the synthesis of particles to introduce bromophenyl surface-functionality which is necessary for the immobilisation of the Pd catalyst.

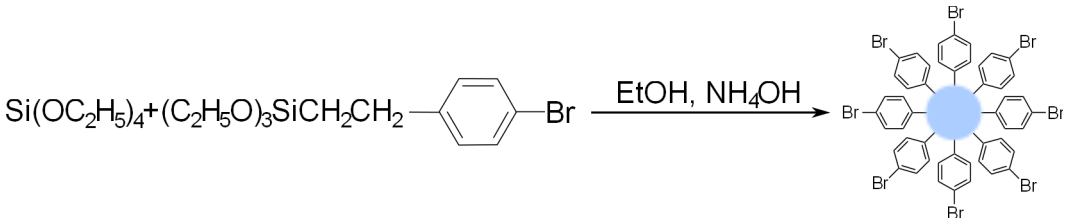

Figure 52: Stöber synthesis of functionalized silica nanoparticles.

Grafting of PF was attempted by the activation of the reactive nanoparticle surface with Pd(PtBu$_3$)$_2$ followed by the SIP process. The prepared particles with an organosilica core and a PF2/6 shell were extensively characterized.

SEM measurements revealed that the SIP attempt resulted in a significant increase in the roughness of the particles surface instead of an increase in diameter (Figure 53), which was probably due to the unavoidable wetting and etching of the particles by the basic water phase during the polymerization process and suppression of the grafting-from process. Additionally, due to the partial wetting of the particles, they tended to coagulate which also caused ineffective grafting.

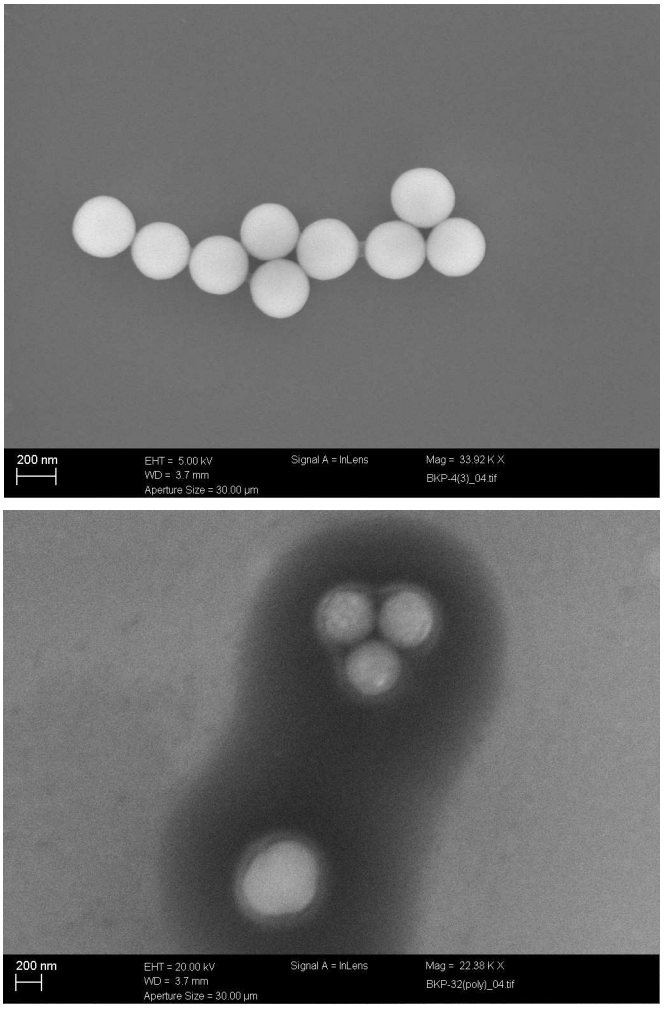

Figure 53: SEM-images of functionalized silica particles a) before SIP; b) after SIP.

The photoluminescence spectrum of PF2/6-SiO_2 nanoparticles showed a low-intensity and relatively well-structured peak at 420 nm with a shoulder at 440 nm (Figure 54, b). The indistinctness of this spectrum reflects the permanent diffusion of nanoparticles in the dispersion. Fluorescent microscopy also detected agglomerated nanoparticles that emitted light in the blue region (Figure 54, a). However, fluorescence intensity was relatively low suggesting an inefficient grafting process.

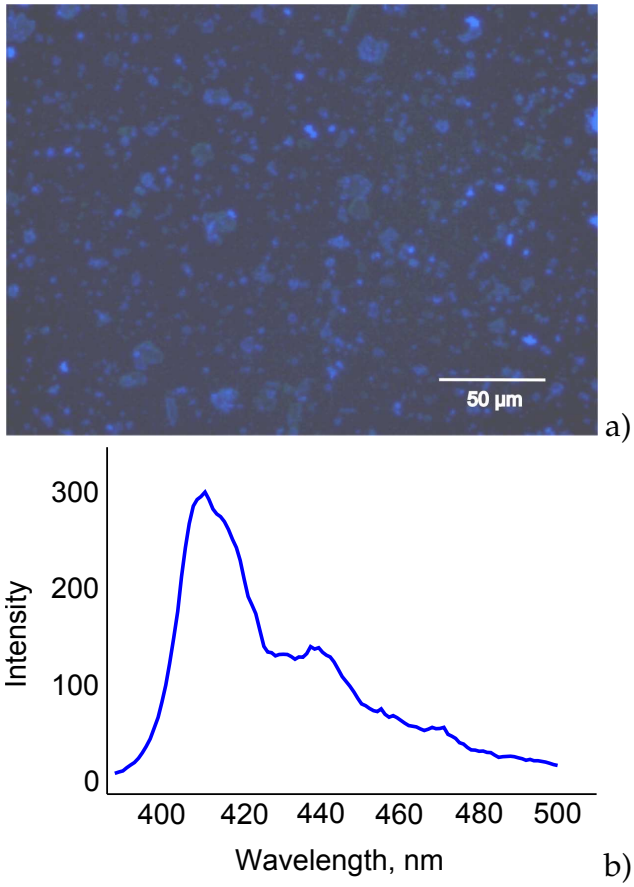

Figure 54: a) Fluorescent micrograph of of Si-graft-PF2/6 nanoparticles deposited on a quartz slide illuminated by UV-light lamp at 360 nm; b) Photoluminescence spectrum of Si-particles after polymerization.

We tried to investigate the thermal behavior of the silica nanoparticles before and after polycondensation by thermogravimetry. Unfortunately, TGA analysis of the PF2/6-SiO_2 particles did not reveal any significant changes compared to initial particles. We thus concluded that only negligible amounts of PF2/6 were grafted to the nanoparticles.

For analytical purposes, grafted PF2/6 chains were detached from the silica core of the SiO_2-PF2/6 particles by dissolution of the latter in a mixture of

aqueous hydrofluoric acid (HF) with toluene for several days. Unfortunately, the mass fraction of the released polymer was too low for GPC investigations. Nevertheless, this reasonable amount of degrafted PF2/6 was enough for NMR analysis. Careful inspection of the ^{1}H NMR spectrum of degrafted PF2/6 (Figure 55) confirmed its identity.

The general conclusion regarding grafting from the particles was that proceeds to a very low extent so that this process, unfortunately, cannot model grafting from planar surfaces.

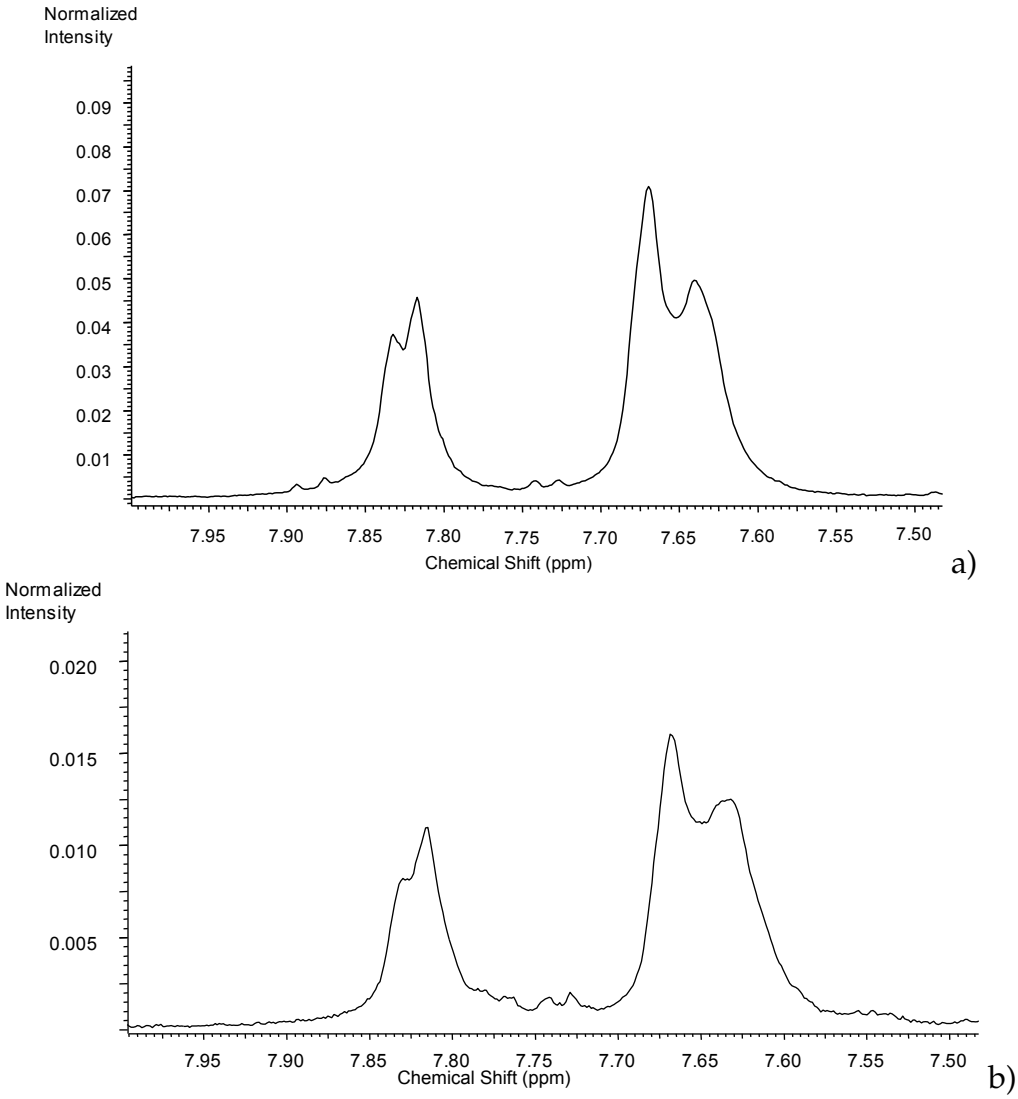

Figure 55: NMR spectrum of a) unbound, high MW PF2/6; b) PF2/6 degrafted from silica nanoparticles.

3.6 Investigation of UV-vis Absorption and Fluorescence Spectra

PFs are a class of promising blue light-emitting materials due to their attractive properties. Owing to a rigid structure and a large band gap, this polymer emits light in a blue region [102, 103]. Figure 56 shows the UV-vis absorption and PL spectra of a dilute chloroform solution of unbound PF2/6 of two different MW. The electronic absorption spectrum of a PF2/6 solution show an unstructured long-wavelength absorption maximum λ_{max} of ∼373-383 nm (which depends on MW). The PL spectrum of PF2/6 has two peaks with maxima at 413 nm and 435 nm assigned to the 0-0 and 0-1 intrachain singlet transition respectively (the 0-0 transition is the most intense).

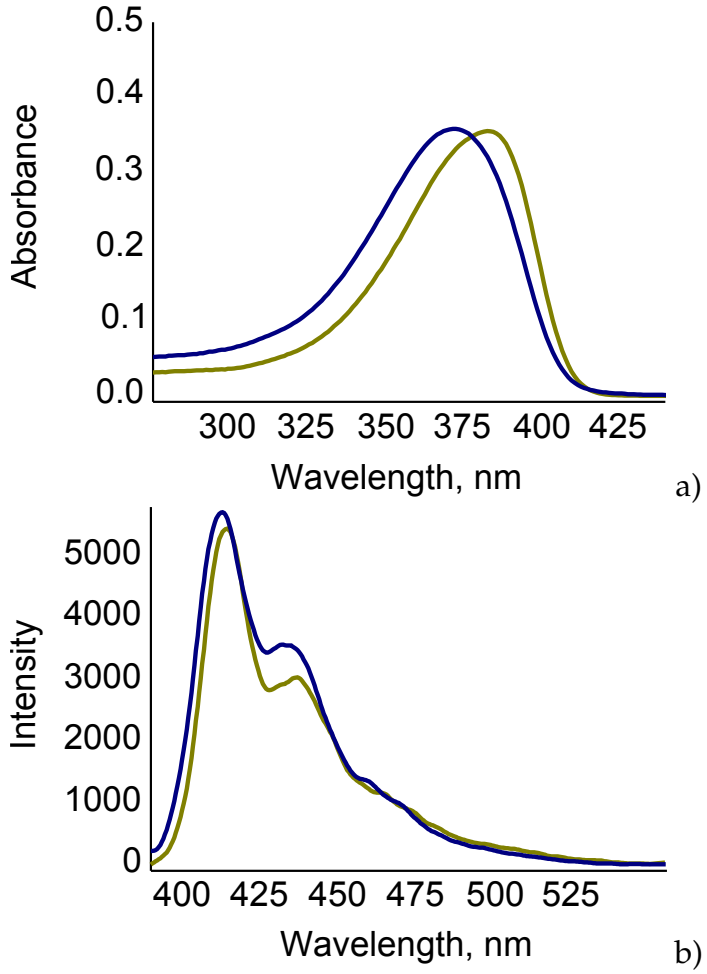

Figure 56: a) UV-vis absorption and b) PL spectra of PF2/6 (M_w=61 000 g/mol, PDI=3.0 (olive curve) and M_w=1100 g/mol, PDI=3.0 (blue curve)) in chloroform solution, c=0.1 mg/mL.

To verify whether the increase of the sample thickness which occurred upon grafting of PF2/6 indeed came solely from the grafted PF2/6, a series of PF2/6 films of different thicknesses on quartz glass slides were prepared and their absorption and emission intensities were compared with those of the grafted PF2/6. The electronic absorption spectra of spin-coated thin solid films reveal a similar structure with a slightly red-shifted peak (most probably due to differences in intermolecular interactions) (Figure 56). The absorption spectra exhibit linear dependence of absorbance on polymer layer thickness (Figure 57). Similar behaviour was also observed for the PL emission spectra (Figure 58).

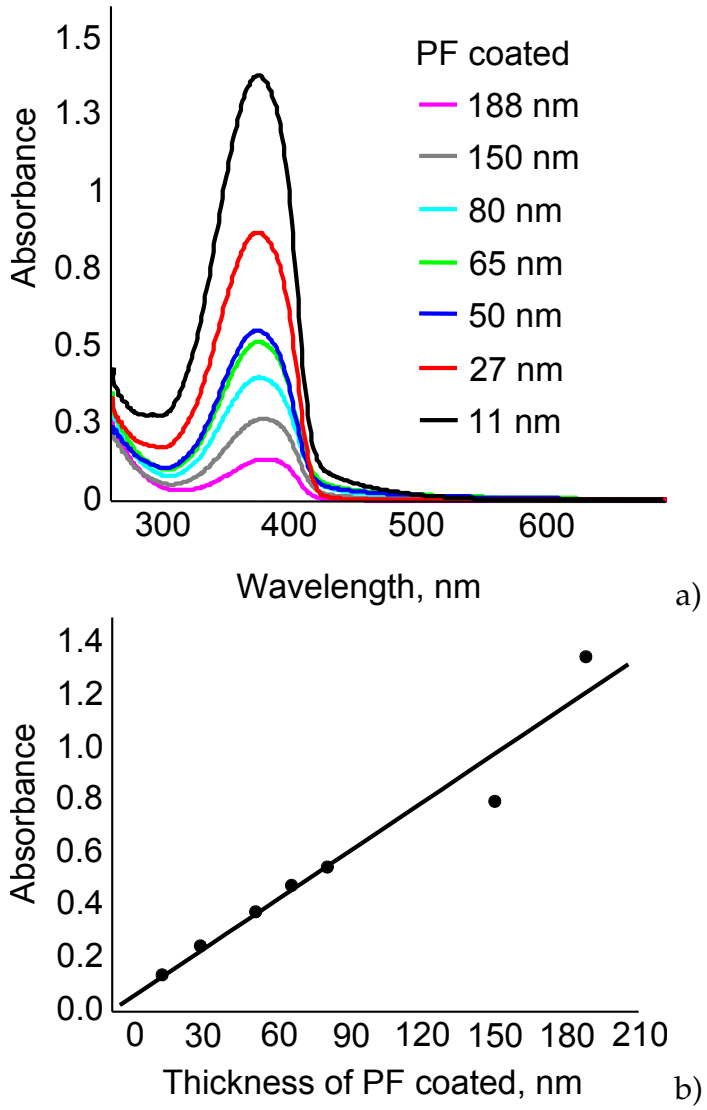

Figure 57: a) Absorption spectra of coated PF2/6 with different thickness, b) dependence of absorbance on thickness of coated PF2/6.

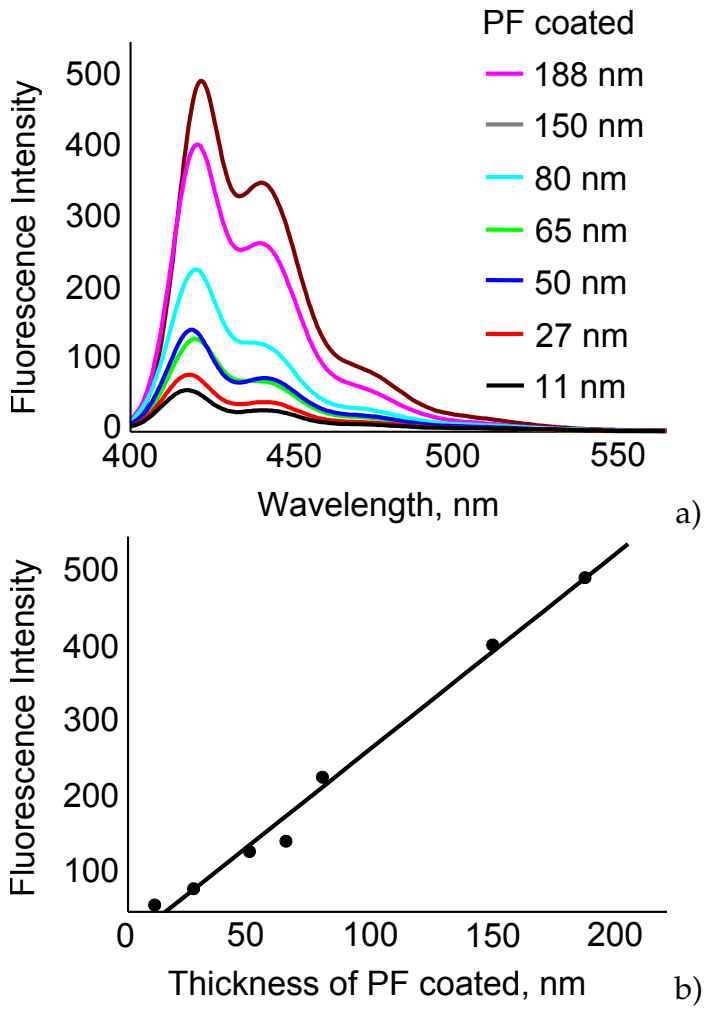

Figure 58: a) Emission spectra of coated PF2/6 with different thickness, b) dependence of intensity on the thickness of coated PF2/6.

It was found that absorption spectra of the grafted PF2/6 films in the dry state and in chloroform (a "good solvent") (Figure 59) are similar to the aforementioned spectrum of unbound PF2/6 (Figure 56). Moreover, the absorption intensity for the grafted films approaches to the one for spin-coated PF2/6 of the same thickness (Figure 57, b) and these data confirm that the grafted material is namely PF2/6.

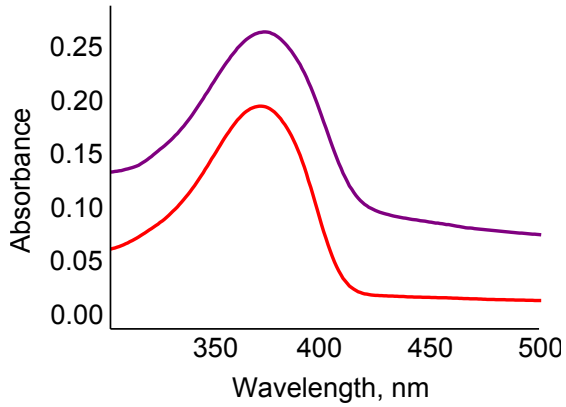

Figure 59: Absorption spectra of grafted PF2/6 in the dry state (red) and in chloroform (violet).

To investigate the dependence of PL intensity on the media, we measured spectra in different solvents (Figure 60). As expected, the highest fluorescence intensity of the grafted PF2/6 was observed for films immersed in $CHCl_3$, which is a good solvent for PF2/6. The emission intensity in THF was approximately two-fold less, whereas the intensity in methanol was one order of magnitude less than the intensity in $CHCl_3$, most likely due to reduced quality of the solvents. The lowest fluorescence intensity (~5% of the intensity in $CHCl_3$) was found for grafted PF2/6 films in the dry state, likely due to an aggregation of PF2/6 chains caused by a well-known self-quenching effect. (The more polar solvent molecules are more closely bound to the excited state, and this favours non-radiative deactivation processes.)

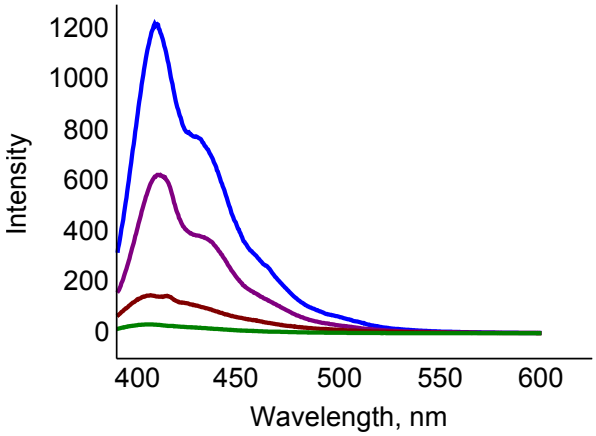

Figure 60: Fluorescence spectra of the 40 nm thick PF2/6 film grafted from 2 nm thick PS(Br) in different solvents (blue - in chloroform, violet - in THF, brown - in methanol, green - in the dry state).

The major problem in the application of PFs in blue PLEDs is color instability. The pure blue emission can be contaminated by an undesired contribution of the green emission band (∼530 nm). It was shown by List and co-workers that the green emission of PF is due to fluoren-9-one defects in the polymer chain [104, 105, 106].

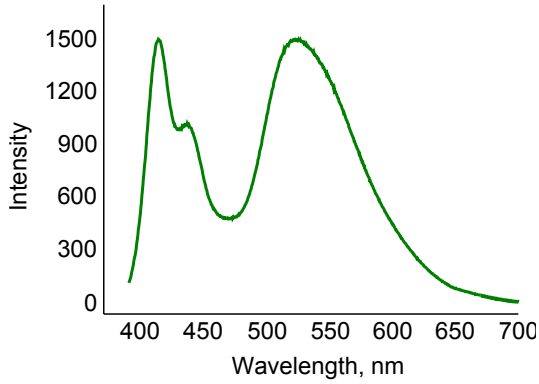

Figure 61: Fluorescence spectrum of the 40 nm thick PF2/6 film grafted from 2 nm thick PS(Br), after annealing at 200°C for 2 hours in air.

The surface-grafted PF2/6 did not exhibit degradation upon storage in contact with air for at least three months. However, air annealing of the samples at 200°C lead to the appearance of a characteristic green emission (Figure 61), presumably due to the formation of fluorenone-defects (λ_{max} = 522 nm) in the PF2/6 structure (Figure 63). The green emission was stronger in the dry state, much lower in THF and is completely suppressed in $CHCl_3$) (Figure 62).

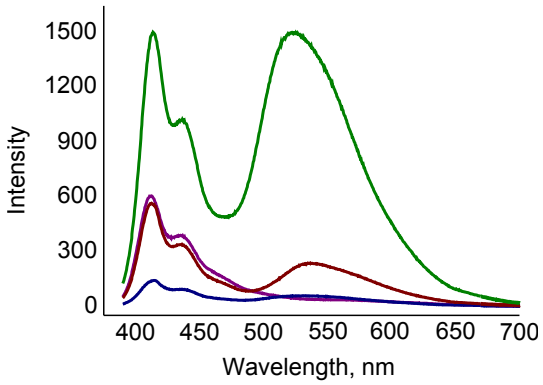

Figure 62: Fluorescence spectra of the 40 nm thick PF2/6 film grafted from 2 nm thick PS(Br) aged for 2 hours at 200°C (blue - in chloroform, violet - in THF, brown - in methanol, green - in the dry state).

Possibly, keto-defects can trap created singlet excitons by dipole-dipole induced Forster-type [107] excitation energy transfer. This is a dominant process in the solid state, whereas in solution Forester-type energy transfer to the keto-defect sites is diminished. The green emission recovers again after the evaporation of $CHCl_3$ which indicates that this "green" emission results from irreversible changes in the backbone chemical structure rather than solely from the chain-aggregation effect, although the green emission manifests itself to a greater extent for more aggregated PFs.

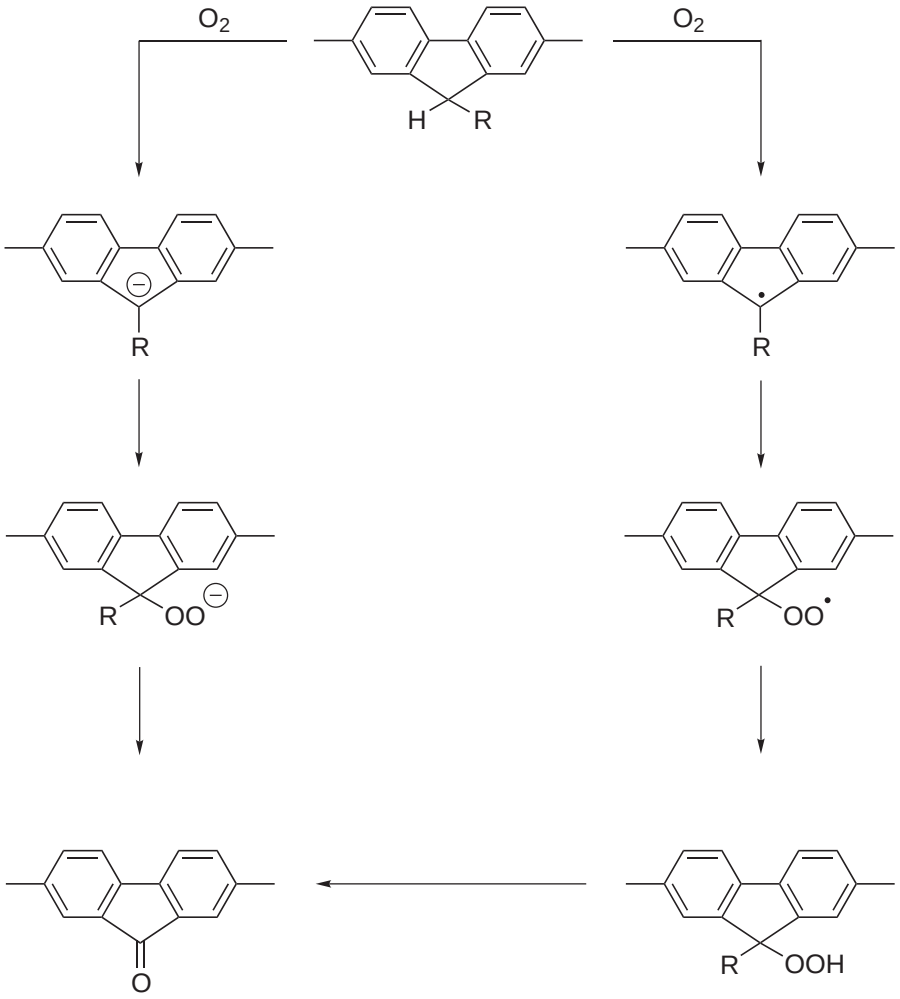

Figure 63: Simplified depiction of the mechanism of fluorenone formation from monosubstituted fluorene repeat units.

3.7 Orientation Studies

The orientational order was studied using polarized UV-visible spectroscopy at different angles. The highly stretch-oriented polymer chains must show strong anisotropy of absorbance parallel and perpendicular to the chain direction. For this purpose the angular dependence was measured using a spectrometer with a step-width of 10°. The investigated films did not reveal any significant change in anisotropy, which means that the polymer chains possess non-uniformly distributed orientation.

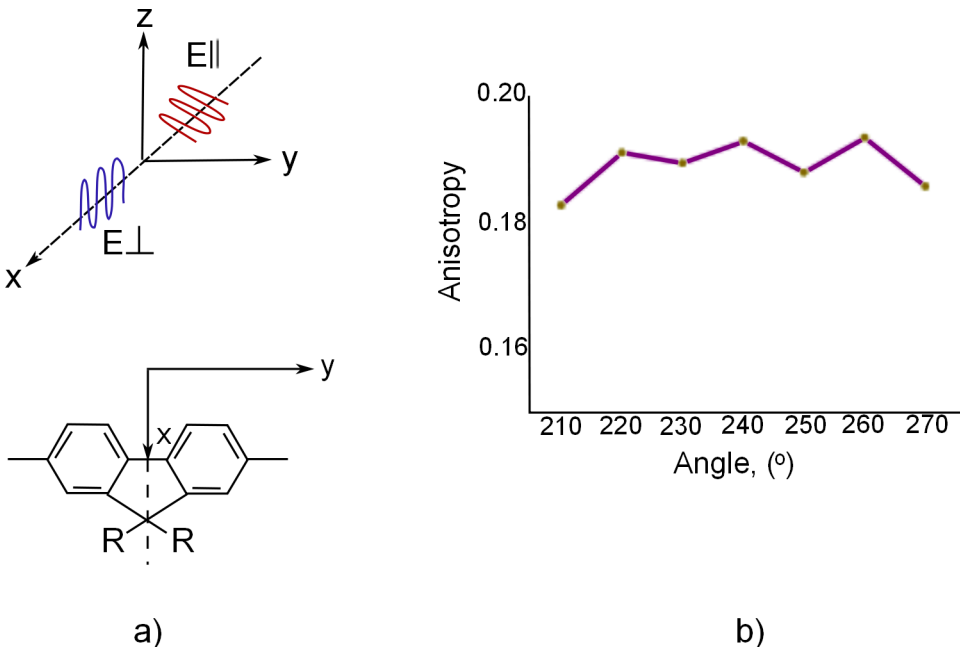

Figure 64: a) Schematic working principle of utilized polarized spectroscopy; b) observed anisotropy of absorbance of grafted PF2/6 at different angles.

3.8 Grafting of PF2/6 from a Patterned Surface

Currently, different patterned structures of conjugated polymers are of significant interest for possible applications in sensors and optical devices. Surface and site-specific polymerization is an excellent tool for the patterning of polymers.

Figure 65 represents a scheme of the patterning procedure. First, submicron hydrogel particles were arranged on Si-wafers by dip coating into a dispersion in water which was then used as a mask. Afterwards, the residual surface was covered with octadecyltrichlorsilane to deactivate (hydrophobize) the space between the particles.

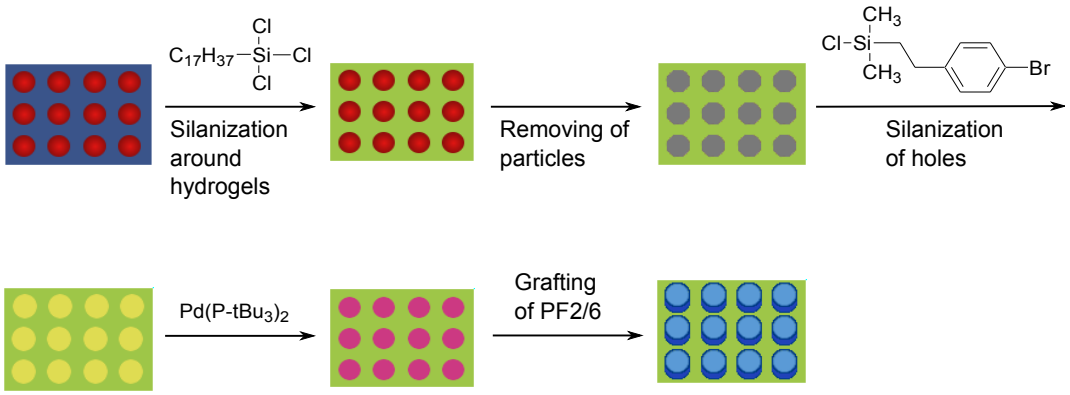

Figure 65: Schematic representation of the patterning: deposition of the arranged hydrogel particles; silanization of the sample with octadecyltrichlorosilane; removal of the particles in an ultrasonic bath; silanization of the holes with [2-(4-bromo-phenyl)-ethyl]-chloro-dimethylsilane; activation with a Pd-catalyst; polymerization.

The particles were removed in an ultrasonic bath and 3-chloropropyltrimethoxysilane was adsorbed selectively onto the remaining hydrophilic holes from the gas phase. AFM revealed the successful deposition and following removing of hydrogel nanoparticles onto the surface resulting in round shaped holes $\sim$1 μm in diameter (Figure 66, a). The subsequent treatment of the samples with a Pd-catalyst and a monomer solution resulted in the selective grafting of PF with a thickness up to 100 nm (Figure 66, d). Moreover, the surface selective polymerization was a perfect proof of the brush-like structure of grafted PF2/6.

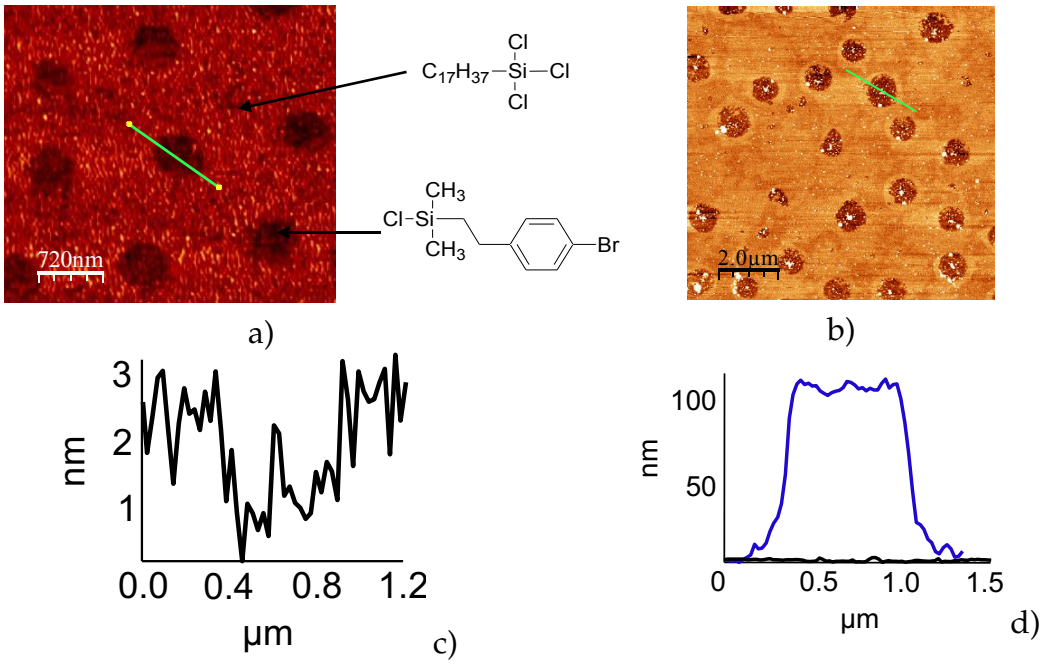

Figure 66: a) AFM topography image of patterned silane before grafting; b) AFM topography image of grafted PF2/6 from patterned silane; c) Cross-section of patterned silane before grafting; d) Cross-section of grafted PF2/6 from patterned silane (black - before and blue - after grafting).

Figure 67: Picture of a PF2/6-patterned Si-wafer.

3.9 Conclusions

In conclusion, we have developed the first surface-initiated and site-specific Suzuki polycondensation to fast and selectively grow polyfluorene from properly functionalized and patterned surfaces at room temperature. This method seems to be very promising tool for fabrication of optoelectronic devices and sensors.

3.10 Experimental Part

Materials. 4-Bromostyrene, Pd(PtBu$_3$)$_2$, 2,7-Dibromo-9,9-bis(2-ethylhexyl)-fluorene, pinacol, n-BuLi, bromobenzene, ammonium, hydrogen peroxide, toluene, hexane, ethanol, toluene, chloroform, dichloromethane, and tetrahydrofuran (THF, stabilizer free, anhydrous) were purchased from Aldrich and used as received without further purification. Poly(glycidyl methacrylate), PGMA (M$_n$=65 000 g/mol, PDI=2.05) was purchased from Polymer Source Inc. Poly(4-bromostyrene) (M$_n$=51 000 g/mol, PDI=2.05) was obtained via radical polymerization of 4-bromostyrene [108]. 7-Bromo-9,9-bis(2ethylhexyl)-9H-fluoren-2-ylboric acid ester [109] and tBu$_3$PPd(Ph)Br were prepared as previously described.

Preparation of [2-(4-bromo-phenyl)-ethyl]-chloro-dimethyl-silane

Hydrosililation was carried out by adding dimethylchlorosilane (100 g) to 4-bromostyrene (18.3 g, 0.1 mol) dropwise in the presence of 160 mg of chloroplatinic acid (2 mL of 1:1 ethanol/diethyl ether solution) as a catalyst and stirring for 1 h. After the excess of dimethylchlorsilane was removed by vacuum distillation, the only residue was fractionized by vacuum distillation. The resulting product is a mixture of Markovnikov and anti-Markovnikov adducts.

Grafting of PF2/6

Highly polished Si-wafers (Wacker-Chemitronics), or quartz slides (Saint-Gobain Quartz PLC.) were firstly cleaned in an ultrasonic bath three times for 5 min with dichloromethane, placed in cleaning mixture of NH_4OH:H_2O_2:H_2O (1:1:2) at 80°C for 1 h and finally rinsed several times with Milipore water (18 MQxcm).

PGMA layers of the same 2 nm thickness (ellipsometry data) were used in all experiments as adhesion promoter between PS(Br) and Si-substrates. It was deposited by spin-coating from chloroform (0.03 mg/ml, 2000 rpm) and the samples were annealed at 150°C during 2 hours in vacuum. PS(Br) layers with variable thickness from 1 to 30 nm were spin-coated onto PGMA from toluene and cross-linked upon a brief irradiation (from 3 to 15 seconds, depending

on the PS(Br) thickness) with UV-light to achieve their insolubility, while keeping the films still swellable in "good" solvents for PS(Br). Alternatively [2-(4-bromo-phenyl)-ethyl]-chloro-dimethyl-silane was deposited from a gas phase onto Si-wafer or quartz slides. 0.1 ml of reactive silane was brought into desiccator, the atmosphere was replaced with vacuum and the samples were annealed at 60°C during 2 hours. Afterwards the samples were extensively rinsed with toluene or chloroforme to remove non-reacted compounds, dried and placed into a round-bottomed flack equipped with septum, and the atmosphere was replaced with argon. Afterward, a solution of $Pd(P\mathit{t}Bu_3)_2$ in dry toluene (3.5 ml, c = 3 mg/ml) was added to the flack in glovebox, and the samples were allowed to react for 2.5 hours at 70°C. The reaction solution was replaced with the mixture of solution of the monomer **2** in dry THF (3.5 ml, c = 10 mg/ml) and 2M aqueous sodium carbonate (0.3 ml). The samples were allowed to polymerize at room temperature for 0.5-60 hours. To stop polymerization, the samples were moved from reactor and rinsed with 2M HCl, water and hot organic solvents (acetone, $CHCl_3$, hexane, THF). Independently on the thickness of the initiating layer, the resulting composit films were very robust against delamination upon extensive rinsing with various different organic solvents in an ultrasonic bath and a Soxhlet apparatus. This proves the covalent grafting of PF2/6.

Grafting of PF2/6 from silica nanoparticles

Silica-core organosilica-shell particles, ∼300 nm in the diameter, were prepared by a modified Stöber method [101] via sequential sol-gel hydrolysis of tetramethyl orthosilicates (TMOS) and [2-(4-bromo-phenyl)-ethyl]-triethoxi-silane.

To immobilize the Pd catalyst, suspensions of silica particles in anhydrous and degassed toluene were mixed with $Pd(P\mathit{t}Bu_3)_2$ in the same solvent under argon at 70°C for 2.5 hours. Prior to polymerization, thus-treated particles were purified from unreacted $Pd(P\mathit{t}Bu_3)_2$ by repeated redispersion/centrifugation cycles. Grafting of PF was attempted by the addition of the monomer **2** in degassed mixture of THF and aqueous sodium carbonate solution followed by stirring overnight. After quenching of the polymerization mixture with 2M HCl, the particles were carefully purified from any ungrafted materials by redispersion in hot chloroform and THF followed by centrifugation. In addition, ethanol was used to remove water residue and allow better redispersion of particles.

4 Effect of Pd Catalysis on the Suzuki Coupling Reaction

4.1 Palladium-Catalyzed Coupling Reactions: Homogeneous and Heterogeneous Catalysis

In the preceding chapter, we described a remarkably efficient process for grafting PF2/6 brushes from slightly cross-linked PS(Br) films via chain-growth Suzuki polycondensation. In particular, it was shown that PF2/6 brushes with thicknesses up to 100 nm can be obtained. In this chapter, we would like to discuss in more detail the possible mechanism of this process. It is important to emphasize that preparation of polymer brushes is possible if the underlying graft-polymerization process involves the chain-growth mechanism, since any step-growth steps occurring during polymerization will inevitably terminate polymerization from the surface process and transfer polymerization to the bulk solution. Furthermore, preparation of rather thick PF2/6 polymer brushes (e.g., 100 nm-thick), requires a significant degree of the chain-growth perfection from the polymerization process. Indeed, to provide a thickness of 100 nm for PF2/6 brushes in the dry state, the grafted PF2/6 should have of minimum DP=125 or M_w = 50 000 g/mol, if the grafted chains are fully stretched. Since in reality the chains are titled or twisted and since the grafting density is always much lower than maximal possible value (at least, by a factor of 3), the real M_w of the grafted polymer to result in the formation of 100 nm-thick PF2/6 brushes should be above 150 000 g/mol. On the other hand, bulk solution experiments have demonstrated that although Suzuki polycondensation involves the chain-growth mechanism, the process is far from perfectly controlled, and it never gave polymers with M_w above 50 000 g/mol. In other words, it is very surprising that such an imperfect process could lead to the formation of polymer brushes of such high thicknesses. Therefore, in this work, an attempt was undertaken to explain this discrepancy. We suggested that there might be some additional factor which would enhance the "stickiness" of the Pd catalyst to the surface, so that the polymerization takes place predominantly at the surface and leads to polymer brushes, even if the underlying polymerization mechanism is not perfectly living. For example, such an extraordinary propensity of the Pd catalyst to be located at the surface would be if the real catalytic species that assist polymerization of monomer **2** (7-Bromo-9,9-bis(2ethylhexyl)-9H-fluoren-2-ylboric acid ester) is not small molecule Pd complexes such as **1** (tBu$_3$PPd(Ph)Br), but Pd nanoparticles (PD NPs). Indeed, the tendency of various species to form nanoparticles, whatever their nature, is well-documented experimentally and explained theoretically. The formation of Pd NPs is, in principle, possible via a thermal decomposition of complex **1**

during Pd catalyst immobilization or afterwards. On the other hand, if formed, such nanoparticles would indeed have an enhanced affinity to aryl- and aryl halide-terminated surfaces, such as PS(Br), because Pd NPs have many coordination sites to bind several aryl halides at a time. The feasibility of this hypothesis is supported by the fact that Suzuki coupling catalyzed by Pd NPs which are stabilized by phosphorous ligands is well-known (see below). It is believed that the cross-coupling mechanism in this case is similar to that for reactions catalyzed by the usual small-molecule complexes, with the only difference that nanoparticles have a plurality of reaction sites with the local structure similar to the structure of small-molecule catalysts. In the following paragraphs, we will briefly review what is known to date about Suzuki cross-coupling catalyzed by Pd NPs. We will further investigate in more detail samples after immobilization of the Pd catalyst using XPS, TEM and NMR techniques in order to understand whether Pd nanoparticles are indeed formed in the activated layers. We will also describe independent synthesis of Pd NPs supported by different ligands and our attempts to catalyze Suzuki polycondensation in bulk solution and at surfaces using these nanoparticles to mimic processes that take place upon surface-initiated polycondensation of PF2/6 as described in Chapter 3.

Pd NPs are widely used as catalysts for Suzuki cross-coupling. The use of NPs in catalysis allows for improving separation of the reaction products from the catalyst. This potentially facilitates decreased catalyst cost due to reduced catalyst loss and simplified product purification [110, 111]. This is especially critical for the synthesis of medical compounds, which must contain $\ll$5 ppm of residual metal in the product [112].

El-Sayed and co-workers synthesized Pd NPs, stabilized by poly(vinyl pyridine) (PVP) and studied their effectiveness in Suzuki reactions in an aqueous solution [113, 114, 115]. The detected TOF (turn off frequency) was up to 90, whereas during the reaction course it decreased as the particle size increased. That suggests that the Suzuki reaction is "structure-sensitive"; that is, the low-coordination number vertex and edge atoms on the particle surface are the active centres for catalysis. Primarily, PVP prevents coagulation of NPs, but the process of refluxing seems to cause Ostwald ripening (a thermodynamically driven process that leads to the dissolution of small NPs and the growth of larger NPs) in which the size of NPs increases. Furthermore, they encapsulated NPs into poly(amidoamine) (PAMAM) dendrimers with 3^{rd} and 4^{th} generations and studied their catalytic activity in the Suzuki C-C coupling reaction [116, 117]. Dendrimers stabilize the metal NPs by preventing their agglomeration, but they do not fully passivate the metal surface. Comparably with PVP-stabilized NPs, TOF was higher for the dendrimer-Pd NP catalyst.

The stabilization of NPs during their synthesis also can be performed by interaction with ligands [118, 119, 120]. In principle, this strategy

potentially allows for good control over the efficiency of catalytic reactions, including enantioselective ones. Pd NPs capped with special ligands such as cyclodextrin were shown to be active for the catalysis of the Suzuki reaction [121]. For instance, iodo- and bromoarenes and iodoferrocenes are coupled to phenyl boronic acid by refluxing in MeCN:H_2O, 1:1 (v/v) in the presence of K_2CO_3 or $Ba(OH)_2$ and 1% perthiolated β-cyclodextrin-Pd NPs. In fact, the simplest dodecathiolate-Pd NPs catalyze the Suzuki reaction of haloarenes, including chloroarenes, with phenylboronic acid, even at ambient temperature, and recycling several times has been achieved [122]. Fujihara and co-workers synthesized small Pd NPs stabilized by bisphosphine BINAP bearing an alkyl chain and performed a carbon-carbon Suzuki coupling reaction catalysed by these NPs [123]. The reaction was carried out at room temperature and resulted in 83 % yield of the coupling product.

Jin et al. reported on a ligand-free Suzuki coupling reaction catalyzed by the $in\ situ$ generated Pd NPs in PEG-400 under aerobic conditions [124]. PEG-400 played versatile roles: as a green reactive medium, reductant, and stabilizer. Moreover, the results showed that this approach was oxygen-promoted.

Furthermore, Pd NPs can be formed in ionic liquids (ILs). This is a valuable media for catalysis with Pd NPs because the substituted imidazolium cation is bulky, favouring the electrosteric stabilization of NPs. Dyson and co-workers used salts of N-butyronitrile pyridinium cation, which reacted with $PdCl_2$ to give a dinitrile complex that turns black upon addition of phenyltributylstannane [125]. The formed Pd NPs catalyzed a Suzuki C-C coupling reaction. However, ILs are non-innocent, as they readily produce Pd-N-heterocyclic carbine complexes upon deprotonation of the imidazolium salt at a sufficiently high temperature.

A large body of reports in the literature focus on the catalytic properties of NPs fixed onto a heterogeneous support such as oxides of Si [126, 127], Al [128, 129], Ti [130], Zr [131, 132], Ca [133], Mg [134] and Zn [135]. Pd NPs on a solid support such as silica which makes the system stable at high temperatures and allows for easy removal from the reaction medium. The fabrication of uniform hollow spheres with nanometre to micrometre dimensions and tailored properties has been studied by Caruse et al. [136, 137]. Monodisperse palladium nanospheres 300 nm in diameter catalyzed Suzuki coupling of iodothiophene with phenylboronic acid using a 3 mol % Pd catalyst in ethanol under reflux. Under the same conditions, a 15 mol % Pd catalyst was used to couple bromobenzene [138].

Another reusable catalyst for the Suzuki-Miyaura coupling reaction is presented by Pd/C. This is one of the most common heterogeneous phosphine-free Pd catalysts, which allows for performing the reaction in aqueous media [139, 140, 141]. Hirao et al. studied the reaction of various halophenols and arylboronic acids and showed that the experimental

procedure is very simple and results in up to 99% yield of the coupling product [142].

Despite the large number of studies which have used Pd NPs as catalysts in Suzuki cross-coupling, it is still an open question as to whether the NPs itself play a catalytic role or whether it just serves as a reservoirs that supplies the molecular Pd species.

For Suzuki reactions, there is conflicting evidence on the reaction mechanism, with some authors supporting the addition of boronic acid to the surface followed by a surface-mediated reaction with an incoming aryl halide [135], while others espouse a leaching mechanism [143] whereby molecular Pd is leached into solution, which then acts as the true catalytic species.

Distinguishing metal-complex homogeneous catalysis from metal-particle heterogeneous catalysis is not trivial; it is a task which has caused considerable examination in the literature. First of all, it is generally difficult to understand whether the soluble colloidal/nanocluster catalyst is involved, partly because colloidal solutions often appear homogeneous to the eye [144, 145]. Additionally, nanoclusters/colloids can be as small as $\sim$1 nm in diameter, which makes them difficult to detect by some methods [146, 147, 148]. In 2003, Leadbeater et al. reported Suzuki coupling of 4-bromoacetophenone and other aryl bromides and phenylboronic acid in the absence of any added transition metal [149, 150]. Careful studies showed that the reactions were catalyzed by trace amounts of Pd in the commercial sodium carbonate reagents [151]. Indeed, even at levels of 50 ppb, traces of Pd were able to catalyze the reaction. A large set of different methods was developed to detect whether heterogeneous NPs or "true" metal-complexes are responsible for catalysis.

The hot filtration technique is an effective test to probe whether leached transition metal species are responsible for the observed catalysis [152]. This is an excellent test to judge heterogeneity: although, when applied alone, it cannot be rigorously used to assess catalysis by leached species due to the speed at which leached Pd species can redeposit back onto the support [153, 145, 154].

It also has been suggested that one can distinguish homogeneous from heterogeneous catalysis by whether or not the kinetics are reproducible. Homogeneous catalysis exhibits reproducible kinetics whereas in case of heterogeneous irreproducible kinetics are observed [155]. However, the discovery of highly reproducible catalytic systems involving nanocluster catalysts shows that such a distinction is not absolute [156]. At the same time, the comparison of the kinetics of the catalytic reaction with the kinetics of precatalyst decomposition also can bring some reliable results. If precatalyst decomposition and the catalyzed reaction occur with the same kinetics and an identical induction period, then this is typically compelling evidence for a heterogeneous catalyst. Despite this, a common scenario involves

introducing the precatalyst and substrate into a reactor, waiting for a given length of time, stopping the reaction, and analyzing the final reaction products. Clearly, the observation of an induction period or of kinetics is impossible in such experiment. Furthermore, in cases where the catalytic reactions proceed to completion before any analysis, it is impossible to judge the kinetic reproducibility.

Another way to determine the type of catalyst is to perform a mercury test. The ability of Hg(0) to poison metal-particle heterogeneous catalysts, via amalgamating the metal or absorbing on the metal surface, has been known for a long time. It was believed that the addition of Hg(0) leading to the suppression of catalysis is evident confirmation of heterogeneous catalysis. However, Hg(0) does quench the activity of Pd(II) pincer precatalysts in coupling reactions [157, 158, 159]. This is a good indication to suggest catalysis via a cycle with a Pd(0) intermediate.

All of the aforementioned indicate that distinguishing between "true" homogeneous and metal-particle heterogeneous catalysis is undoubtedly a complicated task. The field of NP catalysis involves both the homogeneous and heterogeneous catalysis communities, and these catalysts are sometimes therefore called "semi-heterogeneous" [160, 161].

4.2 Results and Discussion

4.2.1 NMR Study of the Oxidative Addition Stage

With the idea in mind to understand the catalyst immobilization process and estimate the feasibility of the formation of Pd nanoparticles, several experiments were carried out. The intriguing question was whether the real catalytically active species is a small-molecule Pd complex or a heterogeneous nanoparticle catalyst.

To directly investigate the oxidative addition stage, NMR ^{1}H and ^{31}P measurements were undertaken during the course of reaction. A model initiator precursor, phenyl bromide, was allowed to react with Pd(PtBu$_3$)$_2$, in degassed toluene-d$_8$ at 70°C directly in an NMR tube.

Figure 68 shows the ^{1}H spectra of the aromatic region during the course of oxidative addition. Peaks at δ ~6.77, 6.85 and 7.21 ppm (A, B and C correspondingly) belong to the protons at the initial phenyl bromide. The resulting product of oxidative addition possesses protons which give peaks at δ ~6.66 (para-position, D), 6.71 (metha-position, E) and 7.25 (ortho-position, F) ppm. Two peaks at δ ~7.39 ppm (G) can be assigned to the biphenyl which is generated as a side decomposition product during the reaction. Peaks at δ ~7.17 and 7.10 ppm (H and I) can be ascribed to the same compound, but protons are situated at metha- and para-positions relative to the biphenyl bond. Hence, this spectrum confirms oxidative addition of phenyl bromide to Pd(PtBu$_3$)$_2$, along with the decomposition process and formation of biphenyl as a homocoupling byproduct. The optimal activation period was found to be 45 min at 70°C which corresponds to the already formed final compound and a negligible amount of biphenyl. On the other hand, the conducted experiment clearly showed the decomposition of initiator **1** and liberation of the free ligand. This process leads to the formation of metallic Pd as seen by a change in colour from yellow to dark brown.

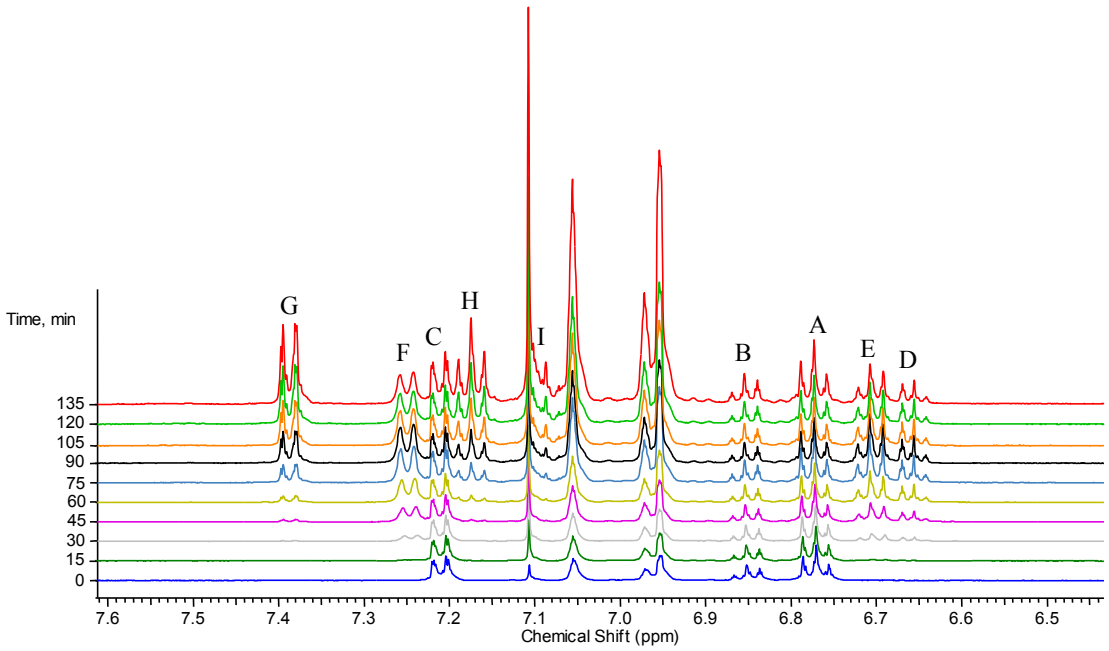

Figure 68: ^{1}H NMR spectra of the aromatic region during the course of oxidative addition.

The ^{31}P spectra also reveals significant changes during the first 90 min (Figure 69). It is clearly seen that consequent changes are minor and it is not necessary to continue the activation process further.

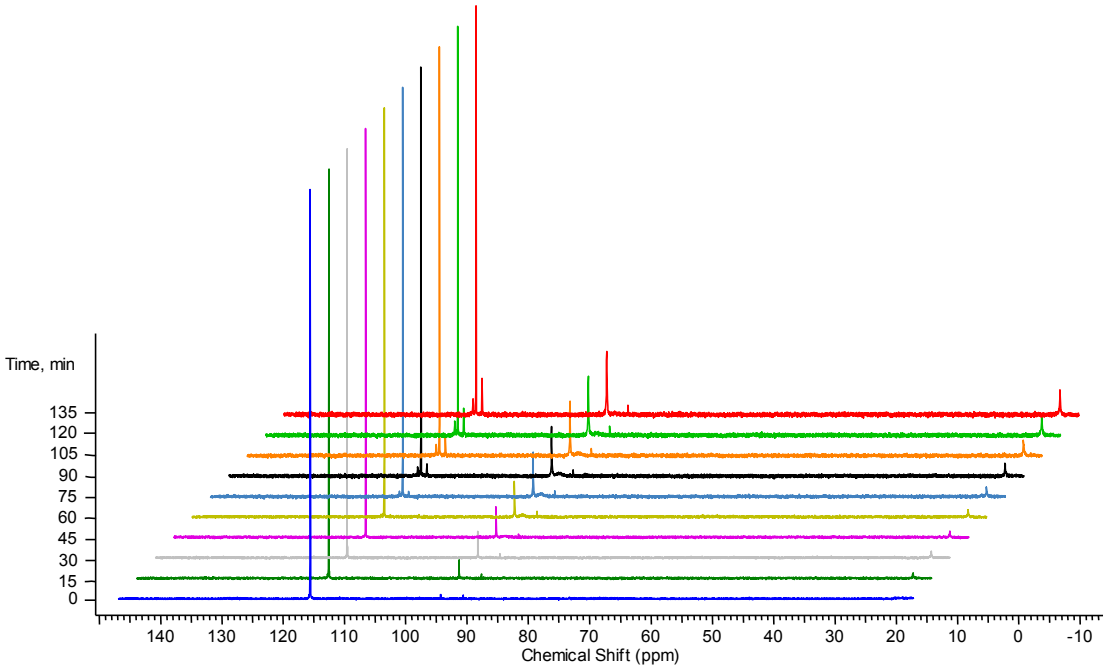

Figure 69: ^{31}P NMR spectra during the course of oxidative addition.

4.2.2 XPS Study of the Oxidative Addition Stage

Additionally, an XPS study was performed to investigate the mechanism of the activation process. Thus, modified substrates were treated with $Pd(P\mathit{t}Bu_3)_2$, in toluene at 70°C followed by washing of the excess catalyst. In the case of the initial 10 nm crosslinked PS(Br) film, the thickness increased by an additional ∼10 nm which was confirmed by ellipsometry. For the reactive silane or PS(Br) monolayer of 1 nm thickness, this resulted in a 3 nm increase. Moreover, extensive rinsing of activated PS(Br) film resulted in much less additional PF thickness than in the case of an non-washed PS(Br) film after the activation stage.

XPS studies of a 10 nm crosslinked PS(Br) film (Figure 70) indeed displayed a high content of C and Br. The observed stoichiometric ratio [Br]/[C] was equal to 0.094 which was less than the calculated value (0.125), mostly because of contamination of the surface with hydrocarbon compounds.

	PS(Br) film	PS(Br) film activated with Pd(PtBu$_3$)$_2$
[N]:[C]$\mid_{spec}$	-	0.032
[O]:[C]$\mid_{spec}$	0.008	0.44
[Na]:[C]$\mid_{spec}$	-	0.001
[Si]:[C]$\mid_{spec}$	0.006	0.158
[P]:[C]$\mid_{spec}$	-	traces
[S]:[C]$\mid_{spec}$	-	0.066
[Cl]:[C]$\mid_{spec}$	-	0.007
[Zn]:[C]$\mid_{spec}$	-	>0.001
[Br]:[C]$\mid_{spec}$	0.094	0.004
[Pd]:[C]$\mid_{spec}$	-	0.0084

Table 3: Elemental ratios determined by XPS of different atoms in a PS(Br) film before and after activation with Pd(PtBu$_3$)$_2$.

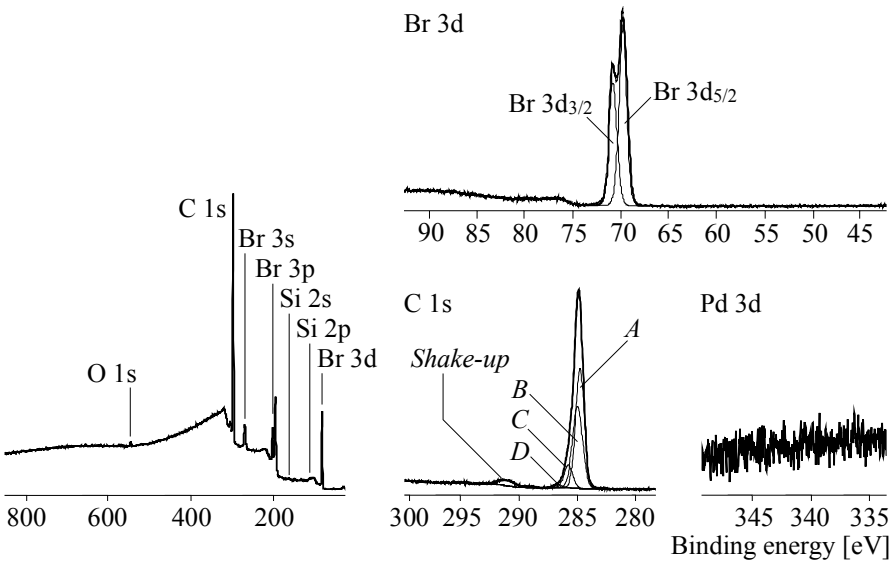

Figure 70: XPS spectra of the crosslinked PS(Br) film.

The C 1s spectra corresponds to the expected C 1s spectra for poly(4-bromostyrene). Peak A shows the carbon atoms of the phenyl ring, B reveals saturated hydrocarbons whereas C corresponds to the carbon bond

to bromine. The intensity ratio [C]/[A] = 0.2 was in agreement with the stoichiometry of PS(Br). The elemental ratio [Br]/[C] determined from the C 1s spectra equialled the [Br]/[C] ratio, which was determined from the wide-scan spectra. Peak A is more intens than expected, mostly because of contamination of the surface with saturated hydrocarbon compounds. An additional small component peak D shows ether (C-O-C) and alcoholic (C-OH) groups resulting from the cross-linked PGMA, which was used as an adhesive layer. Shake-up peaks of the C 1s spectra result from electron transition between the π and π^* orbitals of the phenyl rings.

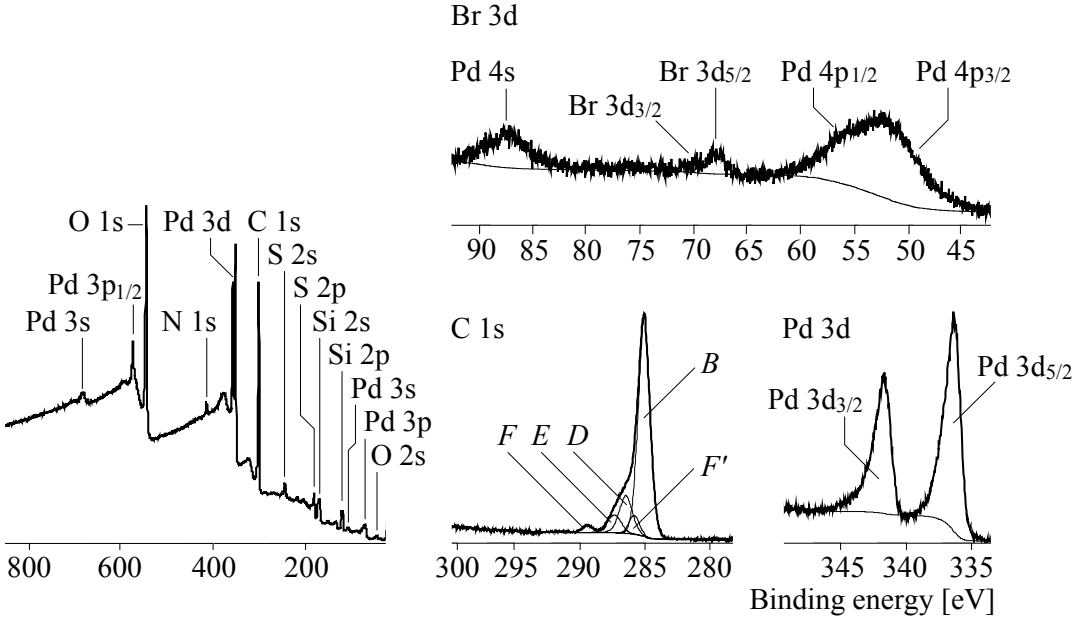

Figure 71: XPS spectra of the crosslinked PS(Br) film treated with Pd(PtBu$_3$)$_2$.

The reaction with Pd(PtBu$_3$)$_2$ lead to the high content of Pd in the polymer film (Figure 71). The [Pd]/[C] = 0.084 was close to the initial ratio [Br]/[C] of the non-treated PS(Br) film. Almost no bromine was found in the sample after the reaction with Pd(PtBu$_3$)$_2$ ([Br]/[C] = 0.004). That concludes that most of the bromophenyl groups were consumed during the reaction. The corresponding Pd 3d spectra shows only one Pd species. The binding energy of the Pd 3d$_{5/2}$ peaks of 336.25 is slightly higher, as expected for the Pd metal. However, it perfectly agrees with PdO. Due to the high catalytic activity of the Pd NPs, the polymer layer was partly decomposed. The C 1s peak is presented with a broad shoulder on its high-energy face, which is very atypical for the PtBu$_3$ compound. The two component peaks D and E correspond to the oxidized carbon species, such as alcoholic (C-OH) and keto groups (C=O). An additional peak F is probably due to carbonic acid groups (-COOH). The

carbon atom in the α-position to these carbonic acid groups (C-COOH) and C-N induced component peak F'. The most intense component peak B shows saturated hydrocarbons and carbon atoms of the residual phenyl rings. No shake-up peaks were detected in the C 1s spectra due to the small number of intact phenyl rings.

All the aforementioned data illustrate that treatment of PS(Br) with Pd($P t Bu_3$)$_2$ lead to the near complete consumption of bromophenyl groups. Although XPS could not confirm the T-shaped monomer structure postulated by Hartwig and co-workers, presumably in the form of Pd clusters were found alone with a deep transformation of PS(Br). It could be proposed that the observed complete decomposition was occurred during storage of the sample before the measurements due to the highly reactive and catalytic nature of Pd complexes. However, it cannot be excluded that freshly prepared samples also contains the molecular Pd complex which is unstable during storage.

4.3 Synthesis of Pd NPs and Utilization as a Catalyst in Suzuki Polycondensation

To verify whether Pd nanoparticles are indeed formed upon activation of PS(Br) with Pd($P t Bu_3$)$_2$, the Pd-activated sample was investigated by AFM (Figure 72) and TEM (Figure 73). Both these measurements confirmed the formation of Pd nanoparticles of sizes ranging from 2 to 10 nm.

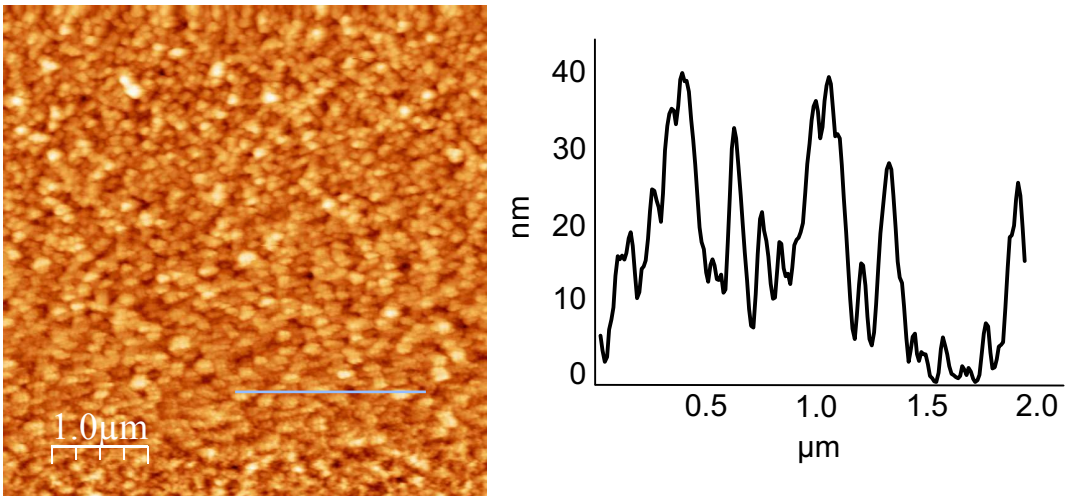

Figure 72: AFM topography image (left) and cross-section (right) of the 10 nm PS(Br) anchoring layer activated with Pd(0)-complex.

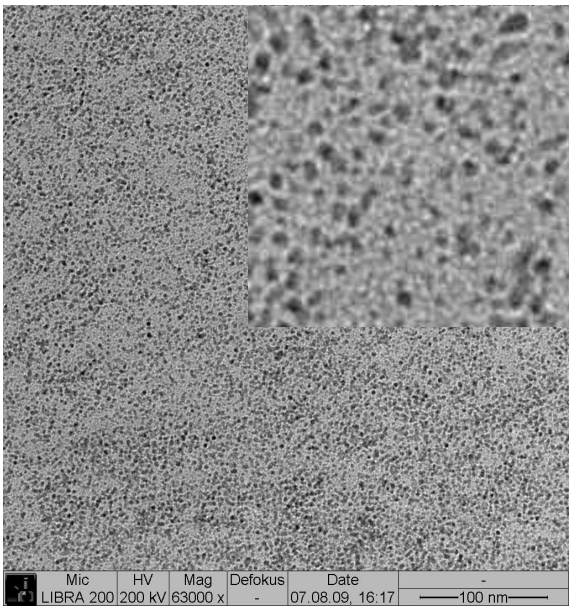

Figure 73: TEM-image of the 10 nm PS(Br) anchoring layer activated with Pd(0)-complex. The film was detached from supporting Si-wafer by treatment with 1 M HF. Zoom image with 5:1 magnification.

In the next step, an attempt was undertaken to prepare Pd nanoparticles independently and to use them for graft- and solution Suzuki polycondensation. It is well known that the initial Pd(II)-complex can be easily converted into palladium black (Pd(0) particles) in the presence of reducing agents. Considering this fact, we tried to prepare Pd-particles, reducing K_2PdCl_4 with $NaBH_4$ and using PtBu$_3$-ligand for stabilization, but unfortunately this was unsuccessful. All Pd-species precipitated during the reaction. That is why we decided to prepare Pd-particles stabilized with BINAP [162] and to exchange BINAP by PtBu$_3$, since synthesis of BINAP-stabilized Pd NPs has previously been reported.

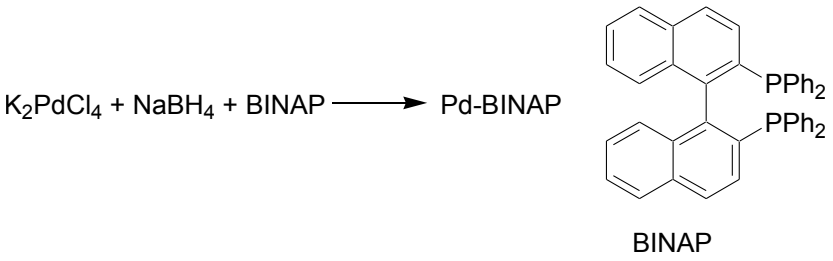

Figure 74: Schematic representation of synthesis of Pd NPs stabilized with BINAP.

The size of the obtained BINAP-stabilized Pd-particles, about 1-10 nm, was proven by TEM investigations (Figure 75). DLS measurments also confirmed this value. Bulk-polymerizations of the monomer (7-bromo-9,9-bis(2-ethylhexyl)-9H-fluoren-2-yl-boronic acid ester) initiated by Pd-BINAP NPs using Na_2CO_3 base did not lead to any significant monomer conversion even after 100 hours of reflux. The same situation was observed in case when the PtBu$_3$ ligand was added to BINAP-stabilized Pd-particles.

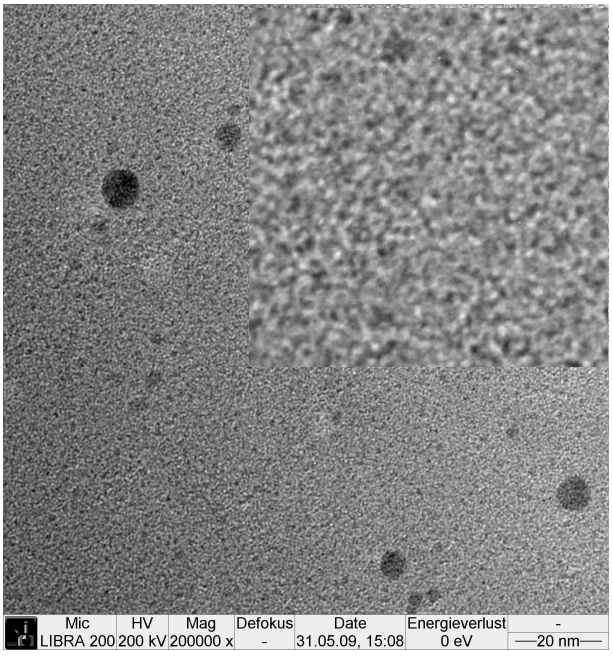

Figure 75: TEM-image of Pd-BINAP nanoparticles deposited onto a PS(Br) film. The film was detached from supporting Si-wafer by treatment with 1 M HF. Zoom image with 4:1 magnification.

Despite of the bulk solution polymerization using BINAP-stabilized Pd NPs, graft-polymerization was also attempted. To this end, activation of surface-immobilized PS(Br) films was performed by BINAP-stabilized Pd-nanoparticles. The TEM image of thus activated and floated PS(Br) film revealed successful immobilization of Pd NPs (Figure 75). Pd NPs are partially agglomerated to give a dots with the size about 10-15 nm.

Afterwards, grafting of PF2/6 brushes from PS(Br) thin films developed on Si-wafers and activated with BINAP-stabilized as well as PtBu$_3$-stabilized Pd NPs was attempted. For the immobilization of Pd NPs, a 10 nm thin PS(Br) film developed on a Si-wafers was dipped into Pd-PtBu$_3$ NPs dispersion either at r.t. or at 70°C and graft-polymerization was attempted afterwards by placing the activated wafers into monomer solution under an argon atmosphere.

The surface after the activation with Pd-PtBu$_3$ and Pd-BINAP NPs remained smooth (RMS = 0.6-1.2 nm) (Figure 76), whereas after polymerization, the RMS value increased up to 39 nm (Figure 77). Possibly, that is due to the reorganisaton of absorbed Pd NPs onto activated PS(Br) film during continuous stirring in organic-water environment. However, no PF2/6 grafting was observed in these experiments, as revealed by UV-vis and ellipsometry measurements. Thus we concluded, that Pd NPs stabilized by BINAP or PtBu$_3$-ligands are inefficient catalysts for Suzuki polycondensation.

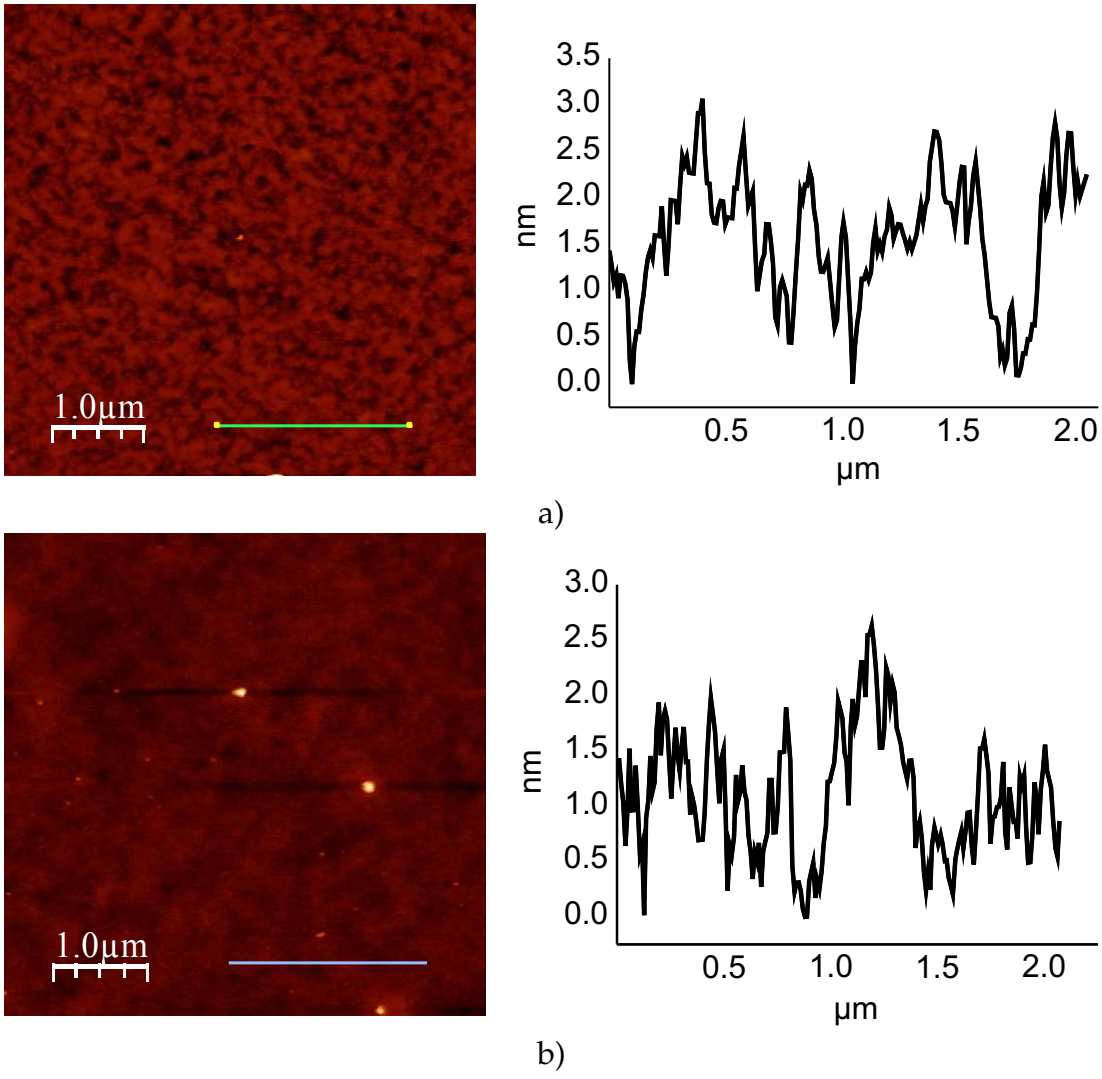

Figure 76: AFM topography image (left) and cross-section (right) of the 10 nm PS(Br) anchoring layer a) activated with Pd-BINAP NPs under 70°C and b) Pd-PtBu$_3$ NPs under 70°C.

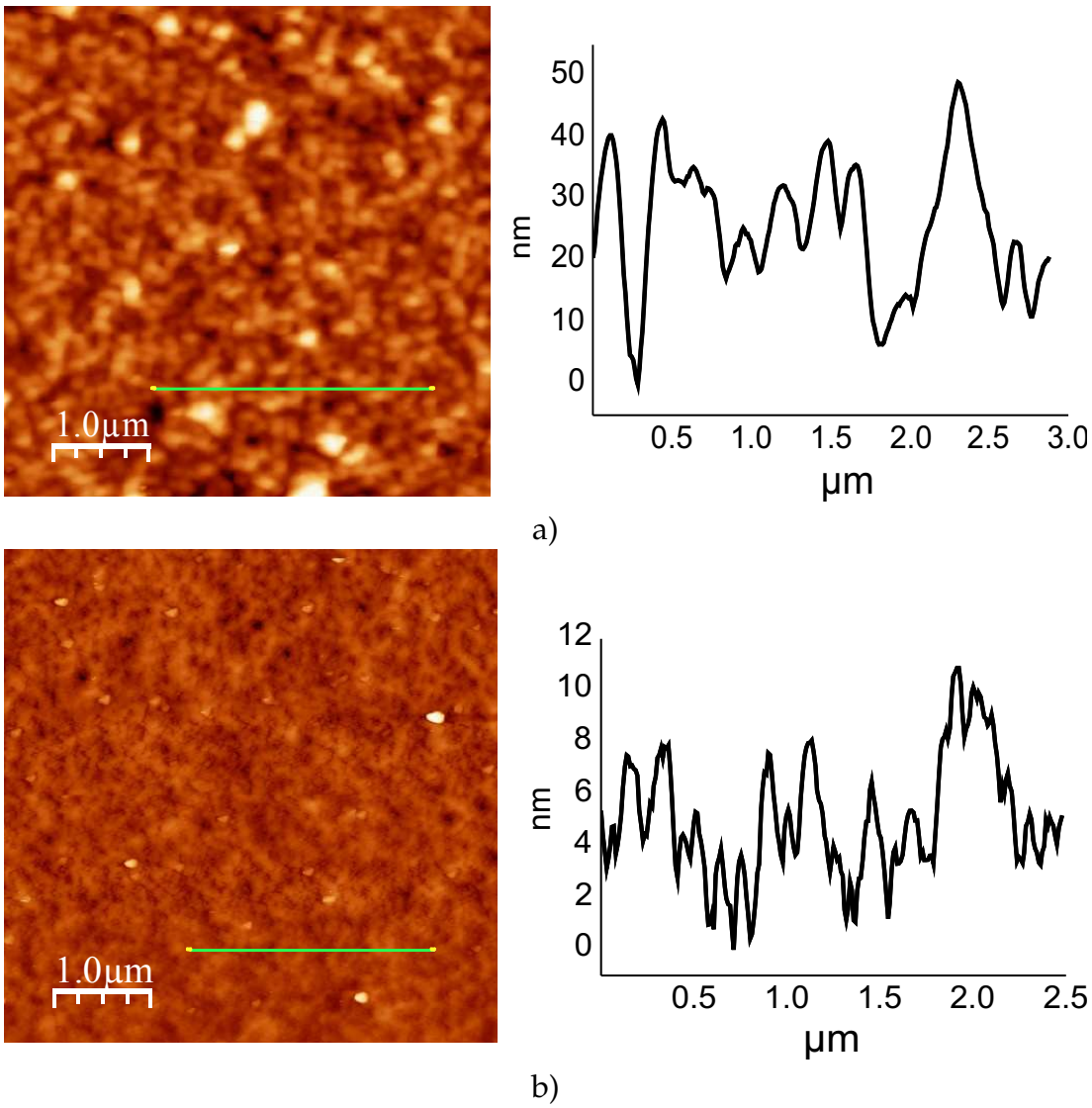

Figure 77: AFM topography image (left) and cross-section (right) of the 10 nm PS(Br) film after treatment with monomer solution activated by a) Pd-BINAP and b) Pd-PtBu$_3$.

4.4 Conclusions

NMR, XPS, AFM and TEM studies were performed to understand the process of preparation of PF2/6 brushes and to optimize grafting conditions.

^{31}P NMR studies of the process of preparation of Pd-based initiators for Suzuki polycondensation allowed us to determine the optimal conditions for activation of the initiator precursor. Investigations also revealed that Pd nanoparticles were indeed formed during activation of the PS(Br) anchoring layer; however, we did not obtain any proof that these NPs play a catalytic role in the grafting-from process. If so, the question of what factor is responsible for the remarkable "stickiness" of the Pd catalyst species to the surface is still open. An alternative explanation would be that the high hydrophobicity of Pd catalyst species supported by PtBu$_3$ ligands and the high polarity of the water-saturated solution forces Pd catalysts to segregate into a highly hydrophobic anchoring layer and further, during the polymerization, into a PF2/6 brush film. In this case, escaping of the Pd species into a water-saturated environment to induce polymerization in bulk solution is a thermodynamically unfavourable process. However, more investigations are necessary to prove this hypothesis.

4.5 Experimental Part

Materials. 2,2'-bis-(diphenylphosphino)-1,1'-binaphthyl (BINAP), sodium borohydride ($NaBH_4$), potassium tetrachloropalladate (K_2PdCl_4), tetraoctylammonium bromide $N(C_8H_{17})_4Br$, dichloromethane, acetone, chloroform, hexane, toluene, PtBu$_3$, hydrofluoric acid (HF), tetrahydrofuran (THF, stabilizer free, anhydrous) were purchased from Aldrich and used as received without further purification. Poly(glycidyl methacrylate), PGMA (M_n=65 000 g/mol, PDI=2.05) was purchased from Polymer Source Inc. Poly(4-bromostyrene) (M_n=51 000 g/mol, PDI=2.05) was obtained via radical polymerization of 4-bromostyrene [108]. 7-Bromo-9,9-bis(2ethylhexyl)-9H-fluoren-2-ylboric acid ester [109], BINAP-Pd NPs were prepared as previously described.

Preparation of PS(Br) film with immobilized Pd NPs for TEM-investigations. Si-wafer with spin-coated PS(Br) and deposited Pd NPs was partially pulled down into the 1M HF and was retained for 1 hour to detach the film from supporting Si-wafer. Detached film was carefully collected by flotation and deposited onto TEM grid.

Activation of PS(Br) film with Pd(PtBu$_3$)$_2$ or Pd-BINAP NPs and grafting of PF2/6 was performed as described in previous Chapter 3. Concentration of synthesized Pd-BINAP NPs utilized in activation process was 3 mg/ml. To perform the ligand-exchange ten-fold excess of PtBu$_3$-ligand was added to the Pd-BINAP NPs solution and heated for 30 min at 70°C.

Polymerization of PF2/6 in bulk initiated by Pd NPs. 7-Bromo-9,9-bis(2ethylhexyl)-9H-fluoren-2-ylboric acid ester (300 mg, 0.504 mmol) was placed in a round-bottomed flask equipped with a magnet stirrer bar, and the atmosphere was replaced with argon. Dry THF (7 ml) and 2M aqueous sodium carbonate (0.3 ml) were added via a syringe. In glovebox Pd-BINAP NPs (2.5 mg, 0.0034 mmol) and PtBu$_3$ (6.9 mg, 0.034 mmol) were placed into a round-bottomed flask and then the mixture was stirred for 30 min at 70°C. Simultaneously Pd-BINAP NPs (2.5 mg, 0.0034 mmol) were dissolved in THF in another round-bottomed flask. Mixture of monomer and aqueous sodium carbonate was equally added to each Pd-containing flask and allowed to react under reflux for several days. The reaction mixture was quenched by 2M hydrochloric acid and the products were extracted with $CHCl_3$. The organic layer was washed with water, dried over anhydrous $MgSO_4$ and concentrated under reduced pressure. NMR-investigations detected pure monomer without any conversion.

5 Grafting of PFO by Kumada Method

5.1 Poly(9,9-dioctyl fluorene) (PFO) Brushes Grafted from PS(Br)-latex Nanoparticles

It is well established that thin-film optoelectronic device properties such as emission color and quantum efficiency are strongly dependent on the organization of the polymer molecules and their interactions with other constituents in multicomponent devices. In general, self-assembly is a powerful and cost-efficient approach in the fabrication of complex nanostructured materials. Possibly, the use of nanoscale, three-dimensional, shape-persistent and covalently preorganized building blocks may enable self-assembly of complex multicomponent functional structures with a higher degree of control. Nanoparticles in which conjugated polymer chains are attached to a particle core by one end and stretched away from the core to form spherical brushes are likely to be the required blocks. In addition, conjugated chains densely grafted to microspheres might lead to the improvement of intermolecular charge transport.

The aforementioned "grafting to" approach usually provides rather low grafting densities, whereas "grafting from" avoids this limitation. Barnes and co-workers tried to attach oligophenylene vinylene to properly modified quantum dots [78]. Following this idea, Schanze et al. grafted polyacetylene from silica microspheres, but the obtained brush thickness was only up to 12 nm [79]. Recently, Kiriy and co-workers developed a new elegant method to grow P3HT brushes from nanoscale silica nanoparticles [163]. The obtained "hairy" nanoparticles possess a high grafting density which corresponds to a "true brush" regime. A PV device based on these particles showed reasonably good performance.

Being interested in optoelectronic devices based on polyfluorenes we tried to apply the "grafting from" approach to grow poly(9,9-dioctyl fluorene) (PFO) brushes from PS(Br) latex nanoparticles (Figure 78).

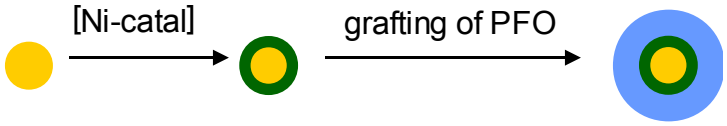

Figure 78: Schematic representation of grafting of PFO from PS(Br) latex nanoparticles.

McCullough et al. reported on a newly developed method to grow PFO using a Grignard Metathesis Method (GRIM) (Figure 79). The addition of lithium chloride to a Grignard reagents turns it into a "turbo-Grignard" which successfully reacts with 9,9-dioctyl-2,7-dibromofluorene so that magnesium halogen exchange results in the formation of a mono-Grignard reagent. The following addition of Ni(dppp)Cl_2 leads to polymerization which is concluded PFO at short reaction time with M_n up to 29 000 g/mol and resulted into a reasonably low PDI=1.5. We made a step further and applied this route to grow PFO brushes from PS(Br) latex nanoparticles.

Figure 79: Synthesis of PFO by the GRIM method.

First, we investigated monomer conversion after treatment of 9,9-dioctyl-2,7-dibromofluorene and 9,9-dioctyl-2,7-diiodofluorene with a "turbo-Grignard" reagent. McCulough reported that the use of i-PrMgCl·LiCl resulted in the formation of the mono-Grignard reagent at 85% yield, whereas our experiments have shown only 30% yield even after several days of stirring. At the same time, the use of 9,9-dioctyl-2-bromo,7-iodofluorene led to almost 100% yield of the mono-Grignard reagent. Thus, in our further experiments, we used 9,9-dioctyl-2-bromo-7-iodofluorene as the monomer precursor.

PS(Br) particles, ∼35 nm in diameter, were prepared by miniemulsion radical copolymerization of styrene bromide with 5% of crosslinker (divinylbenzene). Grafting of PFO was attempted using a recently developed procedure [164]. The prepared particles with a PS(Br) core and a PFO shell were extensively characterized. SEM measurements revealed that SIP induced an increase in particles size up to 40 nm in diameter (Figure 80).

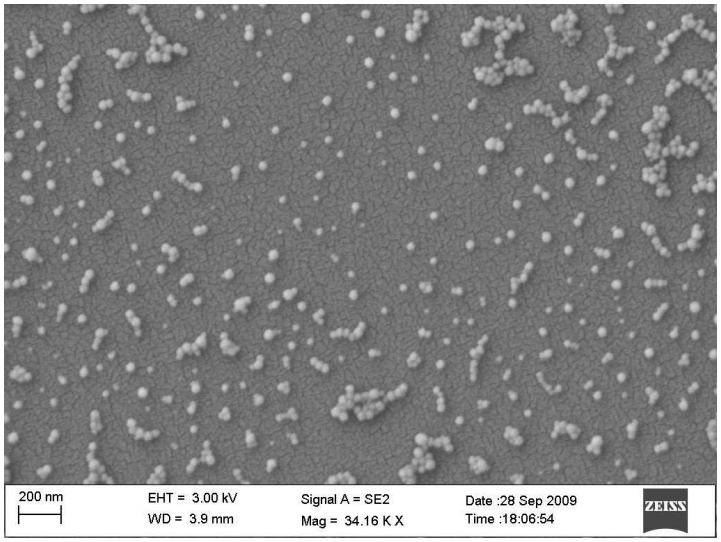

a)

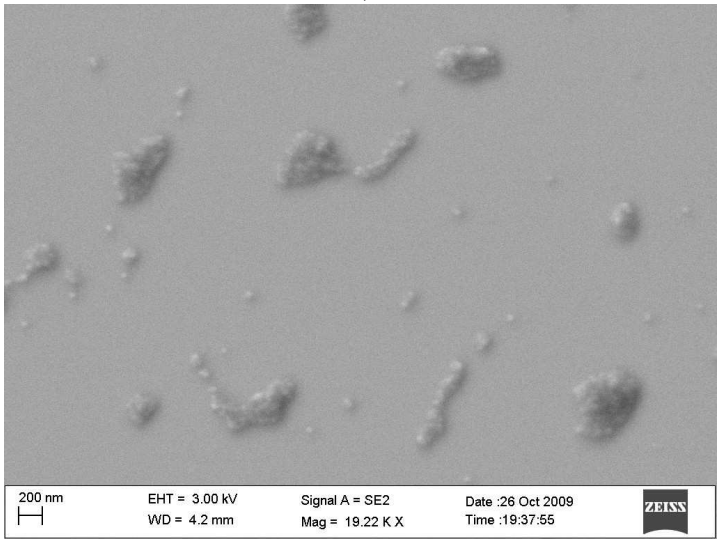

b)

Figure 80: SEM image of a) PS(Br) latex nanoparticles, b) PFO grafted from PS(Br) latex nanoparticles.

Homogeneous layers of PS(Br)-PFO NPs could be prepared by spin-coating the dispersion onto silica or other substrates. The resulting films consisted of a 90 nm thick layer of closely packed particles, as seen by AFM; the micrographs did not reveal any cracks within an area of 2x2 μm^2 (Figure 81, a). It is worth noting that spin-coated linear PFO illustrates self-assembling lamellar structures due to the relatively long symmetrical substituents at the 9^{th} position which induces formation of the β-phase (a highly ordered conformation of planarized chains) (Figure 81, b).

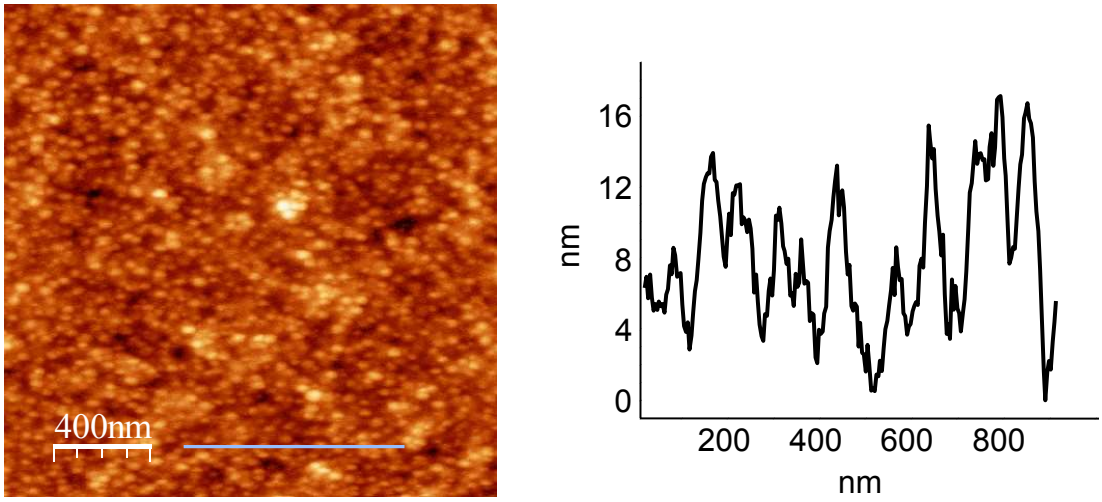

a)

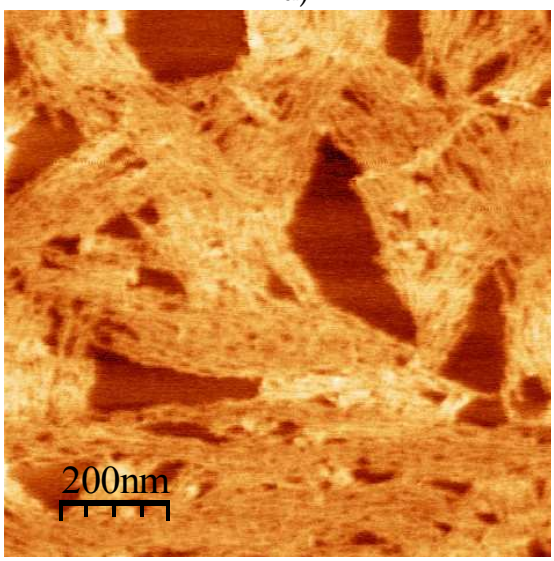

b)

Figure 81: AFM topography image and cross-sections of the a) 90 nm PS(Br)-core PFO-shell nanoparticles and b) AFM phase image of linear PFO.

5.2 UV-vis Absorption and Photoluminescence Investigations

The absorption and photoluminescence spectra of the PS(Br)-core PFO-shell NPs and linear polymer in the dry state are shown in Figure 82. The additional red shifted peak at 440 nm can be assigned to the β-phase of PFO that corresponds to the lower energy state which is induced by extended conformations of the PFO chains [165]. The absorbance of PFO particles is greater than in the case of linear polymer, suggesting that there is a slight increase in photon absorbance due to the spherical structure which brings some disorder to the system.

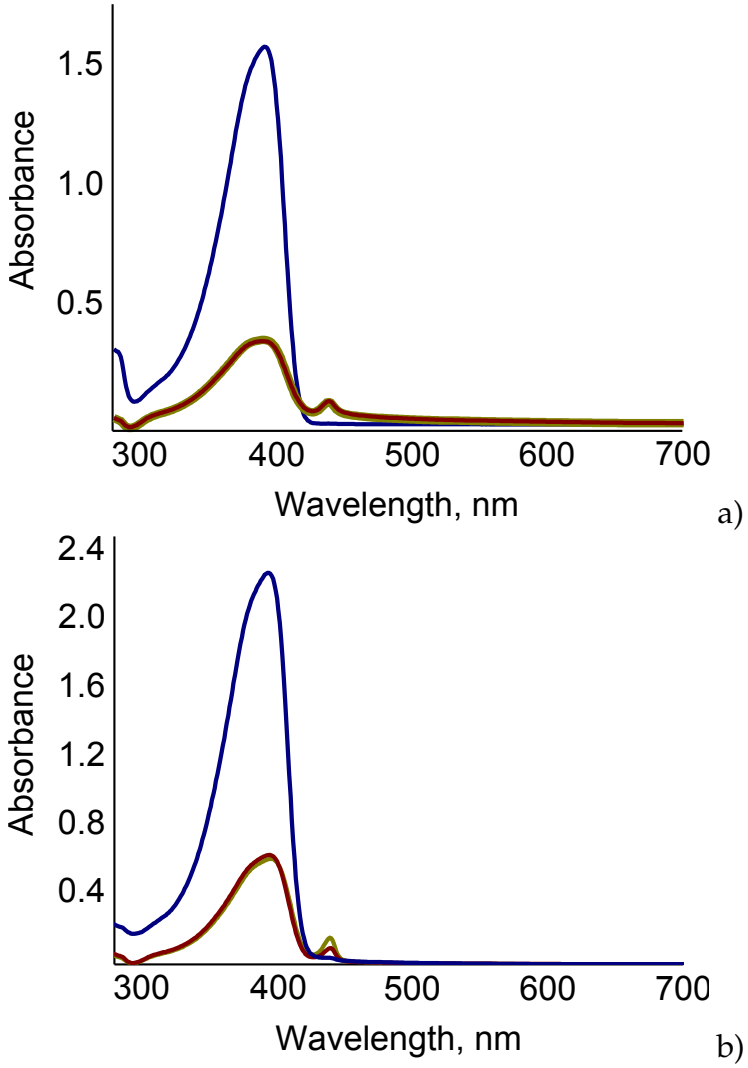

Figure 82: Absorbance spectra of a) linear non-grafted PFO and b) PS(Br)-core PFO-shell nanoparticles. Blue - heating to 70°C followed by a slow cooling to r.t., brown - homogenized system as prepared, olive - cooling to -30°C followed by a slow heating to r.t.

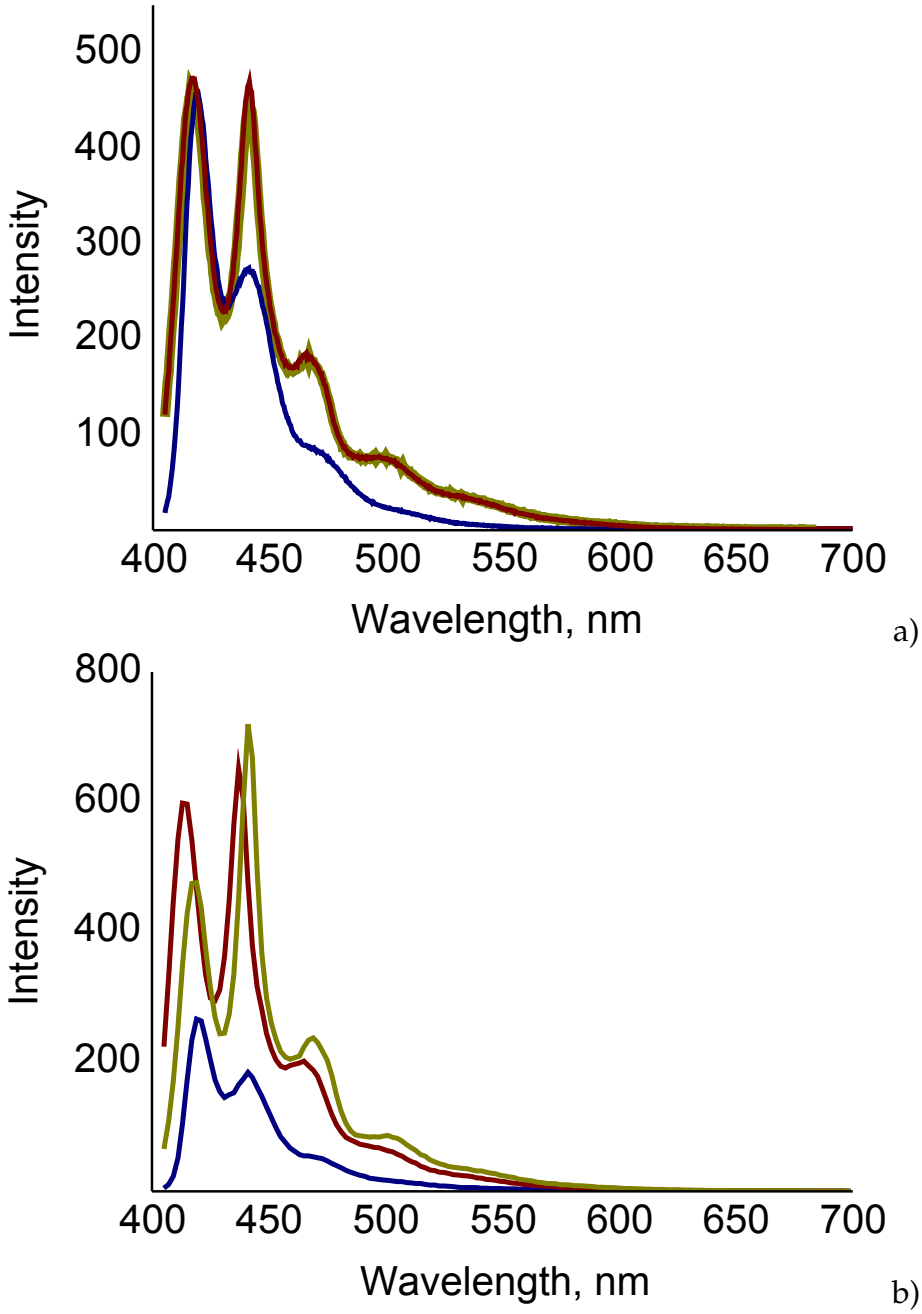

Figure 83: PL spectra of a) linear non-grafted PFO and b) PS(Br)-core PFO-shell nanoparticles. Blue - heating to 70°C followed by a slow cooling to r.t., brown - homogenized system as prepared, olive - cooling to -30°C followed by a slow heating to r.t.

β-phase emission is characterized by well-defined sharp vibronic features with almost no Stokes shift. The enlargement of the β-phase emission comes through efficient Forster energy transfer from the "host" amorphous α- phase PFO to the "guest" β-phase inclusions in the PFO matrix. Such materials can be viewed as self-doped polymer systems. Figure 83 illustrates the PL spectra of PS(Br)-core PFO-shell nanoparticles and non-grafted linear PFO. Thus, the increased absorbance and photoluminescence intensity of PFO nanoparticles, comparably with linear non-grafted polymer, can be assigned to the better structural packing and, as a consequence, improved charge transport properties. We also compared the absorbance and PL spectra of spin-coated films of PFO particles homogenized at room temperature and linear PFO. Both were driven into a crystalline phase by heating to 70°C followed by a slow cooling to room temperature or in the opposite direction, namely cooling to -30°C followed by slow heating to room temperature. We found that the highest emission intensity of peak corresponding to the β-phase was observed for the sample which was slowly heated from -30°C to room temperature. Such an increase in PL intensity is expected from the suggestion regarding a mechanism of crystalline phase formation. During heating, the partially ordered system converts into disordered one, and then as long as it is cooled down, polymer chains tend to pack efficiently in order to reach the minimum energy, but in some sense it is still a more or less disordered state. In the opposite direction, during cooling, the system is quenched, thus the volume of initial glassy (α) and β-phase are preserved. For the time being reversibly slowly heated to room temperature, polymer chains tend to take up favorable packing which leads to an increased β-phase content and, as a consequence, increased emission intensity in some cases.

Prior to use in the device, the PFO nanoparticles were purified properly from the residual Ni-catalyst which can be bound to conjugated polymers. The remaining Ni could not be completely removed using the usual purification techniques. Moreover, the metal contamination (0.0001-1%) often goes undetected due to the concentration limits of common analytical techniques (elemental analysis, NMR, etc.). The presence of residual metal could be the cause of short circuits and lead to poor electrical performance of electroactive devices [166, 167]. We treated the solution of PFO particles with i-PrMgCl at 70°C for 3 hours to react with the residual Ni. Consequently, ethylenediaminetetraacetic acid sodium salt was allowed to stir with the collected substance. The resulting product was extracted, dried and used without further purification.

5.3 Conclusions

Grafting of PFO from PS(Br) latex nanoparticles using surface-initiated Kumada polycondensation was successfully performed. The obtained particles possessed typical PFO structural features which, as a result of β-phase formation, caused additional peak in the absorbance and PL spectra. The largest increment of the β-phase was observed during slow heating of quenched material from -30°C to room temperature. Thus, these particles might be a challenging material for optoelectronic devices capable of efficient polarized emission. The properties of the emitting layer might be improved by mixing with appropriate dopant along with replacement of insulating PS(Br)-core into magnetic, conducting or other substances.

5.4 Experimental Part

Materials. 4-Bromostyrene, aluminum oxide (activated, basic, Brockmann I), Ni(dppp)Cl_2, ethylenebis(diphenylphosphine) (dppe), 9,9-dioctyl-2,7-dibromofluorene, 9,9-dioctyl-2-bromo-7-iodofluorene, i-PrMgCl·LiCl, bromobenzene, divinylbenzene, sodium dodecyl sulfate, potassium persulfate, methanol, chloroform, dichloromethane, acetone, hydrochloric acid, and tetrahydrofuran (THF, stabilizer free, anhydrous) were purchased from Aldrich and used as received without further purification.

Preparation of 9,9-dioctyl-2-chloromagnezium-7-bromofluorene (1a). A round bottomed flask equipped with septum was several times heated under reduced pressure then cooled to room temperature under argon atmosphere. 9,9-dioctyl-2,7-dibromofluorene (1.6465 g, 3 mmol) was placed in the flask. Dry THF (10 ml) was added to the flask via a syringe, and the mixture was stirred at 0°C. i-PrMgCl·LiCl (1.3 M solution in THF, 2.31 ml, 3 mmol) was added via syringe, and the mixture was slowly heated to room temperature and stirred for 3 days.

Alternative route of preparation of 9,9-dioctyl-2-chloromagnezium-7-bromofluorene from 9,9-dioctyl-2-iodo-7-bromofluorene (1.7868 g, 3 mmol) has been the same as shown before.

Preparation of PS(Br)-latex NPs. 4-bromostyrene (3.3 g, 18 mmol) and divinylbenzene (0.66 g, 5 mmol) were purified under aluminum oxide prior to use and placed with sodium dodecyl sulfate (600 mg) into a round bottomed flask equipped with septum. Then solution of potassium persulfate (10 mg) in 60 ml of degassed water was added. The mixture was stirred under 70°C overnight. The resulting product was filtrated, washed several times with mixture of methanol and water then only water and dried in vacuum under 60°C. Yield: 3.68 g.

Preparation of PS(Br)-core PFO-shell NPs. PS(Br) NPs (150 mg) were dispersed in dry THF (35 ml) in a round bottomed flack equipped with septum under inert atmosphere. Et_2NiBiPy (11.475 mg, 0.042 mmol) was dissolved in dry THF (10 ml) and allowed to stir with PS(Br) NPs solution for 1 hour. Dppe (18.41 mg, 0.0462 mmol) was dissolved in 5 ml dry THF, added to the reaction mixture and allowed to stir for 2 hours. Prior to polymerization, thus-treated particles were purified from unreacted dppe by repeated redispersion (in dichloromethane)/centrifugation cycles. Grafting of PFO was attempted by the addition of 9,9-dioctyl-2-chloromagnezium-7-bromofluorene (3 mmol) in THF (50 ml) followed by stirring under 0°C for 30 min. After quenching of the polymerization mixture with 3M EtMgBr and HCl/MeOH, the particles were carefully purified by redispersion in hot chloroform and filtration through silica gel. By following extraction in the Sokslet apparatus in methanol, hexane, dichloromethane and chloroform resulting PS(Br)-PFO NPs were purified from unreacted monomer and linear nongrafted PFO. Yield: 943.2 mg, 81%.

6 Organic Light-Emitting Diodes

6.1 Introduction to Organic Light-Emitting Diodes (OLEDs)

Light-emitting diodes (LEDs), or electroluminescent devices, based on organic materials have been the subject of a number of recent publications. Polymer light-emitting diodes (PLED)-based displays are attractive due to their processing advantages in device manufacturing. The organic materials, used as the emitting layers, are readily soluble in common organic solvents or in water. Uniform and pinhole-free thin films can be steadily cast from solution at room temperature through spin-coating or other techniques. Because of the polymeric nature, they are flexible and can be easily fabricated onto rigid or flexible substrates with different shapes. The colour of the emission depends upon the size of the HOMO-LUMO energy gap. For visible light (380-780 nm), this corresponds to 1.5-3.2 eV. Another advantage of organic semiconductors is that the energy band gap of a given system can be tuned via chemical modification of the polymer structure.

In a full-colour display, each colour pixel contains three subpixels with primary colours in the red, green and blue emission zones, respectively. A popular approach for fabricating such colour pixels is fabricating each colour subpixel with EL materials in the corresponding emission spectra. Currently, PLEDs emitting light in the red and green regions are industrially available. They display pure colour with height efficiency and brightness; however they suffer from thermal destruction during long-time operation process. Nevertheless, efficient and stable saturated blue emission is required and, thus far, remains the main challenge.

The first report of blue emission from a conjugated polymer LED was for poly(p-phenylene) [102]. Poly(alkylfluorene) derivatives are among the most promising blue-emitting materials for PLEDs because of their excellent optical and electronic properties as well as their high thermal and chemical stability. PFs demonstrate a strong blue fluorescence emission, arising from a highly conjugated planar π-electron system. In fact, PFs are the only class of conjugated polymers that can emit a whole range of visible colours with relatively high quantum efficiency (QE). Moreover, the liquid crystalline order of some PFs has opened the way to the fabrication of blue polarized electroluminescent devices.

This chapter gives a brief review of the PLEDs, their main characteristics and our results in the fabrication and characterization of PLEDs using PFO brush nanoparticles, synthesis of which was presented in the previous chapter.

6.2 The Basics of OLEDs

The PLED is typically prepared with a thin layer of semiconducting polymer film sandwiched between two electrodes. A simple schematic picture of the electroluminescence process is depicted in Figure 84. Electrones are injected from the cathode, holes are injected from the anode (1 - charge injection). These electrons and holes generate negative and positive polarons, respectively. After that, carriers migrate along the polymer chain toward the opposite electrode under the influence of the applied electric field (2 - charge transport) and combine in a segment of the polymer chain to form singlet excitons (3 - exciton formation) as produced by photoexcitation in PL. The singlet excitons decay to the ground state by emission of a photon with an energy determined by the polymer composition (4 - radiative exciton recombination, 5 - light emission).

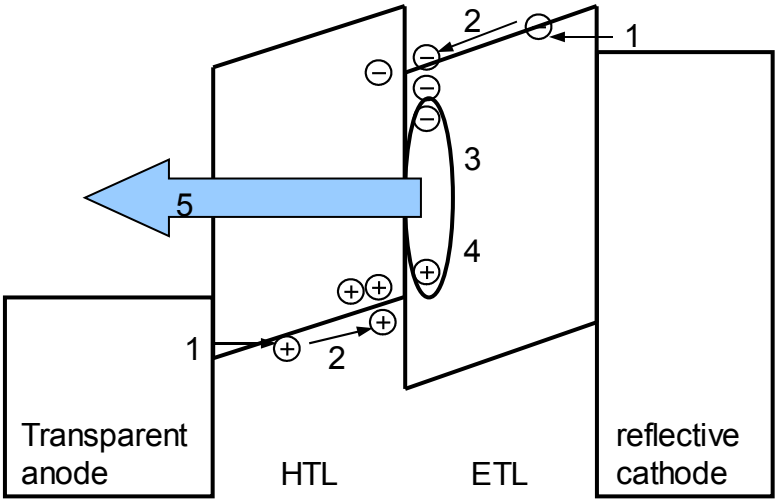

Figure 84: General operation principle of an OLED.

The process of electron-hole capture is crucial to device operation. Only singlet excited states can induce fluorescence emission. High emission requires that S_1, the lowest singlet excited state, be strongly coupled with the ground state S_0 and possesses symmetry opposite to it. Oppositely, triplet excited states do not decay radiatively. Spin statistics states, that the maximum internal quantum efficiency for electroluminescence (EL) cannot exceed 25% of the PL efficiency, since the ratio of triplets to singlets is 3:1. Nevertheless, the triplet excited state induces phosphorescence emission, which has its own drawbacks and benefits.

In order to achieve efficient luminescence, several problems must be overcome. First of all, the polymer layer must be homogeneous and without

any impurities, which can cause charge-trapping with following emission in an undesirable wavelength region, or can lead to nonradiative processes. The latter especially unwanted, because it can cause thermal degradation in the system. The nature of the interfaces between the active light-emitting polymer layer and the ITO (indium-tin oxide) or metal electrode is of paramount importance. The control of these layers may lead to the significant improvement of device performance.

Along with this, the charge balance is strictly required. During device operation, unbalanced carrier mobility means the number of electrons and holes at the emission zone is different, which leads to low current efficiency in device performance. Moreover, the recombination zone can be shifted to the interface that also causes undesired emissions.

The ITO substrate is the most commonly used anode for the fabrication of OLEDs. This is a non-stoichiometric mixture of In, In_2O, InO, In_2O_3, Sn, SnO and Sn_2O_3. Due to its transparency, light generated within the diode is able to leave the device. The value of ITO work-function is typically $\sim$4.7 eV, but can be gently tuned via plasma oxygen treatment up to approx. 5.1 eV. To displace the rigid anode material with a flexible one, several doped conducting polymers have been tried as a native anode layer. For instance, OLEDs employing a polyaniline-poly(styrene sulfonate) (PANI-PSS) blend have shown increased brightness and lifetime, compared to ITO [168]. Yang et al. also tried polypyrrole as an anode [169, 170]. A considerable restriction of these materials is the complexity of device manufacturing. One splendid solution is the utilization of a poly(3,4-ethylenedioxythiophene) poly(styrenesulfonate) (PSS-PEDOT) blend [171, 172, 173, 174, 175].

As mentioned above, PSS-PEDOT can be used as a transparent anode. However, it is now commonly deposited on ITO as an HTL (hole-transport layer). This is a complex of two charged polymers, which possess low resistivity and heigh transmittance. This layer prevents direct contact between the anode and the upper organic layer. The indicated role is very important because it avoids a fast degradation of the devices due to the large number of short-circuits between the two materials. The second purpose of PSS-PEDOT is to enhance the injection of holes from the anode into the organic layers, thus reducing the height of the energetical barrier at the ITO-organic interface. In addition to optimizing hole injection, this buffer layer also serves as a planarization layer to eliminate pin-holes in the EL layer caused by the rough ITO surface. It also serves as a chemical buffer, preventing chemical impurities in the substrate and the transparent ITO electrode from reaching EL polymers, therefore significantly improving PLED operation time [176]. In the near future, elegant flexible electronic devices will be produced utilizing PSS-PEDOT as a native anode layer. Other typical hole-transport layers are illustrated at Figure 85.

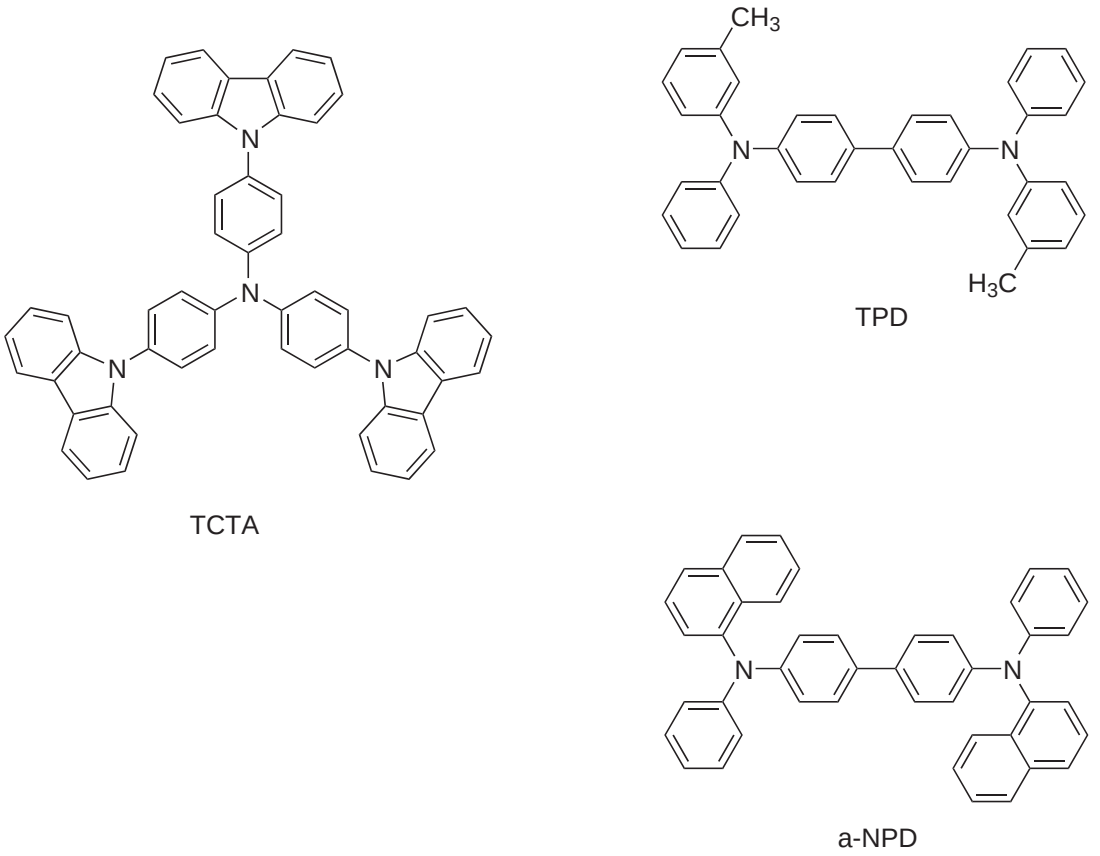

Figure 85: Chemical structures of the typical hole-transport layers: TCTA - 4,4′,4″-tris(N-carbazolyl)-triphenylamine, TPD - N,N′-diphenyl-N,N1-(3-methylphenyl) -[1,1′-biphenyl]-4,4′-diamine, α-NPD - 4,4-bis[N-(1-naphthyl)-N-phenyl-amino]biphenyl.

Electron injection is difficult to achieve without the use of low work-function, reactive materials, such as Al, Ca or Mg. They provide low barriers for electron injection to the semiconductor layer. It has been found that the separation of the cathode from the organic layer with a $\sim$1 nm layer of LiF leads to better device performance. Using a layer of ionic salts between the cathode and the emissive layer prevents atomic diffusion of the metal to the polymer, which can cause covalent bond formation. Also, metal atoms can be easily oxidized, resulting in an interfacial oxide (insulating) layer. In addition, the mobility of electrons is diminished comparably with holes. To improve electron injection, some ETLs are used to be used.

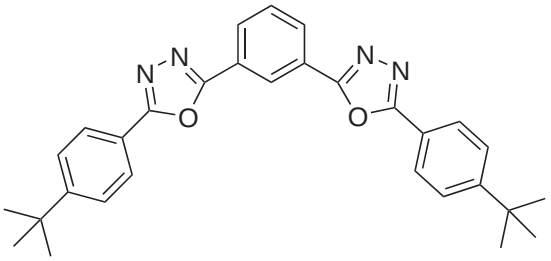

OXD-7

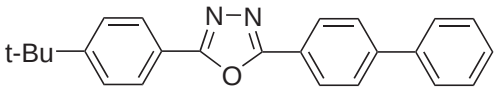

t-Bu-PBD

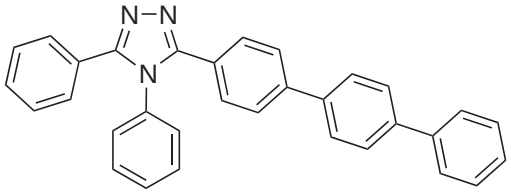

TAZ

Figure 86: Chemical structures of the most common electron-transport layers: OXD-7 - 1,3-Bis[(p-tert-butyl)phenyl-1,3,4-oxadiazoyl]benzene, t-Bu-PBD - 2-(4-Biphenylyl)-5-(p-tert-butylphenyl)-1,3,4-oxadiazole, TAZ - 3-phenyl-4-(1'-naphthyl)-5-phenyl-1,2,4-triazole.

Both layers (electron- and hole-injection) due to the careful band matching control not only injection of carriers, but also the blocking of carriers with opposite sign. This charge blocking function improves the efficiency of charge recombination and turns the charge balance factor.

6.3 Characterization of OLEDs

The criteria for evaluating the performance of an OLED include luminance, efficiency (commonly current efficiency, power efficiency, or external quantum efficiency), turn-on voltage, lifetime and current-density voltage relation.

The current-voltage characteristic is a relationship between current density and the corresponding voltage. A schematic representation of the process is shown in Figure 87. In unbiased (no applied external voltage) conditions, electrons from the n-type side diffuse over to the p-type side where they recombine with holes. A corresponding process occurs with holes that diffuse to the n-type side. This region is known as the depletion region. Upon application of the forward bias voltage, electrons and holes are injected and current flow increases. The carriers diffuse into the regions with the opposite conductivity type where they recombine and emit a photon.

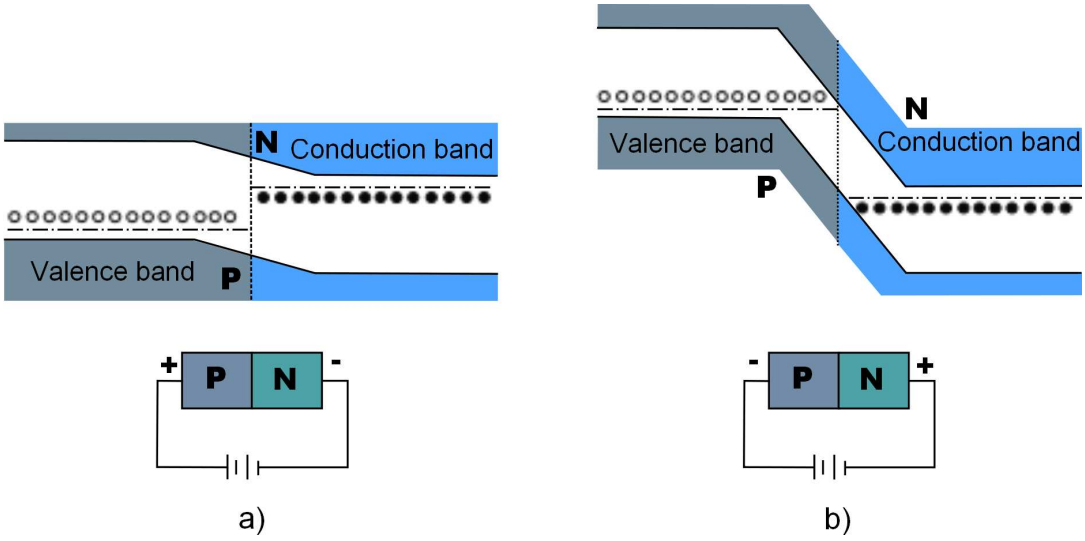

Figure 87: Schematic representation of a) forward biased pn-junction, b) reverse biased pn-junction.

Internal quantum efficiency is defined as the ratio of the number of photons $produced$ within the device to the number of electrons injected into the LED (Equation (13)).

$$\eta_{int} = \gamma r_{st} q \tag{13}$$

r_{st} is the fraction of excitons in a singlet state, q is the efficiency of radiative decay of these singlet excitons. γ is the charge balance factor, which can be defined as the ratio of the electron-hole recombination current density, J, and the measured current density J_r (Equation (14)).

$$\gamma = \frac{J_\gamma}{J} \tag{14}$$

The external quantum efficiency η_{ext} is defined as the ratio of the number of $emitted$ photons outside a device divided by the number of charges injected into a device. As discussed before, the efficiency of radiative decay depends on the device structure.

Turn-on voltage is defined as the voltage corresponding to a luminance of 1 cd/m^2.

Luminance is a luminous intensity per unit area projected in a given direction. The SI unit is the candela per square meter (cd/m^2), which is still sometimes called a nit. The footlambert (fL) is also in common use, with 1 fL=3.426 cd/m^2.

The operating lifetime is defined as the time for the light emission to decay to half of its initial value under continuous, constant current operation.

Additionally, in the application of light emission, the carrier mobility of the polymer plays an important role. Depending on the detailed molecular structures, the morphology and the electric field strength applied, carrier mobility in typical organic semiconductors is in the range of 10^{-7} to 10^{-2} cm^2/(V·s).

6.4 Device Preparation

We assumed that the particles with a modificated PFO brush surface would display improved device performance and charge mobility compared to the spin-coated film of the same linear polymer.

Two sets of PLEDs were fabricated on indium tin oxide (ITO) coated glass substrates, as can be seen in Figure 88. The thickness of ITO layer was ∼100 nm.

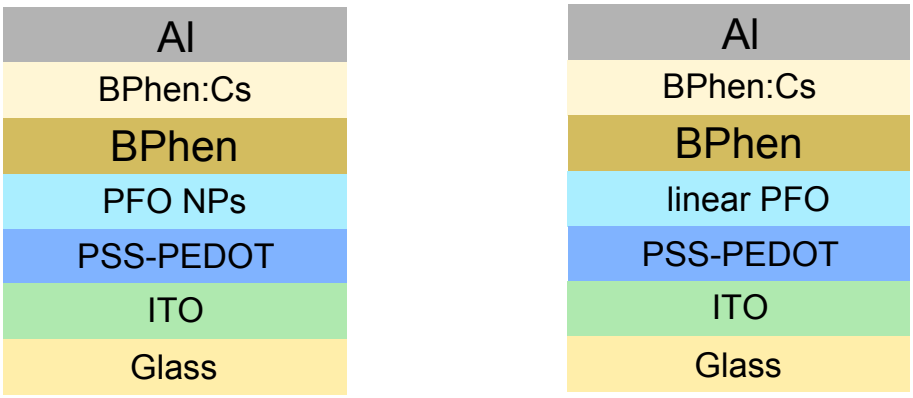

Figure 88: Two types of OLED devices.

First, the PSS-PEDOT hole-transport layer was directly spin-coated on top of ITO in order to improve hole-injection and substrate smoothness and to enhance the performance of the PLEDs. Afterwards, the sample was annealed at 150°C. The annealing lead to further smoothening of the surface (Figure 89) and to improved electron transport as confirmed by measurements of lateral conductivities (from 0.001 Scm^{-1} to 0.04 Scm^{-1}). The obtained thickness was 30 nm. Afterwards, a layer of PS(Br)-core PFO-shell nanoparticles with a thickness of 90 nm was spin-coated. The second type of OLED consisted of the same layers as previously described, but linear PFO of the same 90 nm thickness was used instead of the PS(Br)-core PFO-shell nanoparticles.

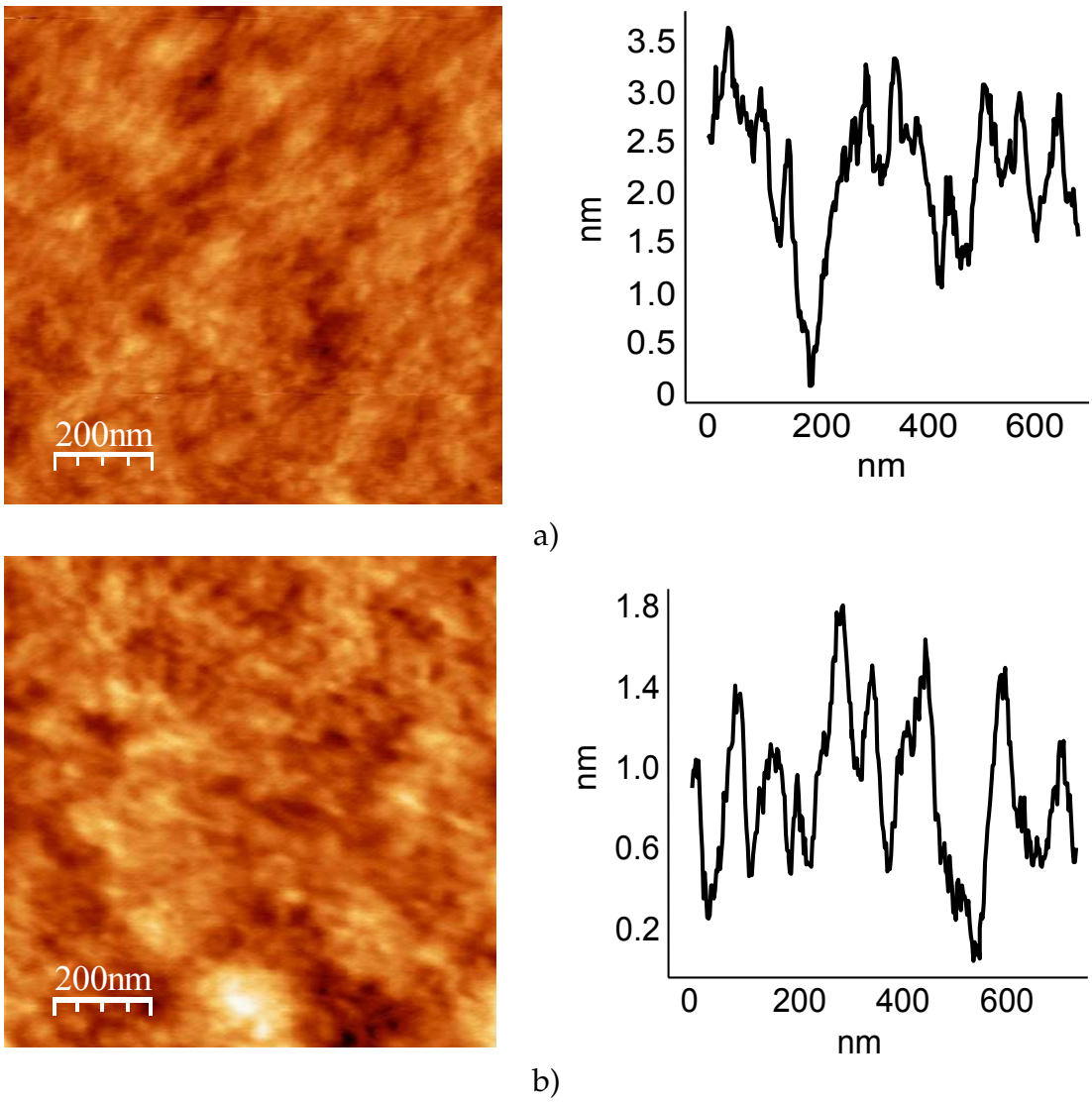

Figure 89: AFM image of a) spin-coated PSS-PEDOT, b) PSS-PEDOT after annealing at 150°C for 2 hours.

Before deposition of the additional layers, the samples were stored under high vacuum ($<10^{-7}$ mbar) for 24 hours. A 90 nm layer of 4,7-diphenyl-1,10-phenantroline (BPhen), a 30 nm thick layer of BPhen doped with caesium (Cs) and a 100 nm aluminium layer (Al) were deposited on the sample through shadow masks on the substrate. The active pixel area, formed by the spatial overlap of the ITO anode and the aluminium cathode, was 0.16 cm^2.

6.5 Optoelectronic Characteristics of OLEDs

The optoelectronic characteristics were investigated at TU Dresden in the group of K. Leo. Figure 90 shows the typical current density - voltage characteristics of the device.

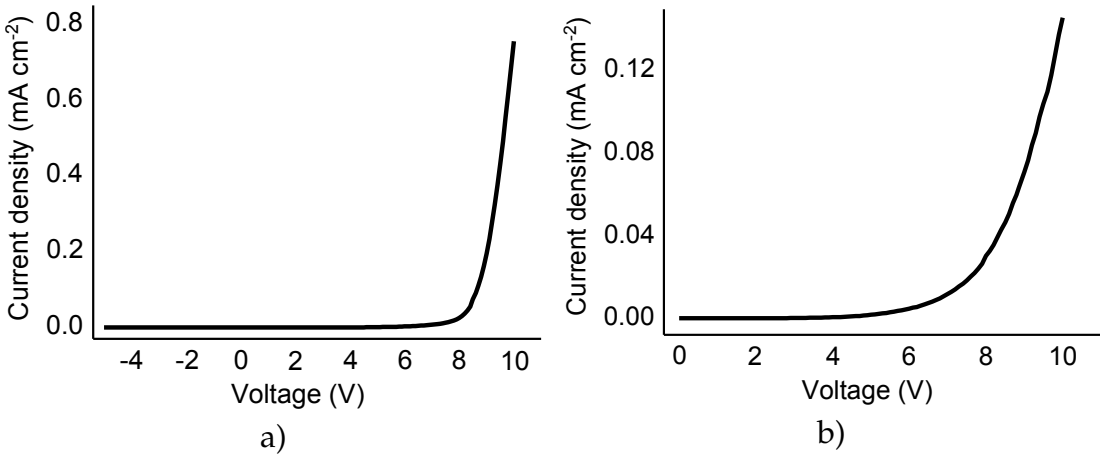

Figure 90: Current density - voltage characteristics of a) ITO/PSS-PEDOT/linear non-grafted PFO/BPhen/Cs:BPhen/Al and b) ITO/PSS-PEDOT/PFO nanoparticles/BPhen/Cs:BPhen/Al.

The driving voltage of devices based on PFO nanoparticles (the device structure is shown at the Figure 88) was 7-8 V which was approximately the same as for linear non-grafted polymer. The IV-curve of NPs based device revealed a remarkably smooth curve in the area of turn-on voltage, whereas in the case of linear PFO, the curve was significantly sharper. The observed effect was a result of a polydispersed NP system. Under a given applied voltage, only a part of present particles were able to transfer charges with the following radiative recombination step. Due to non-homogeneity, some polymer chains were not appropriately in contact with each other, which lead to some energy losses when the voltage was still not high enough to induce all charges to recombine with each other. The observed current density was typical for semiconductors which in the non-doped state demonstrate dielectric properties.

Possibly, due to the fast degradation process (almost no emmision was detected already after 1 minute) we were not able to detect luminance versus voltage characteristics. Nevertheless, Figure 91 illustrates device switched to the working regime. Here one can observe the light emitted in a blue region.

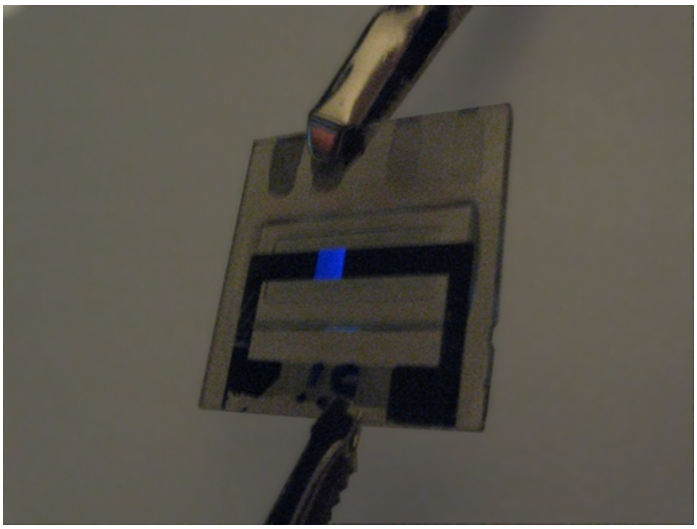

Figure 91: Picture of OLED based on a PFO NPs emitting layer in a working regime.

6.6 Conclusions

It was demonstrated that the NPs covered with a polymer brush surface were suitable for use in optoelectronic devices such as OLEDs. We have shown that particles with grafted polymer brushes can be used as an emitting layer. Unfortunately, we did not observe any reliable electroluminescence efficiency, due to inappropriate device performance. It is well known that highly bright and efficient PLEDs based on PF derivatives can be fabricated using calcium as a cathode [177, 178]. Despite of that, the polymer structures developed herein are promising materials for the manufacturing of optoelectronic devices. There is a great potential to control the properties via tuning of the molecular structure of the core-components which can be replaced by substances with various properties.

6.7 Experimental Part

Materials. The ITO glass (TFD, Inc.) was cleaned by sonication in alcohol to remove all oil dust then treated with mixture of NH_4OH:H_2O_2:H_2O (1:1:2) at 80°C during 1 hour and finally rinsed in Millipore water (18 MQxcm) several times. Purified ITO samples were dried by nitrogen and used immediately.

Preparation of the device. PSS-PEDOT (poly(3,4-ethylenedioxythoiphene) doped with poly(styrene sulfonate); Baytron P AI4083) was ultrasonicated for 15 minutes and spin-coated on the ITO surface to have the thickness of 35 nm and backed at 120°C for 30 min. Dispersion of PS(Br)-core PFO-shell and solution of linear PFO in chloroform were spin-coated (10 mg/ml, 2000 rpm) to have the thickness of 90 nm. Finally, the device was completed by thermal evaporation at a pressure of $2x10^{-6}$ torr of pure BPhen, BPhen doped with caesium (Cs:BPhen), and aluminium (Al), of which the thicknesses are 10, 100 and 100 nm, respectively. Active area of all fabricated devices was 0.16 cm^2 which thereupon was encapsulated and electrical measurements were performed.

7 General Conclusions and Outlook

The main aim of this work, which was the synthesis of covalently grafted conjugated polymer brushes on solid substrates using a "grafting from" approach, was successfully performed.

During the course of this work, the process of surface-initiated polycondensation was investigated. The newly developed method to selectively graft conjugated polymers from different substrates such as Si-wafers, quartz slides or modificated nanoparticles allowed us to produce different architectures which were earlier possible to prepare only non-conductive polymers. Exposure of the substrate with an activated surface layer into the monomer solution produced polymer brushes in a very economical way. Since only monomer was consumed for grafting from the surface.

The grafting process was extensively investigated by different methods, and the thickness of the obtained poly(fluorene) films was elucidated by Null-ellipsometry and confirmed by the AFM scratch-test. Preliminary characteristics of the device, based on PS(Br)-core poly(octylfluorene)-shell nanoparticles, showed satisfactory results (such as turn-on voltage and electroluminescence in a blue region). They could be improved by replacement of the insulating PS(Br)-core of nanoparticles with other substances (semiconductive, etc.). There is still plenty of room for further development and improvement of the synthesis of poly(fluorene)-based polymer brushes.

The polymer structures developed in this work can be utilized as an active layer in lab-on-chip devices. Alkyl groups in the 9^{th} position of the poly(fluorene) monomer unit can be replaced by tailored receptors to detect specific species including small molecules, metal ions and biomolecules due to enhanced sensitivity through sensory signal amplification. Post-polymerization modifications may lead to highly water-swellable conjugated polyelectrolyte brushes. Also, polymerization of initially optically active fluorene-monomers may be the crucial step to the generation of a light source devices with a large degree of circularly polarized electroluminescence. This is of great interest for utilization as backlight for liquid crystalline displays. We believe that the utilization of covalently surface-immobilized conjugated polymers may have a great impact on the development of present-day technological processes.

Abbreviations

AFM	Atomic Force Microscopy
ATRP	Atom Transfer Radical Polymerization
BINAP	2,2′-Bis(diphenylphosphino)-1,1′-binaphthyl
BPhen	4, 7-Diphenyl-1,10-phenanthroline
t-Bu-PBD	2-(4-Biphenylyl)-5-(p-tert-butylphenyl)-1,3,4-oxadiazole
COD	Cyclooctadiene
CP	Conjugated Polymers
DLS	Dynamic Light Scattering
DP	Degree of Polymerization
dppb	1,4-Bis(diphenylphosphino)butane
dppe	1,2-Bis(diphenylphosphino)ethane
dppf	1,1′-Bis(diphenylphosphino)ferrocene
dppp	1,3-Bis(diphenylphosphino)propane
EL	Electroluminescence
ETL	Electron-transport Layer
GPC	Gel Permission Chromatography
GRIM	Grignard Metathesis Method
HOMO	Highest Occupied Molecular Orbital
HT	Hexylthiophene
HTL	Hole-transport Layer
IL	Ionic Liquid
ITO	Indium-tin Oxide
LED	Light-Emitting Diode
LUMO	Lowest Unoccupied Molecular Orbital
MW	Molecular Weight
$Ni(PPh_3)_4$	Tetrakis (triphenylphosphine) Nikel(0)
NMP	Nitroxide Mediated Polymerization
NMR	Nuclear Magnetic Resonance
NP	Nanoparticle
α-NPD	4,4-Bis[N-(1-naphthyl)-N-phenyl-amino]biphenyl
OLED	Organic Light-Emitting Diode
OXD-7	1,3-Bis[(p-tert-butyl)phenyl-1,3,4-oxadiazoyl]benzene
PAMAM	Poly(amidoamine)
PANI-PSS	Polyaniline-poly(styrene sulfonate)
$Pd_2(dba)_3$	Tris(dibenzylideneacetone) dipalladium(0)
PDI	Polydispersity Index
Pd(OAc)	Palladium(II) acetate
$Pd(P\mathit{t}Bu_3)_2$	Bis(tri-tert-butylphosphine) Palladium(0)
$Pd(PPh_3)_4$	Tetrakis (triphenylphosphine) Palladium(0)
PEG	Polyethylene Glycol

PF	Poly(fluorene)
PF2/6	Poly[9,9-bis(2-ethylhexyl)fluorene]
PFO	Poly(9,9-dioctyl fluorene)
PGMA	Poly(glycidyl methacrylate)
P3HT	Poly(3-hexylthiophene)
PL	Photoluminescence
PLED	Polymer Light-Emitting Diode
PPP	Poly(phenyl phenylene)
PPV	Poly(phenyl vinylene)
PS	Polystyrene
PS(Br)	Poly(4-bromostyrene)
PSS-PEDOT	Poly(3,4-ethylenedioxythiophene) poly(styrenesulfonate)
PT	Polythiophene
PV	Photovoltaic
PVK	Poly(vinyl carbazole)
PVK(Br)	Poly-(4-bromo-vinylcarbazole)
PVP	Poly(vinyl pyridine)
Py	Pyridine
QE	Quantum Efficiency
RAFT	Reversible Addition-Fragmentation chain Transfer
RMS	Root Mean Square
ROMP	Ring Opening Metathesis Polymerization
SAM	Self-Assembled Monolayer
SEM	Scanning Electron Microscope
SIP	Surface-Initiated Polymerization
SPM	Scanning Probe Microscopy
STM	Scanning Tunneling Microscope
TAZ	3-Phenyl-4-(1′-naphthyl)-5-phenyl-1,2,4-triazole
TCTA	4,4′,4″-Tris(N-carbazolyl)-triphenylamine
TEM	Transmission Electron Microscopy
TGA	Thermogravimetric Analysis
TMOS	Tetramethyl Orthosilicate
TOF	Turn Off Frequency
TPD	N,N′-Diphenyl-N,N1-(3-methylphenyl) -[1,1′-biphenyl]-4,4′-diamine
UV-vis	Ultravioletvisible
XPS	X-Ray Photoelectron Spectroscopy
d_g	Interval between the grafting points of tethered chains
r_g	Radius of gyration
r.t.	Room Temperature

Acknowledgments

The writing of a dissertation can be a lonely and isolating experience, yet it is obviously not possible without the personal and practical support of numerous people.

Firstly, I would like to thank Prof. Dr. Manfred Stamm for giving me the opportunity to work with his group. Also, I would like to thank Dr. Anton Kiriy for being a great advisor. His ideas and tremendous support had a major influence on this thesis. Thanks a lot to Dr. Volodymyr Senkovskyy for his always great advices as well as his unforgettable jokes.

I also would like to thank Bettina Pilch and Dr. Ulrich Oertel for the UV-vis. measurements. Many thanks to Dr. Hartmut Komber for measuring the NMR spectra and helping in their interpretation. Furthermore, thanks to Petra Treppe for measurements GPC. I am also thankful to Dr. Frank Simon for the XPS measurments. Thanks a lot to Andreas Janke for providing me with AFM measurments along with exciting flying over the Pirna.

Thanks a lot to Dr. Björn Lüssem and Michael Thomschke from group of Prof. Dr. Karl Leo for good collaboration and a nice electronic measurements.

I would like to thank all my colleags and friends in Germany for their help during experiments, fruitfull discussions and of course very nice moments we spent together: Dr. Vera Bocharova, Dr. Konstantin Demidenok, Marta Horecha, Andrey Horechyy, Dr. Tatyana Beroyzkina, Dr. Natalya Khanduyeva, Dr. Roman Tkachov, Ekaterina Svetushkina, Ivan Raguzin, Nikolay Puretskiy.

I would like to thank Viktar Khutko, my very best friend, who did a great job helping me a lot with making up of my thesis. Besides that, thank you, Vitya, for supporting me during all my PhD.

Of course the years before I started my PhD were crucial for my subsequent professional development. Anastasiya Kiprianova and Aleksey Trukhin, who are very close to me, have played a major role in it. They have turn my hate to chemistry into completely opposite direction.

Warmest thanks and my love to my mother Irina for her love, support and understanding.

Last but not least, I would like to thank all fellow students and colleagues from IPF for the fruitful collaborations and equally important the great time in Dresden.

References

[1] Senkovskyy V., Khanduyeva N., Komber H., Oertel U., Stamm M., Kuckling D., and Kiriy A. *J. Am. Chem. Soc.*, 129:6626, 2007.

[2] Chiang C.K., Druy M.A., Gan S.C., Heeger A.J., Louis E.J., McDiarmid A.G., Park Y.W., and Schirakawa H. *J. Am. Chem. Soc.*, 100:1013, 1978.

[3] Berlin A.A. *J Polym Sci*, 55:621, 1961.

[4] Berlin A.A., Popova Z.V., and Yanovskii D.M. *Vysokomol Soedin*, 7:623, 1965.

[5] Speight J.G., Kovacic P., and Koch F.W. *J Macromol Sci C*, 5:295, 1971.

[6] Jones M.B., Kovacic P., and Howe R.F. *Polym Prepr Am Chem Soc*, 21:259, 1980.

[7] Wessling R.A. and Zimmerman R.G. *US Patent*, 3,401,152, 1968.

[8] Wessling R.A. *J Polym Sci Polym Symp*, 72:55, 1985.

[9] Geland J., Vanderzande D., and Louvet F. *European Patent Appl. EP*, 644,217, 1995.

[10] Gilch H.G. and Wheelwright W.L. *J Polym Sci A-1*, 4:1337, 1966.

[11] Papadimitrakopoulos F., Konstadinidis K., Miller T.M., Opila R., Chandross E.A., and Galvin M.E. *Chem. Mater.*, 6 (9):1563, 1994.

[12] Rehahn M., Schlüter A.D., Wegner G., and Feast W.J. *Polymer*, 30:1054–1059, 1989.

[13] Leclerc M., Diaz F.M., and Wegner G. *Macromol Chem*, 190:3105, 1989.

[14] Osterholm J.-E., Laakso J., Nyholm P., Isotalo H., Stubb H., Inganas O., and Salanek W.R. *Synth Met*, 28:C435, 1989.

[15] Yoshino K., Nakajima S., Onoda M., and Sugimoto R. *Synth Met*, 28:C349, 1989.

[16] Kocacic P. and Kyriakis A. *J Am Chem Soc*, 85:454, 1963.

[17] Reddinger J.L. and Reynolds J.R. *Adv Polym Sci*, 145:58, 1999.

[18] Dong B., Song D., Zheng L., Xu J., and Li N. *J Electroanal Chem*, 633:63, 2009.

[19] McMurry J.E. and Fleming M.P. *J Am Chem Soc*, 96:4708, 1974.

[20] McMurry J.E. *Chem Rev*, 89:1513, 1989.

[21] Rehahn M. and Schlüter A.D. *Macromol Chem Rapid Commun*, 11:375, 1990.

[22] Doi S., Osada T., Tsuchida Y., Noguchi T., and Ohnishi T. *Synth Met*, 85:1281, 1997.

[23] Hadziionannou G. and van Hutten P.F. *Semiconducting Polymers*. Wiley, 2000.

[24] Lawrence N.J. *The Wittig Reactions and Related Methods in Preparation of Alkenes: A Practical Approach*. Oxford University Press, New York, 1996.

[25] Laue T. and Plagens A. *Named Organic Reactions, 2nd Ed.* John Wiley and Sons, 1999.

[26] Horhold H.H. and Helbig M. *Macromol Chem Macromol Symp*, 12:229, 1987.

[27] Grignard V. *C.R.Acad Sci*, 130:1322, 1900.

[28] McCullough R.D. *Adv Mater*, 10:93, 1998.

[29] Chen T.A., Wu X.M., and Rieke R.D. *J Am Chem Soc*, 117:233, 1995.

[30] Wu X.M. and Chen T.A. *Macromolecules*, 28:2101, 1995.

[31] Heck R.F. *J Am Chem Soc*, 90:5518, 1968.

[32] Scherf U. *Top Curr Chem*, 201:164, 1999.

[33] Suzuki A. *Pure Appl Chem*, 63:419, 1991.

[34] Tanigaki N., Masuda H., and Kaeriyama K. *Polymer*, 38:1221, 1997.

[35] Remers M., Schulze M., and Wegner G. *Macromol Rapid Commun*, 17:239, 1996.

[36] Stille J.K. *Angew Chem Int Ed*, 25:508, 1986.

[37] Sonogashira K., Tohda Y., and Hagihara N. *Tetrahedron Lett*, 16:4467, 1975.

[38] Yamamoto T., Hayashi Y., and Yamamoto Y. *Bull. Chem Soc. Jpn.*, 51:2091, 1978.

[39] Nothofer H.G., Meisel A., Miteva T., Neher D., Forster M., Oda M., Lieser G., Sainova D., Yasuda A., Lupo D., Knoll W., and Scherf U. *Macromol Symp*, 154:139, 2000.

[40] Dong C.-G. and Hu Q.-S. *J Am Chem Soc*, 127:10006, 2005.

[41] Yokoyama A., Suzuki H., Kubota Y., Ohuchi K., Higashimura H., and Yokozawa T. *J Am Chem Soc*, 129 (23):7236, 2007.

[42] Miyakoshi R., Yokoyama A., and Yokozawa T. *J Am Chem Soc*, 127:17542, 2005.

[43] Mao Y. and Lucht B.L. *J of Polym Sci: Part A*, 42:5538, 2004.

[44] Miyakoshi R., Yokoyama A., and Yokozawa T. *J Polym Sci, Part A: Polym Chem*, 46:753, 2008.

[45] Miyakoshi R., Yokoyama A., and Yokozawa T. *Macromol Rapid Commun*, 25:1663, 2004.

[46] Huang L., Wu S., Qu Y., Geng Y., and Wang F. *Macromolecules*, 41:8944, 2008.

[47] Milner S.T. *Science*, 251:905, 1991.

[48] Halperin A., Tirrell M., and Lodge T.P. *Adv Polym Sci*, 100:31, 1992.

[49] Szleofer I. and Carignano M.A. *Adv Chem Phys*, 94:165, 1996.

[50] de Gennes P.G. *J. Phys. (Paris)*, 37:1445, 1976.

[51] de Gennes P.G. *Macromolecules*, 13:1069, 1980.

[52] Zhao B. and Brittain W.J. *Prog Polym Sci*, 25:677, 2000.

[53] Ruhe J., Ballauff M., Dziezok P., Grohn F., and Johannsmann D. *Adv Polym Sci*, 165:79, 2004.

[54] Minko S. *Polym Rev*, 46:397, 2006.

[55] Soga K., Zuckermann M.J., and Guo H. *Macromolecules*, 29:1998, 1996.

[56] Alexander S. *J Phys (Paris)*, 38:983, 1977.

[57] Szleifer I. and Carignano M. *Adv Chem Phys*, 94:165, 1996.

[58] Zhilina E., Borisov O., Pryamisyn V., and Birshtein T. *Macromolecules*, 24:140, 1991.

[59] Wijmans C., Scheutjens J., and Zhilina E. *Macromolecules*, 25:2657, 1992.

[60] Milner S., Witten T., and Cates M. *Macromolecules*, 21:2610, 1988.

[61] Parsonage E., Tirrell M., Watanabe H., and Nuzzo R. *Macromolecules*, 24:1987, 1987.

[62] Marra J. and Hair M.L. *Colloids Surf*, 34:215, 1989.

[63] Guzonas D., Boils D., and Hair M.L. *Macromolecules*, 24:3383, 1991.

[64] Fleer G.J., Cohen-Stuart M.A., Scheutjens J.M.H., Cosgrovw T., and Vincent B. *Polymers at interfaces*. London: Chapman and Hall, 1993.

[65] Krenkler K.P., Laible R., and Hamann K. *Angew Macromol Chem*, 53:101, 1953.

[66] Tsubokawa N., Hosoya M., Yanadori K., and Sone Y. *J Macromol Sci*, A27:445, 1990.

[67] Tsubokawa N., Kuroda A., and Sone Y. *J Polym Sci, A*, 27:1701, 1989.

[68] Bridger K. and Vincent B. *Eur Polym J*, 16:1017, 1980.

[69] McQuade D.T., Pullen A.E., and Swager T.M. *Chem Rev*, 100:2537, 2000.

[70] Ho H.A., Dore K., Boissinot M., Bergeron M.G., Tanguay R.M., Boudreau D., and Leclerc M. *J Am Chem Soc*, 127:12637, 2005.

[71] Hagberg E.C. and Carter K.R. *Polymer Prepr*, 46:356, 2005.

[72] Beinhoff M., Appapillai A.T., Underwood L.D., Frommer J.E., and Carter K.R. *Langmuir*, 22:2411, 2006.

[73] Brittain W.J. and Minko S.J. *J Polym Sci, Part A: Polym Chem*, 45:3505, 2007.

[74] Nakashima H., Furukawa K., Ajito K., Kashimura Y., and Torimitsu K. *Langmuir*, 21:511, 2005.

[75] Liu J., Tanaka T., Sivula K., Alivisatos A.P., and Frechet J.M. *J Am Chem Soc*, 126:6550, 2004.

[76] Merrifield R. *Science*, 150:178, 1965.

[77] Yokozawa T., Asai T., Ryuji S. Ishigooka S., and Hiraoka S. *J Am Chem Soc*, 122:8313, 2000.

[78] Odoi M.Y., Hammer N.I., Sill K., Emrick T., and Barnes M.D. *J Am Chem Soc*, 128:3506, 2006.

[79] Ogawa K., Chemburu S., Lopez G.P., Whitten D.G., and Schanze K.S. *Langmuir*, 23:4541, 2007.

[80] Edmondson S., Osborne V.L., and Huck W.T.S. *Chem Soc Rev*, 33:14, 2004.

[81] Iovu M.C., Sheina E.E., Gil R.R., and McCullough R.D. *Macromolecules*, 38:8649, 2005.

[82] Joseph R. Lakowicz. *Principles of Fluorescence Spectroscopy*. Springer, 1999.

[83] Jablonski A. *Z Phys*, 94:38, 1935.

[84] Stokes G.G. *Phil Trans R Soc (London)*, 142:463, 1852.

[85] Azzam R.M.A. and Bashara N.M. *Ellipsometry and Polarized Light*. North Holland, 1988.

[86] Tompkins H. *A User's Guide to Ellipsometry*. Academic Press, San Diego., 1992.

[87] Iyer K. S., Zdyrko B., Malz H., J. Pionteck, and I. Luzinov. *Macromolecules*, 36(17):6519, 2003.

[88] Binning G., Roher H., Gerber C., and Weibel E. *Phys Rev Lett*, 49:57, 1982.

[89] Binnig G., Quate C. F., and Gerber Ch. *Phys Rev Lett*, 56:930, 1986.

[90] Frommer J. *An*, 31:1298, 1992.

[91] Tsukruk V. *Rubber Chemistry and Technology*, 14:446, 1998.

[92] Schlüter A.D. *J Polym Sci A: Polym Chem*, 39:1533, 2001.

[93] Stambuli J.P., Incarnito C.D., Bühl M., and Hartwig J.F. *J Am Chem Soc*, 126:1184, 2004.

[94] Weber S. K., Galbrecht F., and Scherf U. *Org Letters*, 8:4039, 2006.

[95] Liversedge I.A., Higgins S.J., Giles M., Heeney M., and McCulloch I. *Tetrahedron Lett*, 47:5143, 2006.

[96] Khanduyeva N., Senkovskyy V., Beryozkina T., Simon F., Nitschke M., Stamm M., Grötzschel R., and Kiriy A. *Macromolecules*, 41:7383, 2008.

[97] Khanduyeva N., Senkovskyy V., Beryozkina T., Horecha M., Stamm M., Ulrich C., Riede M., Leo K., and Kiriy A. *J Am Chem Soc*, 131:153, 2009.

[98] Bradley D.D.C., Grell M., Long X., Mellor H., Grice A., Inbasekaran M., and Woo E.P. *Opt Probes Conjugated Polym*, 254:3145, 1997.

[99] Grell M., Bradley D.D.C., Long X., Chamberlain T., Inbasekaran M., Woo E.P., and Soliman M. *Acta Polymerica*, 49(8):439, 1998.

[100] Stöber W. and Fink A. *J of Colloid and Interface Sci*, page 62, 1968.

[101] Nozawa K., Gailhanou H., Raison L., Sellier E., Delille J.P., and Delville M.N. *Langmuir*, 21:1516, 2005.

[102] Grem G., Leditzky G., Ullrich B., and Leising G. *Adv Mater*, 4:36, 1992.

[103] Cimrova V., Remmers M., Neher D., and Wegner G. *Adv M*, 8:146, 1996.

[104] List E.J.W., Guenter R., de Freitas P.S., and Scherf U. *Adv Mater*, 14:374, 2002.

[105] Gaal M., List E.J.W., and Scherf U. *Macromole*, 36:4236, 2003.

[106] Romaner L., Pogantsch A., de Frietas P.S., Scherf U., Gaal M., Zojer E., and List E.J.W. *Adv Funct Mater*, 13:597, 2003.

[107] Forster T. *Ann Phys*, 2:55, 1948.

[108] Youshida E.J. *Polym Sci*, 34:2937, 1996.

[109] Zhang X., Tian H., Liu Q., Wang L., Geng Y., and Wang F. *J Org Chem*, 71(11):4332, 2006.

[110] Bhanage B.M. and Arai M. *Catal Rev*, 43:315, 2001.

[111] Biffis A., Zecca M., and Basato M. *J Mol Catal A: Chem*, 173:294, 2001.

[112] Garret C.E. *Adv Synth Catal*, 346:889, 2004.

[113] Li Y., Xiaoyong M. Hong, David M. Collard, and Mostafa A. El-Sayed. *Org Lett*, 2:2385, 2000.

[114] Li Y., Boone E., and El-Sayed A. Mostafa. *Langmuir*, 18:4921, 2002.

[115] Narayanan R. and El-Sayed A. Mostafa. *J Am Chem Soc*, 125:8340, 2003.

[116] Li Y. and El-Sayed A. Mostafa. *J Phys Chem B*, 105:8938, 2001.

[117] Narayanan R. and El-Sayed A. Mostafa. *J Phys Chem B*, 108:8572, 2004.

[118] Daniel M.-C. and Astruc D. *Chem Rev*, 104:293, 2004.

[119] Gittins D.I. and Caruso F. *Angew Chem Int Ed*, 40:3001, 2001.

[120] Besson C., Finney E.E., and Finke R.R. *Chem Mater*, 17:4925, 2005.

[121] Strimbu L., Liu J., and Kaifer A.E. *Langmuir*, 19:483, 2003.

[122] Lu F., Ruiz J., and Astruc D. *Tetrahedron Lett*, 45:9443, 2004.

[123] Tatumi R., Akita T., and Fujihara H. *Chem Comm*, page 3349, 2006.

[124] Han W., Liu C., and Jin Z.-L. *Org Lett*, 9(20):4005, 2007.

[125] Zhao D., Fei Z., Geldbach T., Scopelliti R., and Dyson P.J. *J Am Chem Soc*, 126:15876, 2004.

[126] Lang H.-F., May R.A., Iversen B.L., and Chandler B.D. *J Am Chem Soc*, 125:14832, 2003.

[127] Lang H.-F., Maldonado S., Stevenson K.J., and Chandler B.D. *J Am Chem Soc*, 126:12949, 2004.

[128] Schauermann S., Hoffmann J., Johanek V., Hartmann J., Libuda J., and Freund H.-J. *Angew Chem Int Ed*, 41:2532, 2002.

[129] Heemeier M., Carlsson A.F., Naschitzki M., Schmal M., Baumer M., and Freund H.-J. *Angew Chem Int Ed*, 114:4242, 2002.

[130] Ebitani K., Fujie Y., and Kaneda K. *Langmuir*, 15:190, 1999.

[131] Djakovitch L. and Kohler K. *J Am Chem Soc*, 123:5990, 2001.

[132] Prockl S., Kleist W., Gruber M.A., and Kohler K. *Angew Chem Int Ed*, 43:1881, 2004.

[133] Mori K., Hara T., Mizugaki T., Ebitani K., and Kaneda K. *J Am Chem Soc*, 126:10657, 2004.

[134] Choudary B.M., Mahdi S., Chowdari N.S., Kantam M.L., and Streedhar B. *J Am Chem Soc*, 124:14127, 2002.

[135] Bertarione S., Scarano D., Zecchina A., Johanek V., Hoffmann J., Schauermann S., Libuda J., Rupprechter G., and Freund H.-J. *J Catal*, 123:64, 2004.

[136] Caruso F., Caruso R.A., and Mohwald H. *Science*, 282:1111, 1998.

[137] Caruso F. *Adv Mater*, 13:11, 2001.

[138] Kim S.-W., Kim M., Lee W.Y., and Hyeon T. *J Am Chem Soc*, 124:7642, 2002.

[139] Marck G., Villiger A., and Buchker R. *Tetrahedron Lett*, 35:3277, 1994.

[140] Wallow T.I. and Novak B.M. *J Org Chem*, 59:5034, 1994.

[141] Reetz M.T. and Westermann E. *Angew Chem Int Ed*, 39:165, 2000.

[142] Sakurai H., Tsukuda T., and Hirao T. *J Org Chem*, 67:2721, 2002.

[143] Hu J. and Liu Y.B. *Langmuir*, 21:2121, 2005.

[144] Beller M., Fischer H., Kuhlein K., Reisinger C.P., and Herrmann W.A. *J Organomet Chem*, 520:257, 1996.

[145] Zhao F., Murakami K., Shirai M., and Arai M. *J Catal*, 194:479, 2000.

[146] Whitesides G.M., Hackett M., Brainard R.L., Lavalleye J.P.P.M., Sowinski A.F., Izumi A.N., Moore S.S., Brown D.W., and Staudt E.M. *Organometallics*, 4:1819, 1985.

[147] Crabtree R.H., Mellea M.F., Mihelcic J.M., and Quirk J.M. *J Am Chem Soc*, 104:107, 1982.

[148] Collman J.P., Kosydar K.M., Bressan M., Lamanna W., and Garret T. *J Am Chem Soc*, 106:2569, 1984.

[149] Leadbeater N.E. and Marco M. *J Org Chem*, 68:5660, 2003.

[150] Leadbeater N.E. and Marko M. *Angew Chem Int Ed*, 42:1407, 2003.

[151] Arvela R.K., Leadbeater N.E., Sangi M.S., Williams V.A., Granados P., and Singer R.D. *J Org Chem*, 70:161, 2005.

[152] Sheldon R.A., Wallau M., Arendes I.W.C.E., and Schuchardt U. *Acc Chem Res*, 31:485, 1998.

[153] Zhao F.Y., Bhanage B.M., Shirai M., and Arai M. *Chem Eur J*, 6:843, 2000.

[154] Zhao F.Y., Shirai M., and Arai M. *J Mol Catal A: Chem*, 154:39, 2000.

[155] Laine R.M. *J Mol Catal*, 14:137, 1982.

[156] Lin Y. and Finke R.G. *Inorg Chem*, 33:4891, 1994.

[157] Yu K.Q., Sommer W., Richardson J.M., Weck M., and Jones C.W. *Adv Synth Catal*, 347:161, 2005.

[158] Eberhard M.R. *Org Lett*, 6:2125, 2004.

[159] Olsson D., Nilsson P., El Masnaouy M., and Wendt O.F. *Dalton Trans*, page 1924, 2005.

[160] Astruc D., Lu F., and Ruiz J.A. *Angew Chem Int Ed*, 44:7399, 2005.

[161] De Vries J.G. *Dalton Trans*, page 421, 2006.

[162] Tamura M. and Fujihara H. *J Am Chem Soc*, 125:15742, 2003.

[163] Senkovskyy V., Tkachov R., Beryozkina T., Komber H., Oertel U., Horecha M., Bocharova V., Stamm M., Gevorgyan S.A., Krebs F.C., and Kiriy A. *J Am Chem Soc*, 131:16445, 2009.

[164] Tkachev R., Senkovskyy V., Horecha M., Oertel U., Stamm M., and Kiriy A. *Chem Comm*, 46:1425, 2010.

[165] Brinkmann M. *Macromolecules*, 40:7532, 2007.

[166] Krebs F.C., Nyberg R.B., and Jorgesen M. *Chem Mater*, 16:1313, 2004.

[167] Nielsen K.T., Bechgaard K., and Krebs F.C. *Macromolecules*, 38:658, 2005.

[168] Karg S., Scott J.C., Salem J.R., and Angelopoulos M. *Synth Met*, 80:111, 1996.

[169] Yang Y., Westerweele W., Zhang C., Smith P., and Heeger A.J. *J Appl Phys*, 77:695, 1995.

[170] Gao Y., Heeger A.J., Lee J.Y., and Kim C.Y. *Synth Met*, 82:221, 1996.

[171] Cao Y., Yu G., Zhang C., Menon R., and Heeger A.J. *Synth Met*, 87:171, 1997.

[172] Brown T.M., Kim J.S., Friend R.H., Cacialli F., Daik R., and Feast W.J. *Appl Phys Lett*, 75:1679, 1999.

[173] Yan H., Huang Q., Scott B.J., and Marks T.J. *Appl Phys Lett*, 84:3873, 2004.

[174] Choulis S.A., Choong V.E., Mathai M.K., and So F. *Appl Phys Lett*, 87:113503, 2005.

[175] Seo S.M., Kim J.H., Park J.Y., and Lee H.H. *Appl Phys Lett*, 87:183503, 2005.

[176] Zhang C., Yu G., and Cao Y. *US Patent*, page 5798170, 1998.

[177] Grice A.W., Bradley D.D.C., Bernius M.T., Inbasekaran M., Wu W.W., and Woo E.P. *Appl Phys Lett*, 73:629, 1998.

[178] Weinfurtner K.-H., Fujikawa H., Tokito S., and Taga Y. *Appl Phys Lett*, 76:2502, 2000.

Curriculum Vitae

Boyko Kseniya

Personal

- Born on February 18, 1985.
- Russian nationality.

Qualification

since 07.2007	PhD student in the department of Chemistry of Technical University of Dresden (Supervisor: Prof. M. Stamm)
09.2002-06.2007	M.S. degree (in chemistry) at the Department of Chemistry of Saint-Petersburg State University
09.1999-06.2002	Gymnasium Nr. 45, Saint Petersburg, Russia
09.1992-06.1999	Secondary school Nr. 23, Vladivostok, Russia

Versicherung

Hiermit versichere ich, dass ich die vorliegende Arbeit ohne unzulässige Hilfe Dritter und ohne Benutzung anderer als der angegebenen Hilfsmittel angefertigt habe; die aus fremden Quellen direkt oder indirekt übernommenen Gedanken sind als solche kenntlich gemacht. Die Arbeit wurde bisher weder im Inland noch im Ausland in gleicher oder ähnlicher Form einer anderen Prüfungsbehörde vorgelegt. Die vorliegende Arbeit wurde unter der wissenschaftlichen Betreuung von Prof. Dr. Manfred Stamm an dem Leibniz-Institut für Polymerforschung Dresden angefertigt. Keine frühere erfolglose Promotionsverfahren statt gefunden haben. Ich erkenne die Promotionsordnung der Technischen Universität Dresden der Fakultät Mathematik und Naturwissenschaft vom 16.04.2003 an.

Boyko Kseniya

Dresden